Jihye Jung, M.Eng.

Studies of the catalytic mechanism of nitrile reductase from *Escherichia coli*

DOCTORAL THESIS

to achieve the university degree of

Doktorin der Naturwissenschaften

submitted to

Graz University of Technology

Supervisor

Univ. -Prof. Dipl. -Ing. Dr. techn. Bernd Nidetzky

Institute of Biotechnology and Biochemical Engineering
Faculty of Technical Chemistry, Chemical and Process Engineering and Biotechnology

Graz, Oct 2018

AFFIDAVIT

I declare that I have authored this thesis independently, that I have not used other than the declared sources/resources, and that I have explicitly indicated all material which has been quoted either literally or by content from the sources used. The text document uploaded to TUGRAZonline is identical to the present doctoral thesis.

Date	Signature

ABSTRACT

The nitrile reductase QueF catalyzes a biologically unique four-electron reduction of a nitrile to an amine. The natural reaction of QueF is the NADPH-dependent conversion of 7-cyano-7-deazaguanine ($preQ_0$) to 7-aminomethyl-7-deazaguanine ($preQ_1$). $preQ_0$ and $preQ_1$ belong to the biosynthesis pathway of the tRNA-inserted nucleoside queuosine. Queuosine modulates codon-anticodon binding efficiency for decoding NAC/U codons to Asn, Asp, His, and Tyr. The biosynthesis of queuosine is observed exclusively in bacteria and therefore represents a possible target for antibacterial strategies. Besides its fundamental relevance in mechanistic enzymology, the mechanism of QueF is therefore of considerable interest in this biological and medicinal context. The proposed QueF mechanism involves a covalent thioimidate adduct between $preQ_0$ and a cysteine nucleophile in the enzyme. The formed adduct is subsequently converted into $preQ_1$ in two NADPH-dependent reduction steps, presumably via an imine intermediate.

First, we show that the *Escherichia coli* QueF binds $preQ_0$ in a strongly exothermic process whereby the thioimidate adduct is formed with half-of-the-sites reactivity in the homodimeric enzyme. Both steps of $preQ_0$ reduction proceed about 4-7-fold more slowly than trapping of the enzyme-bound $preQ_0$ as covalent thioimidate and are thus mainly rate-limiting for the enzyme's k_{cat}. Kinetic studies combined with simulation reveal a large primary deuterium kinetic isotope effect of 3.3 on the covalent thioimidate reduction and a smaller kinetic isotope effect of 1.8 on the imine reduction to $preQ_1$. A model of QueF substrate recognition and a catalytic pathway for the enzyme are proposed based on these data.

The $preQ_0$-derived imine, which is an intermediate of nitrile reduction, might immediately hydrolyze to the corresponding aldehyde on being exposed to water. Protecting a labile imine from interception by water thus is fundamental to QueF catalysis for proper enzyme function. In the QueF from *E. coli*, the conserved Glu^{89} and Phe^{228} residues together with a mobile structural element comprising the catalytic Cys^{190} form a substrate-binding pocket that secludes the bound $preQ_0$ completely from solvent. We show that residue substitutions (E89A, E89L, and F228A) targeted at opening up the binding pocket weakened $preQ_0$ binding at the preadduct stage by up to +10 kJ/mol and profoundly affected catalysis. The E89A, E89L, and F228A variants performed primarily (≥90%) a two-electron reduction of $preQ_0$, releasing hydrolyzed imine as the product. The $preQ_0$ reduction by L191A and I192A gave $preQ_1$ and 7-formyl-7-deazaguanine at a 4:1 and 1:1 ratio, respectively. Collectively, these results provide direct evidence for the intermediacy of an imine in the QueF-catalyzed reaction.

The covalent catalysis in *E. coli* QueF requires assistance from catalytic proton transfer. Conversion of nitrile to the covalent intermediate and further on to product necessitates acid-base catalysis. The QueF active site comprises a cysteine nucleophile flanked by an aspartic acid and additionally contains a histidine. Here, we used mutagenesis of *E. coli* QueF (C190A, C190S, D197A, D197H, H229A) to study functional interplay between these enzyme residues in covalent catalysis. Substitution of Cys^{190} or Asp^{197} annihilates $preQ_0$ covalent binding and largely disrupts the nitrile-to-amine reductase activity. The H229A variant readily forms the thioimidate adduct and is 24-fold less active for $preQ_0$ reduction than wild-type ecQueF. Using isothermal titration calorimetry we show that the non-covalent step of $preQ_0$ binding involves proton uptake mediated by Asp^{197} with His^{229} as the likely protonated group. We suggest that protonated (charged) His^{229} facilitates polarization of the substrate nitrile for nucleophilic attack on carbon by Cys^{190}; and through proton relay via Asp^{197}, it could provide the proton for re-protonating Cys^{190} during formation of the imine intermediate.

ZUSAMMENFASSUNG

Die Nitrilreduktase QueF katalysiert eine biologisch einzigartige Vierelektronenreduktion einer Nitrilgruppe zu einem primären Amin. Die natürliche Reaktion von QueF ist die NADPH abhängige Umsetzung von 7-Cyano-7-deazaguanin ($preQ_0$) zu 7-Aminomethyl-7-deazaguanin ($preQ_1$). $preQ_0$ und $preQ_1$ gehören zum Biosyntheseweg des in tRNA eingebauten Nukleosids Queuosin. Neben seiner fundamentalen Bedeutung in der mechanistischen Enzymologie ist der katalytische Mechanismus auch von Interesse im bio-medizinischen Kontext. Der vorgeschlagene Mechanismus beinhaltet ein kovalentes Thioimidat zwischen einem Cystein Nukleophil im Enzyms und $preQ_0$. Das Intermediat wird in zwei NADPH abhängigen Reduktionsschritten, wahrscheinlich unter Beteiligung eines Imin Intermediat, zu $preQ_1$ umgesetzt.

Wir zeigen, dass QueF aus *Escherichia coli* das $preQ_0$ in einem exothermen Prozess bindet. Das Thioimidat Intermediat wird unter sogenannter Halbseitenreaktivität des homodimeren Enzyms gebildet. Beide Reduktionsschritte sind stereoselektiv für den 4-pro-*R* Wasserstoff am NADPH. Sie sind 4 bis 7 mal langsamer als die Bildung des kovalenten Thioimidats und geschwindigkeitsbestimmend für die Wechselzahl des Enzyms. Kinetische Studien in Kombination mit Computersimulation zeigen einen primären Deuteriumisotopeneffekte auf die Reduktion des Thioimidats und des Imins. Ein Modell der Substraterkennung durch QueF und ein katalytischer Weg für das Enzym konnten auf Basis dieser Daten vorgeschlagen werden.

Das Imin Intermediat könnte zum korrespondierenden Aldehyd hydrolysieren. Es vor Wasser zu schützen ist daher zentraler Aspekt der Katalyse von QueF und wesentlich für die korrekte Enzymfunktion. QueF aus *E. coli* nutzt die konservierten Reste Glu^{89} und Phe^{228}gemeinsam mit einer beweglichen Schleife, die das katalytische Cys^{190} enthält, um eine Substratbindungstasche auszubilden, die $preQ_0$ von Wasser abschließt. Wir zeigen, dass Substitutionen (E89A, E89L und F228A) zu einer Schwächung der Bindung von $preQ_0$ vor der Adduktbildung führen und dass sie starken Effekt auf die Katalyse haben. Die Varianten E89A, E89L und F228A führten hauptsächlich ($\geq$ 90%) eine Zweielektronenreduktion von $preQ_0$ durch und setzten hydrolysiertes Imin (7-Formyl-7-deazaguanin) als Produkt frei. Die Reduktion von $preQ_0$ durch die Varianten L191A und I192A ergab $preQ_1$ und 7-Formyl-7-deazaguanin. Zusammengefasst zeigen diese Resultate erstmals direkt ein Imin Intermediat in der Reaktion von QueF.

Die kovalente Katalyse von QueF aus *E. coli* erfordert katalytischen Protonentransfer. Umsetzung des Nitrils zum kovalenten Intermediat erfordert weiterhin Säure-Basenkatalyse. Das aktive Zentrum von QueF enthält ein Cystein, das von einer Asparaginsäure flankiert wird, und enthält darüber hinaus ein Histidin. Hier wurde Mutagenese von QueF aus *E. coli* (C190A, C190S, D197A, D197H, H229A) verwendet, um das Zusammenspiel dieser Formen der Katalyse zu studieren. Substitution von Cys^{190} oder Asp^{197} führt zur Zerstörung der kovalenten Bindung von $preQ_0$ und unterbricht weitgehend die Aktivität der Nitril-zu-Amin Reduktase. Die Variante H229A kann das Thioimidat Intermediat bilden und ist 24 mal weniger aktiv als das Wildtypenzym. Mittels isothermer Titrationskalorimetrie zeigen wir, dass der nicht kovalente Schritt der Bindung von $preQ_0$ mit einer Protonenaufnahme durch das Enzym, vermittelt durch Asp^{197} und mit His^{229} als der wahrscheinlich protonierten Gruppe, einhergeht. Der katalytische Protonentransfer von Cys^{190} via Asp^{197} auf den Stickstoff des Nitrils treiben die Bildung des kovalenten Intermediats voran. Wir schlagen vor, dass das protonierte (geladene) His^{229} die Polarisierung der Nitrilgruppe des Substrats erhöht und somit die nukleophile Attacke von Cys^{190} auf den Kohlenstoff des Nitrils erleichtert. Ebenfalls schlagen wir vor, dass durch Verlagerung des Protons im Wege von Asp^{197} das His^{229} das Proton für die Reprotonierung von Cys^{190} während der Bildung des Imin Intermediats bereitstellt.

Table of contents

Kinetic analysis and probing with substrate analogues of the reaction pathway of the nitrile reductase QueF from *Escherichia coli*

THE JOURNAL OF BIOLOGICAL CHEMISTRY VOL. 291, NO. 49, pp. 25411–25426, December 2, 2016

Kinetic Analysis and Probing with Substrate Analogues of the Reaction Pathway of the Nitrile Reductase QueF from *Escherichia coli*[*]

Received for publication, July 6, 2016, and in revised form, October 1, 2016 Published, JBC Papers in Press, October 17, 2016, DOI 10.1074/jbc.M116.747014

Jihye Jung[‡§], **Tibor Czabany**[§], **Birgit Wilding**[‡¶], **Norbert Klempier**[¶], **and Bernd Nidetzky**[‡§1]

From the [‡]*Austrian Centre of Industrial Biotechnology, Petersgasse 14, the* [§]*Institute of Biotechnology and Biochemical Engineering, Graz University of Technology, NAWIGraz, Petersgasse 12/1, and the* [¶]*Institute of Organic Chemistry, Graz University of Technology, Stremayrgasse 9, A-8010 Graz, Austria*

Edited by John Denu

The enzyme QueF catalyzes a four-electron reduction of a nitrile group into an amine, the only reaction of this kind known in biology. In nature, QueF converts 7-cyano-7-deazaguanine ($preQ_0$) into 7-aminomethyl-7-deazaguanine ($preQ_1$) for the biosynthesis of the tRNA-inserted nucleoside queuosine. The proposed QueF mechanism involves a covalent thioimide adduct between $preQ_0$ and a cysteine nucleophile in the enzyme, and this adduct is subsequently converted into $preQ_1$ in two NADPH-dependent reduction steps. Here, we show that the *Escherichia coli* QueF binds $preQ_0$ in a strongly exothermic process ($\Delta H = -80.3$ kJ/mol; $-T\Delta S = 37.9$ kJ/mol, $K_d = 39$ nM) whereby the thioimide adduct is formed with half-of-the-sites reactivity in the homodimeric enzyme. Both steps of $preQ_0$ reduction involve transfer of the 4-pro-*R*-hydrogen from NADPH. They proceed about 4–7-fold more slowly than trapping of the enzyme-bound $preQ_0$ as covalent thioimide (1.63 s^{-1}) and are thus mainly rate-limiting for the enzyme's k_{cat} (=0.12 s^{-1}). Kinetic studies combined with simulation reveal a large primary deuterium kinetic isotope effect of 3.3 on the covalent thioimide reduction and a smaller kinetic isotope effect of 1.8 on the imine reduction to $preQ_1$. 7-Formyl-7-deazaguanine, a carbonyl analogue of the imine intermediate, was synthesized chemically and is shown to be recognized by QueF as weak ligand for binding ($\Delta H = -2.3$ kJ/mol; $-T\Delta S = -19.5$ kJ/mol) but not as substrate for reduction or oxidation. A model of QueF substrate recognition and a catalytic pathway for the enzyme are proposed based on these data.

Reduction of a nitrile group to a primary amine is a transformation well known and important to synthetic chemistry (1–4). Its unique biological equivalent is the reaction catalyzed by QueF enzymes (5). QueF was discovered from the biosynthetic pathway of the tRNA-modified nucleobase queuosine (Q)[2] where it was shown to utilize NADPH for the conversion of 7-cyano-7-deazaguanine ($preQ_0$) into 7-aminomethyl-7-deazaguanine ($preQ_1$) (Fig. 1). Until today, QueF remains the only enzyme known to promote the intricate nitrile-to-amine chemistry. The catalytic mechanism of QueF is therefore of significant fundamental interest. In addition, it also has potential application relevance. Q is a nucleoside from the wobble position of the tRNAs for Asn, Asp, His, and Tyr, and it is thus required for translation efficiency and fidelity (6). Despite its ubiquitous occurrence in nature, Q is synthesized *de novo* only in bacteria (7–9). The enzymes of the Q pathway, QueF in particular, due to its apparent uniqueness, therefore represent promising drug targets to combat bacterial infections selectively. Moreover, due to the hazardous conditions required in the chemical reaction (1–4), "greener" routes of nitrile reduction are highly demanded. A biocatalytic route going by the QueF mechanism presents an interesting option.

QueF enzymes have been characterized structurally from unimodular and bimodular classes (10, 11), and the herein studied QueF from *Escherichia coli* is a bimodular protein. The bimodular QueF is a functional homodimer, whereas the unimodular QueF folds into a homodecamer (a dimer of pentamers) (5, 10, 11). In both types of QueF, the active site is positioned at a structural interface, created from different subunits in the unimodular QueF and from the tandem tunneling-fold domains of the same subunit in the bimodular QueF. The arrangement of catalytic groups is highly conserved in both enzymes (10–12).

The basic QueF mechanism was delineated in biochemical and structural studies of the unimodular enzyme from *Bacillus subtilis* (Fig. 1) (11, 13). The binding of $preQ_0$ involves a large induced fit, resulting in the functional active site to be formed and to become completely secluded from solvent. Cys^{55} then attacks the nitrile group to build a covalent thioimide, where it was possible to trap both in the crystal and in solution. QM/MM calculations on the bimodular QueF from *Vibrio cholerae* suggested a role for Asp^{201} (Asp^{62} in *B. subtilis* QueF)

[*] This work was supported by the Federal Ministry of Economy, Family and Youth (BMWFW), the Federal Ministry for Transport, Innovation and Technology (BMVIT), the Styrian Business Promotion Agency (SFG), the Vienna Business Agency, the Standortagentur Tirol, the Government of Lower Austria, and the Styrian Provincial Government Economic Affairs and Innovation through the COMET-Funding Program managed by the Austrian Research Promotion Agency (FFG). The authors declare that they have no conflicts of interest with the contents of this article.

[1] To whom correspondence should be addressed. Tel.: 43-316-873-8400; Fax: 43-316-873-8434; E-mail: bernd.nidetzky@tugraz.at.

[2] The abbreviations used are: Q, queuosine; $preQ_0$, 7-cyano-7-deazaguanine; $preQ_1$, 7-aminomethyl-7-deazaguanine; QM/MM, quantum mechanics/molecular mechanics; 7-formyl-$preQ_0$, 7-formyl-7-deazaguanine; ecQueF, *E. coli* QueF; 2-deamino-$preQ_0$, 7-cyano-2-deamino-7-deazaguanine; 6-deoxo-$preQ_0$, 7-cyano-6-deoxo-7-deazaguanine; LTQ, linear ion trap; FT, Fourier transform; KIE, kinetic isotope effect; ITC, isothermal titration calorimetry.

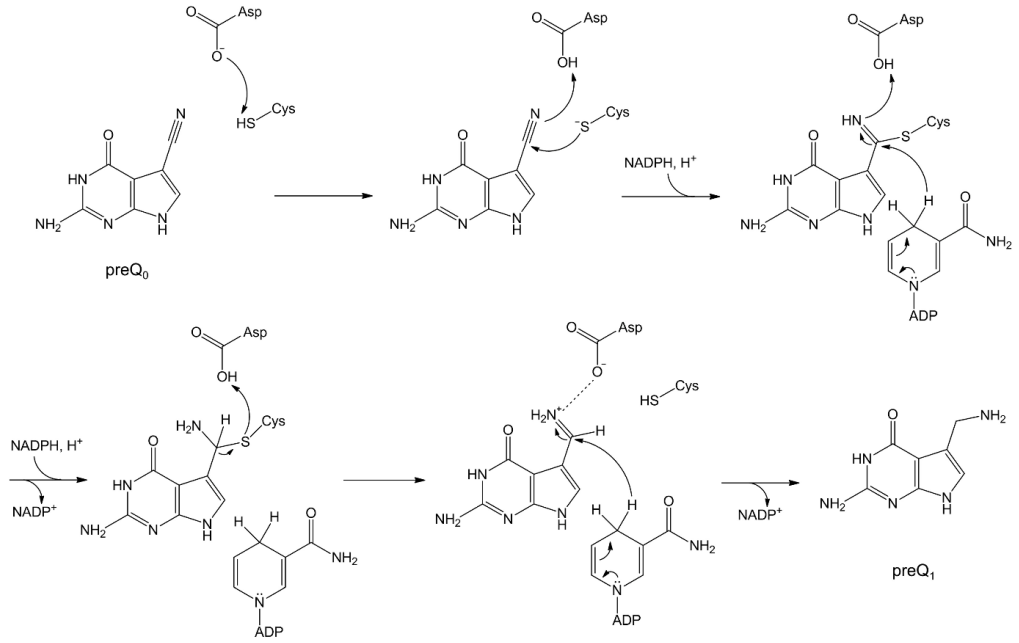

FIGURE 1. **Proposed mechanism of QueF in the reduction of $preQ_0$ to $preQ_1$.** The *dashed line* indicates an electrostatic stabilization.

as a proton shuttle during the thioimide formation (14) (Fig. 1). Hydride reduction of the thioimide by NADPH, also under protonic assistance by Asp, subsequently gives a covalent hemithioaminal. $NADP^+$ is exchanged by NADPH and the C–S bond cleaved to yield a non-covalent imine intermediate, which is finally reduced to $preQ_1$. The QM/MM calculations suggested that Asp^{201} protonates the Cys^{194} in *V. cholerae* QueF on hemithioaminal breakdown and provides electrostatic stabilization during the subsequent hydride transfer (14). Free energy barrier analysis indicated that the imine reduction is slowest among the chemical steps of the computed reaction pathway for the *V. cholerae* QueF. In *B. subtilis* QueF, the k_{cat} (0.011 s^{-1}) (5, 13) is much smaller than the rate constant of thioimide formation (2.78 s^{-1}) (11). Therefore, this also locates the rate-determining step in the sequence of steps involved in the NADPH-dependent reductions.

Despite these preceding insights into QueF structure and function, fundamental issues of the enzymatic mechanism remain. Which interactions between QueF and $preQ_0$ are required in the induced-fit binding of the substrate or in the formation of a competent thioimide intermediate? How does NADPH bind and which of its diastereotopic hydrogens at the nicotinamide C4 is used for hydride transfer in each reduction step? Is the very small k_{cat} of QueF really limited by one of the hydride transfer steps, as QM/MM calculations have suggested (14), or are rather the associated physical steps (which were not analyzed computationally) slow? To address these questions, we prepared tailored analogues of $preQ_0$, in which specific recognition sites for QueF binding were removed or altered by

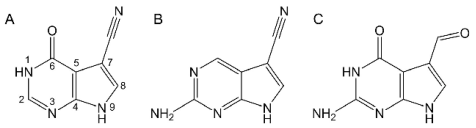

FIGURE 2. **Structures of 2-deamino-$preQ_0$ (*A*), 6-deoxo-$preQ_0$ (*B*), and 7-formyl-$preQ_0$ (*C*).**

targeted organic synthesis (Fig. 2). Together with the native $preQ_0$, we used these analogues to characterize the kinetics and thermodynamics of substrate binding by the QueF enzyme from *E. coli* (ecQueF). We applied transient and steady-state kinetic analysis in combination with kinetic simulations to characterize and to determine rate constants for the individual steps of the enzymatic reaction pathway. We also developed a synthesis of 7-formyl-7-deazaguanine (Fig. 2) as a carbonyl surrogate of the imine intermediate of the QueF reaction. We characterized the binding of this analogue to ecQueF and examined its reactivity as substrate for enzymatic reduction or oxidation. A model of substrate binding recognition by ecQueF is suggested based on the evidence presented. We show that each reduction step by the enzyme involves transfer of the pro-4-*R*-hydrogen of NADPH. We also show that the hydride transfer steps are rate-determining in the overall reaction.

Results

ITC Study of Substrate and Coenzyme Binding to ecQueF—ITC experiments were conducted to determine the thermodynamic characteristics of substrate and NADPH binding to

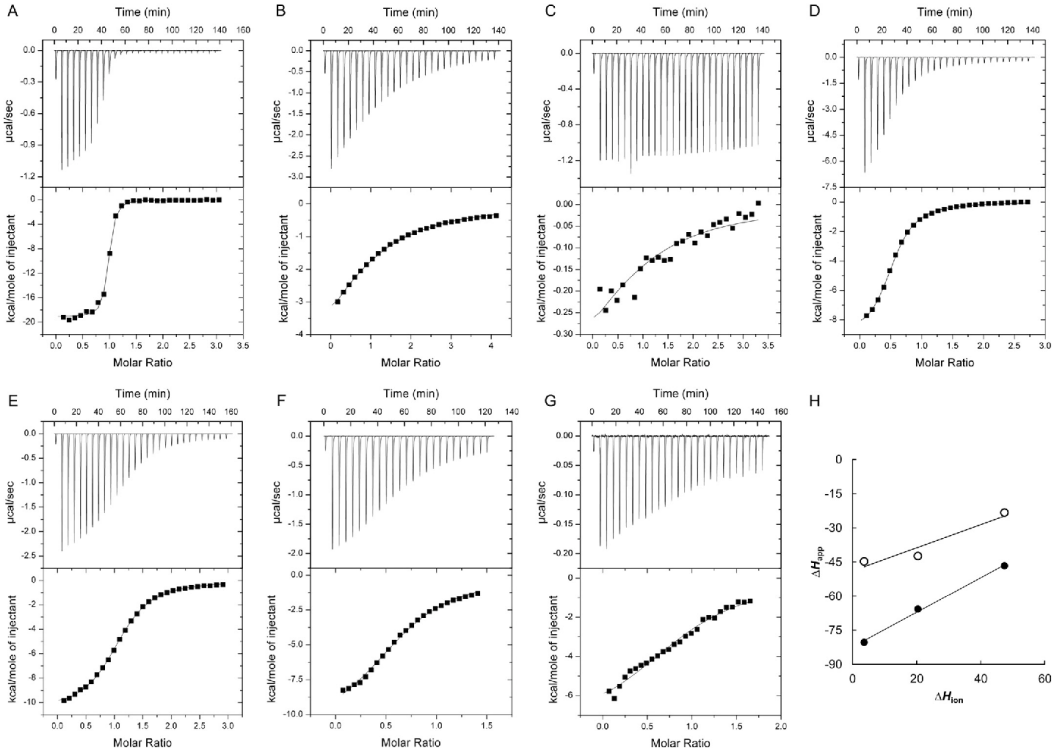

FIGURE 3. **ITC analysis for the binding of substrates and NADPH to wild type ecQueF (*A–D*) and to the C190A variant (*E–G*) is shown.** Each enzyme and ligand solution was prepared in the sodium phosphate buffer (100 mM, pH 7.5). The obtained thermodynamic parameters are summarized in Table 1. *A–D*, $preQ_0$ (0.25 mM, *A*), 2-deamino-$preQ_0$ (5 mM, *B*), 7-formyl-$preQ_0$ (3 mM, *C*), and NADPH (2.9 mM, *D*) were titrated to wild type ecQueF solution (10 μM for $preQ_0$, 200 μM for 2-deamino-$preQ_0$ and NADPH, and 150 μM for 7-formyl-$preQ_0$). The DMSO concentration of the enzyme solutions varied as follows: 1.2% for $preQ_0$, 2.5% for 2-deamino, and 7-formyl-$preQ_0$ and no DMSO for NADPH. The *c* values (c = [protein]/K_d) obtained from the experiments were 259 for $preQ_0$ and 12 for NADPH. Because of the relatively low *c* values for 2-deamino-$preQ_0$ and 7-formyl-$preQ_0$ (0.9 and 1.1, respectively), thermodynamic parameters for the two ligands were calculated under a fixed molar stoichiometry (ligand bound/ecQueF homodimer) of 1 that was obtained from the $preQ_0$ binding measurement. *E* and *F*, $preQ_0$ (0.8 mM, *E*) and NADPH (1.2 mM, *F*) were titrated to a solution of the C190A variant (60 μM, *E*; 92 μM, *F*). The thermodynamic characteristics of NADPH binding to the C190A variant were not affected by the presence of DMSO. *G*, solution of the $preQ_0$-C190A complex (104 μM) was titrated into the NADPH solution (11 μM). The DMSO concentration in both ligand and substrate solution was 2% for $preQ_0$ and 1.4% for NADPH. The *c* values were 11 for $preQ_0$ and 5 (C190A) or 4 (the $preQ_0$-C190A complex) for NADPH. *H*, dependence of the apparent binding enthalpies (ΔH_{app}) of $preQ_0$ binding to the wild type (*closed circles*) and C190A variant (*open circles*) as a function of buffer ionization enthalpy (ΔH_{ion}) is shown. The slope is +0.76 for the wild type enzyme ($R^2 = 0.996$) and +0.51 for C190A variant ($R^2 = 0.921$). The thermodynamic parameters are summarized in Tables 1 and 2.

ecQueF (25 °C, pH 7.5; 100 mM sodium phosphate buffer). The results are shown in Fig. 3 and the parameters calculated from the data are summarized in Table 1. The binding of $preQ_0$ was a strongly exergonic process ($\Delta G < 0$) in which a highly favorable enthalpy term (ΔH) overcompensated the non-favorable contribution from the binding entropy ($-T\Delta S$). The 39 nM dissociation constant (K_d) thus determined was in good agreement with the K_d estimate of 36 nM obtained from a gel filtration analysis of the unimodular QueF from *B. subtilis* (11). The number of $preQ_0$-binding sites occupied in the ecQueF homodimer was determined from the ITC data to be unity (±5%). Binding models comprising two equivalent or distinct binding sites/enzyme homodimer were also examined but were inconsistent with the experimental results. The half-of-the-sites reactivity of ecQueF implied by these findings was in line with the structural suggestion that the minimal catalytic unit of *V. cholerae* QueF should be the protein homodimer (10).

Besides analyzing $preQ_0$ binding in the standard phosphate buffer, we also determined the ΔH of $preQ_0$ binding in Tris and HEPES buffer (Table 2 and Fig. 3*H*). Because the three buffers differ strongly in ionization enthalpy (ΔH_{ion}), the proton release or uptake in conjunction with ligand binding can be determined from the difference in the ΔH of binding. We showed that in terms of ΔG, the overall $preQ_0$ binding to ecQueF was hardly affected by the buffer used (Tables 1 and 2). The binding stoichiometry was also unchanged on variation of the buffer. However, there was a large buffer effect on ΔH (Table 2), and we determined that 0.78 ± 0.09 protons were taken up by each ecQueF dimer on binding of $preQ_0$ under the conditions used (pH 7.5, Table 1).

TABLE 1

Kinetic and thermodynamic parameters for ecQueF

ND indicates not detectable; NM indicates not measured.

	$PreQ_0$	2-Deamino-$preQ_0$	6-Deoxo-$preQ_0$	7-Formyl-$preQ_0$	NADPH
$k_{cat,\ app}$ (s^{-1})	0.120 ± 0.002	0.140 ± 0.014	ND	ND	
$K_{m,\ app}$ (μM)	< 1	50 ± 12	ND	ND	7.80 ± 0.48,[a] 35 ± 18[b]
K_d[c] (μM)	0.039 ± 0.004 (5.5 ± 0.1)[d]	(2.29 ± 0.04) × 10^2	NM	(1.6 ± 0.3) × 10^2	16.0 ± 0.5 (18.1 ± 1.1[e], 3.6 ± 0.6[f])
ΔH (kJ/mol)	−80.3 ± 0.5 (−44.7 ± 0.2)[d]	−28.9 ± 0.2	NM	−2.3 ± 0.2	−38.9 ± 0.4 (−47.5 ± 1.2[e], −31.3 ± 1.2[f])
$-T\Delta S$ (kJ/mol)	37.9 (14.6)[d]	8.1	NM	−19.5	11.5 (20.3[e], 0.07[f])
ΔG (kJ/mol)	−42.4 ± 0.5 (−30.1 ± 0.2)[d]	−20.9 ± 0.2	NM	−21.8 ± 0.2	−27.5 ± 0.4 (−27.2 ± 1.2[e], −31.2 ± 1.2[f])
n_{H+}[g]	0.78 ± 0.09 (0.46 ± 0.27)[d]	NM	NM	N.D	NM

[a] Data were obtained with $preQ_0$.
[b] Data were obtained with 2-deamino-$preQ_0$.
[c] Dissociation constants were obtained from ITC measurements.
[d] Data of $preQ_0$ binding were obtained with the C190A variant.
[e] Data were obtained with the substrate-free C190A variant.
[f] Data were obtained with the noncovalent C190A-$preQ_0$ complex.
[g] The number of protons (n_{H+}) taken up by the enzyme on $preQ_0$ binding was obtained from the measured enthalpies in sodium phosphate (shown in this table), HEPES, and Tris buffers at pH 7.5 (for the thermodynamic data of $preQ_0$ binding in HEPES and Tris buffers, see Table 2).

TABLE 2

Thermodynamic parameters of $preQ_0$ binding to wild type and C190A ecQueF in HEPES and Tris buffers

	K_d	ΔH	$-T\Delta S$	ΔG	ΔH_{ion}[a]
	μM	*kJ/mol*	*kJ/mol*	*kJ/mol*	*kJ/mol*
Wild type[b]					
HEPES	0.034 ± 0.003	−65.7 ± 0.4	22.9	−42.8 ± 0.4	20.40
Tris	0.054 ± 0.005	−47.7 ± 0.3	5.1	−41.6 ± 0.3	47.45
C190A[c]					
HEPES	4.26 ± 0.11	−42.3 ± 0.2	11.5	−30.8 ± 0.2	20.40
Tris	4.05 ± 0.16	−23.2 ± 0.2	−7.7	−30.9 ± 0.2	47.45

[a] The ionization enthalpy of the buffer was obtained from literature (27).
[b] The $preQ_0$ solution (250 μM) was titrated to the wild type enzyme solution (10 μM). DMSO concentration was 1.2% in both solutions. The *c* values were 294 and 184 in HEPES and Tris, respectively.
[c] The $preQ_0$ solution (800 μM) was titrated to the C190A variant solution (60 μM). DMSO concentration was 2% in both solutions. The *c* values were 9 in both HEPES and Tris.

The 2-deamination of $preQ_0$ resulted in a drastic weakening of the substrate binding, reflected in a 21.5 kJ/mol loss in the ΔG stabilizing the ecQueF-bound state, comparing 2-deamino-$preQ_0$ to $preQ_0$. This is equivalent to a 6×10^3-fold increase in the K_d of the 2-deaminated substrate. The effect in ΔG was due to a strongly lowered enthalpy contribution to the binding of 2-deamino-$preQ_0$ as compared with $preQ_0$ ($\Delta\Delta H$ = +51.4 kJ/mol). The entropy term was, however, less unfavorable for the binding of 2-deamino-$preQ_0$ than it was for the binding of $preQ_0$. It thus compensated to some degree for the very large binding enthalpy change due to removal of the 2-amino group. We also examined the binding of 6-deoxo-$preQ_0$ but were unable to obtain a binding isotherm due to the low water solubility of this compound.

Contrary to the binding of $preQ_0$ and 2-deamino-$preQ_0$ in which both were enthalpy-driven processes, the binding of 7-formyl-$preQ_0$ was hardly exothermic. It therefore relied completely on a favorable entropy contribution to become a spontaneous process characterized by a negative ΔG. Indeed, the $-T\Delta S$ term exhibited sign change from positive to negative and hence turned from being non-favorable to favorable for binding when the binding of $preQ_0$ (or 2-deamino-$preQ_0$) was compared with that of 7-formyl-$preQ_0$. Despite the completely different thermodynamic signatures of the binding of 2-deamino-$preQ_0$ and 7-formyl-$preQ_0$, the dissociation constants of these two ligands were similar (Table 1).

Removal of the active-site nucleophile in an inactive C190A variant of ecQueF weakened the binding of $preQ_0$ (K_d = 5.5 μM) about 141-fold compared with $preQ_0$ binding to the wild type enzyme. This reflected a drastically lowered enthalpy contribution to the binding ($\Delta\Delta H$ = +35.6 kJ/mol) in the enzyme variant as compared with wild type ecQueF. The entropy term of $preQ_0$ binding to the C190A variant was positive ($-T\Delta S$ = +14.6 kJ/mol). The results are summarized in Table 1. As in the wild type enzyme, the ΔH of $preQ_0$ binding to the C190A variant was strongly dependent on the buffer used (phosphate, HEPES, Tris). The ΔG of binding was however hardly affected by the buffer (Table 2). We determined from the data that 0.46 ± 0.27 protons were taken up by the C190A variant on binding of $preQ_0$ (pH 7.5; Table 1).

The binding of NADPH by QueF is generally not well understood. We show here (Fig. 3; Table 1) that NADPH was bound by the free forms of wild type ecQueF and the C190A variant thereof. With both enzymes the binding occurred in an enthalpy-driven fashion. The overall binding was highly exergonic and characterized by 16.0 and 18.1 μM dissociation constants for the wild type enzyme and the C190A variant, respectively. These thermodynamic characteristics appear consistent with a binding process involving biological recognition and are unlikely to reflect a merely adventitious binding of NADPH. If so, then the binding of NADPH to ecQueF would not require $preQ_0$ to have been bound to the enzyme before. Additionally, we determined that NADPH binds to the binary complex of C190A and $preQ_0$ with about 5-fold enhanced affinity (K_d = 3.6 μM) compared with its binding to the free enzyme. The binding stoichiometry was 1 NADPH/enzyme dimer. Despite the relatively small difference in ΔG of binding ($\Delta\Delta G$ = −4 kJ/mol), the thermodynamic signature of NADPH binding to the C190A-$preQ_0$ complex was quite distinct from that of NADPH binding to the free enzyme. The binding of NADPH to the C190A-

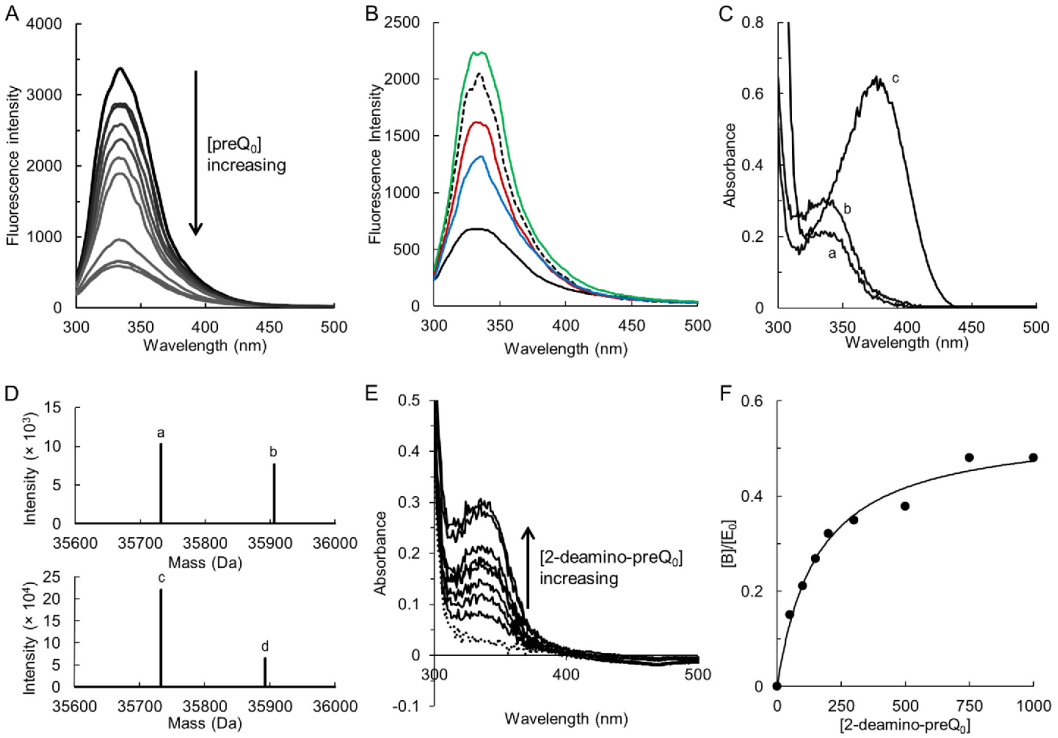

FIGURE 4. **Nitrile substrate binding to ecQueF was analyzed by fluorescence titration (*A* and *B*), spectrophotometric titration measuring covalent thioimide formation (*C, E,* and *F*), and protein mass analysis of ecQueF after incubation with preQ$_0$ or 2-deamino-preQ$_0$ (*D*).** The DMSO concentration in the enzyme solution was 1%. *A,* protein fluorescence intensities of ecQueF (2.8 ± 0.4 μM) decreased gradually until the ratio of ecQueF to preQ$_0$ reached a value of 1 (*top to bottom*: 0.0–10 μM, [preQ$_0$]). *B,* fluorescence intensities of ecQueF (*black dashed line*, 2.8 ± 0.4 μM) were changed by addition of ligands (*black,* preQ$_0$; *red,* 2-deamino-preQ$_0$; *blue,* 3-deoxo-preQ$_0$; *green,* 7-formyl-preQ$_0$; each 3 μM). *C,* absorbance spectra for the covalent thioimide adduct of ecQueF (60 μM) with 2-deamino-preQ$_0$ (*a*, 500 μM, and *b*, 1.00 mM) and the shifted spectrum of the enzyme adduct with 2-deamino-preQ$_0$ (500 μM) upon addition of preQ$_0$ (*c*, 60 μM) are shown. *D,* sample of ecQueF (130 μM) incubated with preQ$_0$ (*top*, 130 μM) is shown to contain preQ$_0$-free monomeric ecQueF (*a*, 35,732.1 ± 0.5 Da) and covalent adduct of monomeric ecQueF with preQ$_0$ (*b*, 35,906.0 ± 1.7 Da). The sample of ecQueF (130 μM) incubated with 2-deamino-preQ$_0$ (*bottom,* 2.6 mM) is shown to contain substrate-free monomeric ecQueF (*c*, 35732.7 ± 0.1 Da) and monomeric adduct with 2-deamino-preQ$_0$ (*d*, 35892.7 ± 0.1 Da). *E,* absorbance spectra of covalent thioimide (ecQueF, 50 μM) with 2-deamino-preQ$_0$ (*bottom to top*: 50–1000 μM, [2-deamino-preQ$_0$]) were obtained. The spectra of enzyme and adduct are represented by *dotted* and *solid lines*, respectively. *F,* binding stoichiometry ([*B*]/[E_0], *closed circle*) dependent on the 2-deamino-preQ$_0$ concentration is shown. The data are taken from *E*. [*B*] and [E_0] are the concentrations of 2-deamino-preQ$_0$ bound to the enzyme and the initial concentration of free enzyme, respectively. The *black line* is a hyperbolic fit of the data.

preQ$_0$ complex lacked a contribution from entropy ($-T\Delta S$ = +0.07 kJ/mol), and the enthalpy contribution was lowered ($\Delta\Delta H$ = +16.2 kJ/mol) in comparison with NADPH binding to the free enzyme. Note: NADPH binding to the covalent adduct between wild type enzyme and preQ$_0$ does not give a stable complex because catalytic reduction takes place. It was therefore not examined with ITC.

Substrate Binding and Covalent Thioimide Formation—As in *B. subtilis* QueF (11), the substrate binding in ecQueF was traceable by both quenching and blue shifting of the protein's Trp fluorescence (Fig. 4, *A* and *B*). Trp^{57} and Trp^{198} in the substrate-binding pocket (Fig. 5) are the likely reporter groups. On addition of preQ$_0$, the ecQueF fluorescence (excitation, 280 nm) was quenched, and a slight blue shift in the maximum wavelength of emission (λ_{max}, 334 → 330 nm) was observed. The quenching yield increased dependent on the molar ratio of preQ$_0$ and the enzyme homodimer used. It reached a maximum of about 0.7 when this ratio was approximately unity (Fig. 4*A*). The titration of ecQueF with 2-deamino-preQ$_0$ and 6-deoxo-preQ$_0$ also produced fluorescence quenching, but the corresponding yields were lower, 0.21 and 0.36, respectively (Fig. 4*B*), than for preQ$_0$. The 7-formyl-preQ$_0$ behaved differently. Its incubation with ecQueF caused a slight enhancement of the protein fluorescence (~10%), and the λ_{max} was up-shifted (334 → 336 nm), as shown in Fig. 4*B*. Binding of preQ$_0$ to the C190A variant of ecQueF caused only a small amount of fluorescence quenching (~15%).

Formation of the covalent thioimide between ecQueF and preQ$_0$ was detectable by appearance of an absorbance band with maximum absorption at 380 nm (Fig. 4*C*). A molar extinction coefficient of 10.02 ± 0.14 mM^{-1} cm^{-1} was determined. With this, we could show that the preQ$_0$ was linked to each

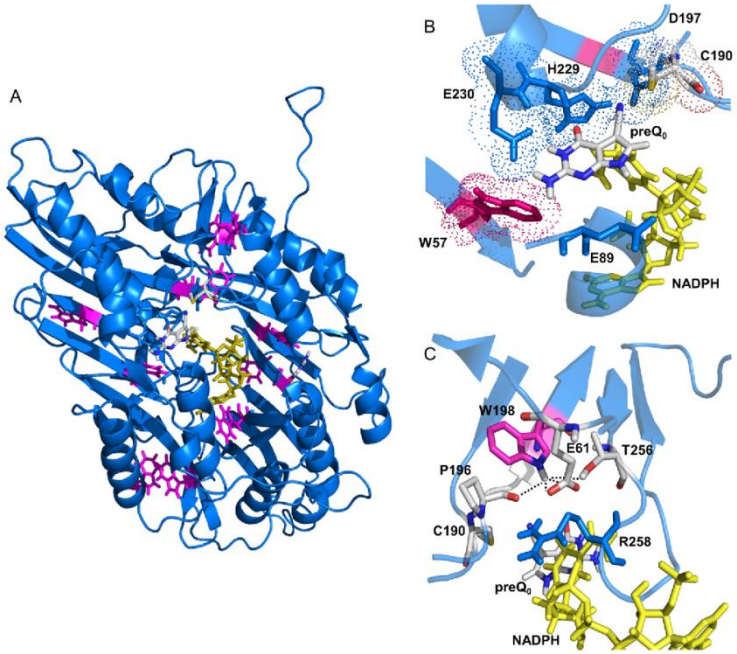

FIGURE 5. **Overall structure model (*A*) of ecQueF with $preQ_0$ and NADPH and close-up view of Trp^{57} (*B*) and Trp^{198} (*C*).** Tryptophan is shown in *magenta*. Other amino acids in the active site and NADPH are shown in *blue* and *yellow*, respectively. Cys^{190}, $preQ_0$, and amino acids having hydrophilic interaction with Trp^{198} are indicated by element-based colors. The model of ecQueF is from Ref. 12.

ecQueF dimer in a 1:1 stoichiometry. Results of protein mass analysis (Fig. 4*D*) were in good agreement with these findings, showing that the sample from incubation of ecQueF with $preQ_0$ was composed of about equal amounts of the monomeric enzyme-$preQ_0$ adduct (43%) and also the monomeric apoenzyme (57%). Reactivity of half-of-the-sites in the ecQueF dimer was thus strongly supported. Time-resolved titration analysis in stopped-flow experiments also revealed that a molar $preQ_0$ concentration equivalent to that of the ecQueF dimer was sufficient for complete covalent conversion of the available active sites (Fig. 6).

Incubation of ecQueF in the presence of 2-deamino-$preQ_0$ also gave rise to a new absorbance band, but compared with the $preQ_0$ thioimide adduct, its maximum absorption was at a lower wavelength of around 340 nm (Fig. 4*C*). A molar extinction coefficient of 10.50 ± 0.04 mM^{-1} cm^{-1} was determined. Contrary to $preQ_0$, a substrate/enzyme molar ratio of about 13 was required so that covalent conversion of ecQueF with 2-deamino-$preQ_0$ was complete (Fig. 4*E*). Protein mass analysis confirmed the presence of the covalent adduct and furthermore revealed that the portion of total ecQueF covalently modified (maximum, ~40–50% of dimer) was strongly dependent on the amount of 2-deamino-$preQ_0$ offered (Fig. 4*D*). A K_d of 155 μM was determined for 2-deamino-$preQ_0$ binding to ecQueF (Fig. 4*F*), in useful accordance with the results of the ITC experiments (Table 1). No evidence of covalent linkage formation between ecQueF and 6-deoxo-$preQ_0$ or ecQueF and 7-formyl-

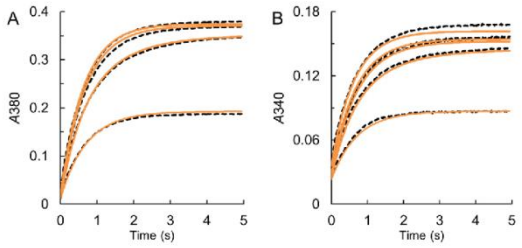

FIGURE 6. **Stopped-flow progress curves of $preQ_0$ binding to ecQueF are shown together with results of model fitting.** Thioimide adduct formation in the absence of NADPH is shown, recording absorbance at 380 nm (*A*) and at 340 nm (*B*). The ecQueF (33 μM) was mixed with $preQ_0$ (*bottom to top*: 17, 32, 45, 60, and 120 μM). *Black dashed lines* show the averaged data in triplicate measurements. *Orange solid lines* are the fit of a two-step binding mechanism, described in Scheme 1 and text, to the data.

$preQ_0$ was found in spectrophotometric titration analysis. Likewise, the C190A variant did not show evidence of covalent binding of $preQ_0$, as expected.

Addition of $preQ_0$ to a pre-incubated mixture of ecQueF with any of the three $preQ_0$ analogues reinstated in each case the effect on fluorescence quenching and "thioimide absorbance band" formation that $preQ_0$ alone had. Therefore, this showed effective competition of $preQ_0$ with the other ligands for binding to ecQueF and also demonstrated the reversibility of thioimide covalent linkage formation by 2-deamino-$preQ_0$ (Fig. 4*C*).

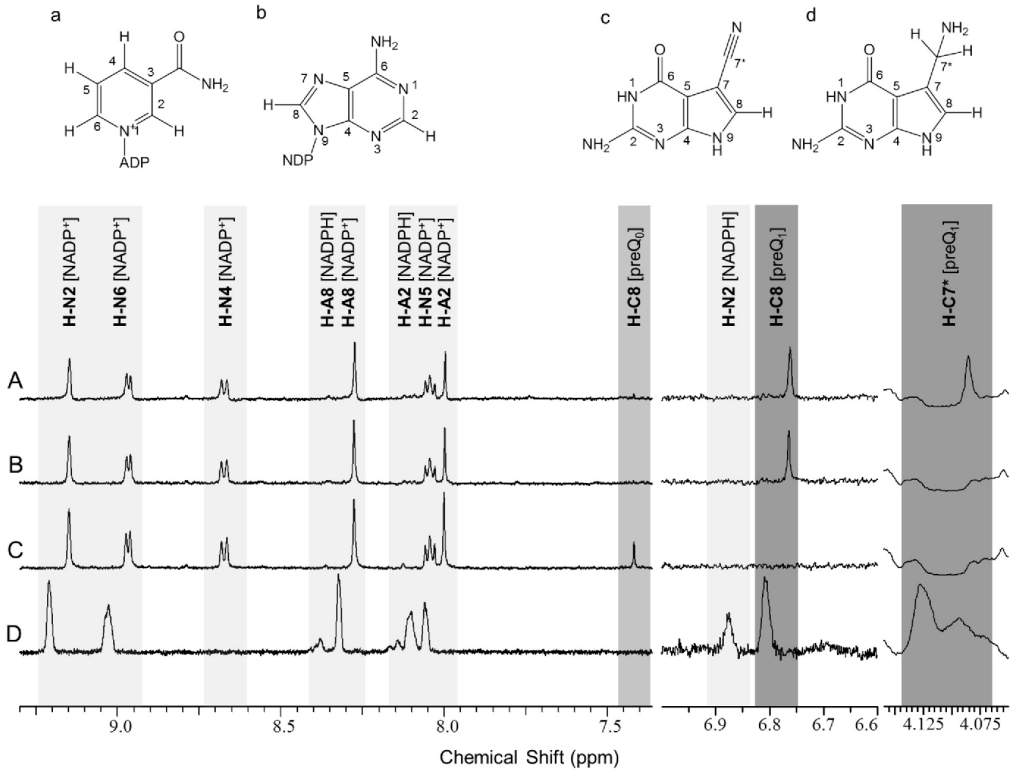

FIGURE 7. **^{1}H NMR analysis is shown of the enzymatic reduction of preQ$_0$ by NADPH (*A*), 4*R*-[^{2}H]NADPH (*B*), or 4*S*-[^{2}H]NADPH (*D*).** *C shows a control comprising NADP$^+$* (475 μM) and preQ$_0$ (238 μM). The chemical structures from which signals were recorded are shown in *a–d*. *A–C*, Tris buffer (25 mM, D_2O, 99.8% D; pD 7.5) containing 50 mM KCl and 1.15 mM tris(2-carboxyethyl)phosphine was used. NADPH or (4*R*)-[^{2}H]NADPH (475 μM) was incubated with ecQueF (29 μM) and preQ$_0$ (238 μM) at 25 °C. The DMSO concentration was 0.5%. When about 90% of the coenzyme had been consumed, the enzyme was filtered off, and the filtrate was analyzed by ^{1}H NMR. *D*, 4*S*-[^{2}H]NADPH solution (1.9 mM, 1.0 ml) was mixed with preQ$_0$ (800 μM) and ecQueF (10 μM). The DMSO concentration was 4%. When 1.6 mM of the NADPH was consumed, enzyme was removed. D_2O (10%, by volume) was added to the solution prior to ^{1}H NMR analysis. Note: all peaks were broadened and shifted by 0.05–0.10 ppm in the spectra of the ecQueF reaction with 4*S*-[^{2}H]NADPH due to the presence of H_2O.

Stereospecificity of ecQueF for Hydrogen Transfer from NADPH—This central characteristic of the QueF mechanism has not been elucidated in previous biochemical and structural studies of the enzyme. We used NADPH, (4*R*)-[^{2}H]NADPH, or (4*S*)-[^{2}H]NADPH for the reduction of preQ$_0$ and analyzed with ^{1}H NMR the products formed, NADP$^+$ and preQ$_1$. Results are shown in Fig. 7. In all reactions, the conversion of preQ$_0$ into preQ$_1$ was traced by monitoring the singlet signal of the deazaguanine C8 hydrogen, which appears at 7.42 ppm in substrate and at 6.76 ppm in product. When NADPH was used, the proton spectra of the product exhibited a singlet peak at 4.08 ppm, which is assigned to the hydrogens of the aminomethyl carbon of preQ$_1$ (Fig. 7*A*). This peak was absent from the spectra of the preQ$_1$ released in the reaction with (4*R*)-[^{2}H]NADPH (Fig. 7*B*). Besides, the product of the oxidation of (4*R*)-[^{2}H]NADPH was NADP$^+$ and not 4-[^{2}H]NADP$^+$. The hydrogen at position C4 on the nicotinamide ring was identified unequivocally from the doublet signal at 8.67–8.68 ppm (Fig. 7*B*). When the alternatively deuterium-labeled (4*S*)-[^{2}H]NADPH was used, only the hydrogen was transferred in the enzymatic reaction of preQ$_0$, and authentic preQ$_1$ was obtained together with 4-[^{2}H]NADP$^+$ (Fig. 7*D*). These results are clear in showing that ecQueF is specific for transferring the 4-pro-*R*-hydrogen from NADPH, and it does so in both hydride reduction steps of the catalytic conversion of preQ$_0$ to preQ$_1$.

Steady-state Kinetic Study of ecQueF—Based on the measurement of both NADPH consumption and amine product formation (Fig. 8), we showed that besides preQ$_0$ the 2-deamino derivative was also a workable substrate of ecQueF (see below). The 6-deoxo-preQ$_0$ was inactive within the detection limits of the assay used. The 7-formyl-preQ$_0$ (100 μM) was not reduced by ecQueF in the presence of NADPH (150 or 300 μM) nor was it oxidized in the presence of NADP$^+$ (300 μM). Absence of activity with this substrate was shown at different pH values in the range 5.5–7.5 (100 mM ammonium acetate buffer, pH 5.5 or pH 6.7; 100 mM Tris buffer, pH 7.5). Considering the poor solubility of 7-formyl-preQ$_0$ in water, we added 7-formyl-preQ$_0$ (dissolved in DMSO) directly to the enzyme solution contain-

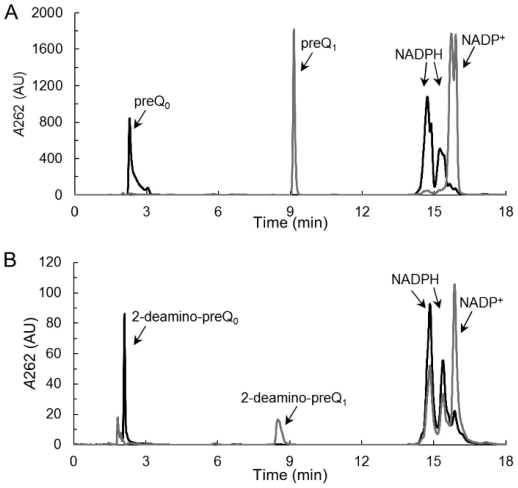

FIGURE 8. **Enzymatic reduction of preQ$_0$ (*A*) or 2-deamino-preQ$_0$ (*B*) by ecQueF was analyzed by HPLC.** *A*, enzyme (21 μM) was mixed with preQ$_0$ (1 mM) and NADPH (3 mM). *B*, enzyme (11 μM) was mixed with 2-deamino-preQ$_0$ (100 μM) and NADPH (300 μM). *Black lines* indicate control sample containing NADPH and nitrile substrate, and *gray lines* indicate the enzymatic reduction. Incubation was at 25 °C for 10–20 min.

TABLE 3
Kinetic constants obtained by using the kinetic model of the ecQueF reaction shown in Scheme 1

		Kinetic constants
K_d	k_2/k_1	$(2.63 \pm 0.01) \times 10^{-6}$ M
	k_3 (k_4)[a]	1.63 ± 0.01 s^{-1} (0.024 s^{-1})[a]
K_1	k_6/k_5	$(20.4 \pm 2.0) \times 10^{-6}$ M
K_2	k_8/k_7	$(3.23 \pm 0.02) \times 10^{-6}$ M
	k_9 (k_{10})[b]	5.9 ± 0.2 s^{-1} (0.56 s^{-1})[b]
	k_{11}	0.234 ± 0.002 s^{-1} (3.3 ± 0.1)[c]
K_3	k_{13}/k_{12}	$\leqq 0.1 \times 10^{-6}$ M
	k_{14}	0.447 ± 0.006 s^{-1} (1.8 ± 0.1)[c]
	k_{cat}	0.150 ± 0.001 s^{-1} (2.8 ± 0.2)[c]
	K_M (NADPH)	$(23.7 \pm 2.0) \times 10^{-6}$ M

[a] k_4 was obtained from the relationship K_d_overall = K_d_kinetic/$(1 + k_3/k_4)$. The K_d_overall is 39 nM. k_4 was not included in the global fitting in COPASI. If it was included, its value was close to zero. Therefore, the k_4 value shown probably gives an upper bound for the dissociation rate constant.
[b] k_{10} was obtained from the relationship $k_3k_5/k_4k_6 = k_7k_9/k_8k_{10}$. Note that k_{10} was not included in the global fitting in COPASI. If it was included, its value was close to zero. The k_{10} value shown probably gives an upper bound for the dissociation rate constant.
[c] KIEs were obtained by comparing rate constants of preQ$_0$ reduction by NADPH, as shown in the table, and 4*R*-[^{2}H]NADPH ($k_{11} = 0.069 \pm 0.001$ s^{-1}, $k_{14} = 0.25 \pm 0.01$ s^{-1}, $k_{cat} = 0.053 \pm 0.001$ s^{-1}).

ing NADPH so that enzymatic reduction could precede substrate precipitation. However, no reaction was observed, despite the use of ecQueF concentrations (7.6–30.0 μM) that would have allowed detection of just 0.1 enzyme turnover. Just to note, oxidation by NADP$^+$ might have involved the 7-formyl group in native or hydrated form, requiring nucleophilic catalysis from active-site cysteine in the former but not the latter (15–18). Enzymatic conversion of 7-formyl-preQ$_0$ was also analyzed in the presence of $(NH_4)_2SO_4$ or NH_4Cl (each at 50 mM), considering that addition of the ammonium ions might facilitate the formation of an incipient imine to be reduced by QueF. However, no reaction was observed under these conditions.

We furthermore examined the reverse reaction of ecQueF, measuring reduction of NADP$^+$ (100 μM), and product formation associated with it, in the presence of preQ$_1$ (40 μM). Using the standard pH of 7.5 but also elevated pH values of up to 9.0 in order to facilitate deprotonation of the 7-amino group, there was no conversion of preQ$_1$ above the detection limit, which was roughly 0.1 turnover of the molar enzyme concentration used (20–80 μM). To prevent the product attached to the enzyme from escaping detection, we denatured the protein with methanol and repeated the HPLC analysis, thereby confirming the absence of an oxidation of preQ$_1$ under the conditions used.

Initial rate analysis showed that the K_M value for NADPH was not affected by variation of the preQ$_0$ concentration in the range 5–100 μM. The lower end limit of the substrate concentration was defined by the time resolution and sensitivity of the spectrophotometric assay. Considering the 39 nM K_d value for preQ$_0$, only a negligible portion of free enzyme could have existed at steady state under these conditions. Therefore, this explains a coenzyme K_M apparently independent of the substrate concentration. Results are summarized in Table 1. In terms of k_{cat}, 2-deamino-preQ$_0$ was an equally good nitrile substrate as was preQ$_0$. The NADPH K_M was, however, elevated about 4-fold in the reaction with 2-deamino-preQ$_0$ (Table 1). A huge difference existed in the substrate K_M, consistent with results of the ITC binding study of preQ$_0$ and 2-deamino-preQ$_0$.

Transient Kinetic Study and Kinetic Simulation—To characterize individual steps of the ecQueF reaction, a transient kinetic analysis in stopped-flow experiments was performed. Fig. 6 shows representative time courses of thioimide formation upon mixing the enzyme with preQ$_0$ in the absence of NADPH. The absorbance increased exponentially with an amplitude determined by the limiting concentration of ecQueF dimer or preQ$_0$. The rate constants k_{obs} (1.35 ± 0.15 s^{-1}) were independent of the initial concentrations of enzyme and preQ$_0$. Using global fitting with COPASI, a two-step binding-reaction model, $E + S \leftrightarrows E{\cdot}S \rightarrow E\text{-}S$, was useful to describe the data recorded at varied enzyme and substrate concentrations (Fig. 6, *A* and *B*). It involved a relatively fast binding of preQ$_0$ with a dissociation constant (K_d_kinetic) of 2.63 ($\pm$0.01) μM that was followed by a slower and, within the limit of accuracy of the method used, effectively irreversible transformation of the non-covalent *E*·S into the covalent complex *E*-S with a rate constant (k_3) of 1.63 ($\pm$ 0.01) s^{-1} (Table 3). The obtained k_3 was in a good agreement with the experimentally determined k_{obs}. The relationship between the overall 39 nM dissociation constant determined by ITC and the kinetically determined parameters, *i.e.* K_d_overall = K_d_kinetic/$(1 + k_3/k_4)$, can be used to calculate an approximate value of 0.024 s^{-1} for the thioimide release rate constant (k_4).

Fig. 9*A* shows absorbance time traces at 340 and 380 nm for a reaction under conditions of a single turnover of the enzyme present. Time traces for reactions under multiple turnover conditions in which a limiting enzyme concentration (5 μM) was used are shown additionally in Fig. 9, *B–D*. The single-turnover time traces were characterized by a fast initial increase in absor-

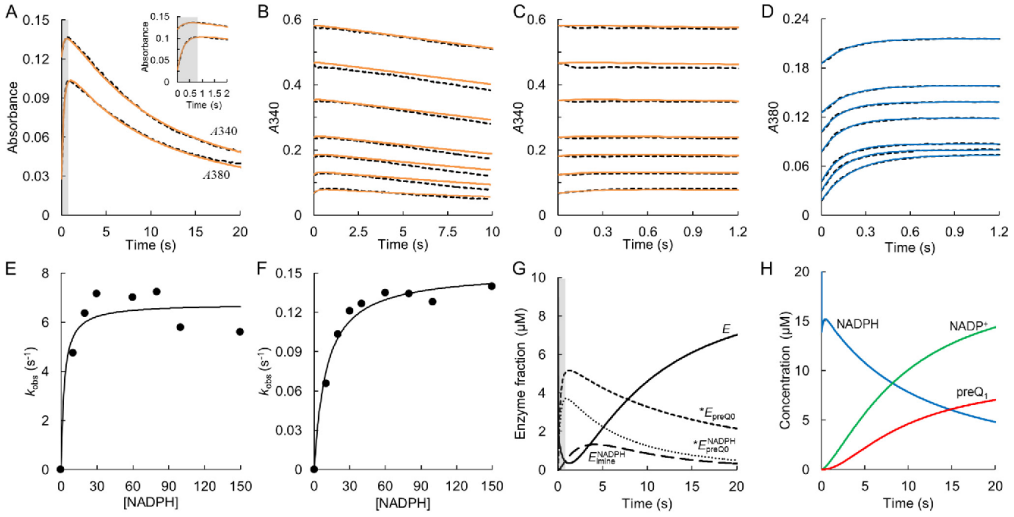

FIGURE 9. **Stopped-flow progress curves of enzymatic reactions under single-turnover and multiple-turnover conditions are shown together with results of kinetic simulation.** *A,* single-turnover reaction of $preQ_0$ reduction is shown. The *gray shaded area* indicates the phase of covalent thioimide formation, and a close-up view of this phase is shown in the *inset* (*top,* 340 nm; *bottom,* 380 nm). The ecQueF (10 μM) was mixed with $preQ_0$ (10 μM) and NADPH (20 μM). *B,* multiple-turnover reaction was recorded at 340 nm. The concentrations of enzyme and $preQ_0$ were constant at 5 and 60 μM, respectively. The NADPH concentration varied (*bottom to top*: 10, 20, 30, 40, 60, 80, and 100 μM). *C* and *D,* close-up views of covalent thioimide formation in multiple-turnover reactions are shown at 340 nm (*C*) and at 380 nm (*D*). *A–D, black dashed lines* show the experimental data. *Orange solid lines* in *A–C* present fit of the data to the kinetic mechanism described in Scheme 1, and *blue solid lines* in *D* indicate single exponential fit of the data. *E* and *F,* dependence of stopped-flow rate constants (k_{obs}) on the NADPH concentration is shown. The *circles* are the data, and the *solid line* is a hyperbolic fit. k_{obs} of formation of the thioimide adduct is shown in *E*. It was obtained from single exponential fits of the data in *D*. k_{obs} of the NADPH consumption is shown in *F*. It was obtained from linear fits on the data in *B* (1–10 s range). *G* and *H,* reaction simulation under single-turnover conditions applying the kinetic parameters from Table 3 is shown. *G,* enzyme forms are represented as in Scheme 1. The time-dependent concentrations of enzyme forms bound to $preQ_0$ (E_{preQ0}), present as imine intermediate (E_{imine}), and bound to NADPH (E^{NADPH}) were negligible and are therefore not shown. The *gray shaded area* in *G* indicates the phase of covalent thioimide formation also shown in *A*. *H,* simulated curves of NADPH consumption and of formation of $NADP^+$ and $preQ_1$ are shown. The disappearance of free $preQ_0$ was too fast to be represented here (≤1 s).

bance, at 380 nm in particular, which reflected formation of the covalent intermediate (Fig. 9*A*). The subsequent decrease in absorbance was due to NADPH consumption mainly but also included the effect of the concomitant decay of the intermediate, especially when single-turnover conditions were used. Fitting the initial increase in absorbance with an exponential function (Fig. 9*D*), the corresponding k_{obs} showed a hyperbolic dependence on the NADPH concentration, with a K_d of 3.0 (± 1.6) μM and a maximum value of 7.32 (± 0.46) s^{-1} (Fig. 9*E*). The presence of NADPH therefore resulted in a 4.5-fold speeding up of the formation of the thioimide intermediate. The decrease in absorbance at both 340 and 380 nm was best fit with a single exponential (single-turnover reactions) or a straight line (multiple-turnover reactions). The rate constants calculated from these fits were hyperbolically dependent on the NADPH concentration, with a K_d of 10 (± 2) μM and a maximum value of 0.15 (± 0.01) s^{-1}, which is similar to the k_{cat} (Fig. 9*F*).

The kinetic model in Scheme 1 was used to fit the data from all experiments, comprising a large set of averaged stopped-flow time traces from 28 independent reaction conditions, involving variation in NADPH concentration between 10 and 150 μM. Fig. 9, *A–C*, compares the experimental progress curves to the corresponding fitting results, which reveals useful agreement between the two. Table 3 summarizes the rate and binding constants thus determined. The kinetic steps of thioimide and imine reduction were the slowest in the enzymatic pathway, and their corresponding rate constants were similar. Note that based on a decrease in NADPH absorbance (at 340 nm) alone, it would not have been possible to distinguish the two steps. However, because the thioimide reduction also involves concomitant decrease in absorbance at 380 nm, the first hydride transfer step has a spectral signature different from the second. This could be used to determine the rate constant associated with each step. The rate constants of the microscopic reaction steps (Table 3) were consistent with the k_{cat} measured at steady state (Table 1) and also with the rate constants from stopped-flow experiments. Fig. 9*G* shows the distribution of different enzyme forms in a single-turnover stopped-flow reaction. The enzyme complexes with $preQ_0$ prevail during the reaction. Because of the comparably weak binding of NADPH to the covalent enzyme-$preQ_0$ complex, NADPH that was initially bound to enzyme prior to formation of the covalent adduct was partly released from the enzyme once the thioimide intermediate had been formed. This can be seen in the very early phase of the reaction shown in Fig. 9*H*.

Three features of the kinetic model in Scheme 1 should be emphasized. First, there are three binding steps for NADPH (K_1 to K_3). Simpler models, in which NADPH binding for thioimide reduction occurred only to the covalent enzyme-$preQ_0$ adduct or NADPH binding occurred to the non-covalent ternary com-

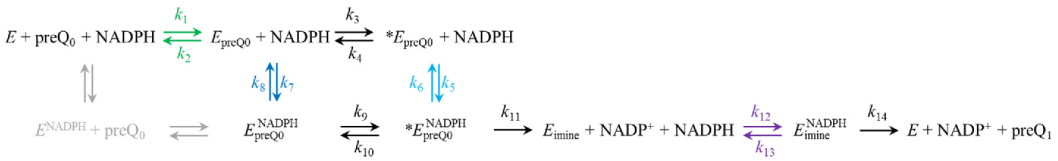

SCHEME 1. **Proposed kinetic mechanism of preQ$_0$ reduction by ecQueF is shown.** *E* is the free ecQueF, and the enzyme-bound preQ$_0$ and NADPH are indicated by *subscript* and *superscript*, respectively. An *asterisk* on *E* indicates the covalent thioimide linkage between preQ$_0$ and enzyme. E_{imine} indicates enzyme with bound imine intermediate. The steps included in kinetic simulations are indicated in *black*. NADPH binding to *E* was excluded from the kinetic simulation and is indicated in *light gray*. The kinetic constants from simulation and fitting of reaction time courses are shown in Table 3. The following rate constants were obtained only as ratios to give the corresponding dissociation constants in rapid equilibrium: $K_d = k_2/k_1$ (*green*); $K_1 = k_6/k_5$ (*light blue*); $K_2 = k_8/k_7$ (*blue*); and $K_3 = k_{13}/k_{12}$ (*purple*). The chemical and isotope-sensitive steps are thioimide reduction (k_{11}) and imine reduction (k_{14}). These steps were assumed to be effectively irreversible under the reaction conditions used. Likewise, formation of the thioimide intermediate (k_3 and k_9) was assumed to be irreversible in the fitting because the rate constants of the reverse reaction (k_4 and k_{10}) are very small in comparison.

plex and NADPH dissociation from the covalent adduct was not allowed, failed to describe the experimental time courses properly. Second, the extremely small dissociation constant for NADPH binding to the hemithioaminal/imine intermediate is worth noting. It suggests that NADPH was bound almost irreversibly by ecQueF at this step. Unless having this small value of K_3, the dependence of the reaction on the NADPH concentration could not be properly explained. Third, the covalent ternary complex showed a much lower absorbance both at 340 nm (~54%) and 380 nm (~60%) than expected from the sum of the corresponding individual absorbances of NADPH and thioimide adduct. Note that the absorbance of NADPH was not affected by binding to ecQueF. The result is interesting as it suggests that the thioimide adduct and NADPH perturb each other electronically in the ternary complex. More interestingly, even the extent of this electronic perturbation was attenuated strongly when the ternary complex was formed from (4*R*)-[^{2}H]NADPH instead of NADPH. The electronic effect and its dependence on the isotopic substitution in NADPH might be explained by a "near-attack" ground-state conformer that involves close alignment, and perhaps even partial bonding, between the thioimide carbon and the C4 nicotinamide hydrogen of NADPH. Electronic preorganization of the ternary complex for efficient hydride reduction is therefore suggested.

KIE Study—Substitution of the reactive 4-pro-*R*-hydrogen of NADPH by deuterium caused a slowdown of the enzymatic preQ$_0$ reduction. The effect was expressed in a substantial primary KIE on both the maximum rate ($^DV_{max} = 2.40 \pm 0.12$) and the catalytic efficiency for coenzyme ($^DV_{max}/K_M = 2.68 \pm 0.41$).

Stopped-flow progress curves of preQ$_0$ reduction by (4*R*)-[^{2}H]NADPH under multiple-turnover reaction conditions are shown in Fig. 10. The corresponding single-turnover reactions are also presented there. Exponential fit of the initial absorbance increase revealed that the deuteration of NADPH did not cause slowdown of the formation of the thioimide intermediate ($k_{obs} = 6.4 \pm 0.3\ s^{-1}$), as expected. The dependence of k_{obs} on the NADPH concentration was also unaffected ($K_d = 3.0 \pm 1.5$ μM), as shown in Fig. 10, *D* and *E*. Rate constants determined from fits of the absorbance decrease in individual stopped-flow traces are shown on Fig. 10*F*. From the hyperbolic dependence of k_{obs} on the NADPH concentration, a maximum rate constant of 0.055 (± 0.003) s^{-1} was obtained, and the corresponding K_d was 14 (± 3) μM. Therefore, the deuteration of NADPH affected strongly the enzymatic rate, although the apparent binding was hardly influenced.

Results of a global fit of Scheme 1 to the data are shown in the figures, and the reaction constants determined are summarized in Table 3. Deuteration of the coenzyme caused slowdown of both reduction steps, but the effect was by far more pronounced on the thioimide conversion. The corresponding KIEs were determined as 3.3 ± 0.1 (thioimide reduction) and 1.8 ± 0.1 (imine reduction). The value of $^DV_{max}$ can be explained from these two KIEs (Table 3).

Discussion

Groups of preQ$_0$ Required for Binding Recognition and Covalent Adduct Formation by ecQueF—Structural and sequence-based comparisons reveal the bimodular QueFs (from *V. cholerae* and *E. coli*) to exhibit substrate binding pockets highly similar to that of their unimodular counterpart (from *B. subtilis*) for which a preQ$_0$ complex structure has been determined (10–12). Evidence characterizing the substrate binding in ecQueF is therefore interpreted on the basis of a high degree of functional residue conservation in these enzymes. Comparing the changes in protein fluorescence, the heat released, and the amount of covalent thioimide adduct formed in titrations of ecQueF with preQ$_0$ (or analogues thereof), the overall substrate binding is found to be composed of three main elements. The initial accommodation of the substrate in the binding pocket lacks a spectroscopic signature in absorbance and fluorescence, but by analyzing the binding of the non-reactive substrate analogue 7-formyl-preQ$_0$, it becomes traceable with ITC. Results show that this first step in the binding is driven exclusively by loss in entropy, which probably reflects the desolvation of the substrate, the binding site in ecQueF, or both. The complete lack of an enthalpic contribution to the binding of 7-formyl-preQ$_0$ (Table 1) suggests that specific interactions are not developed between this ligand and the enzyme. The second step involves a protein conformational rearrangement, detectable mainly by ITC but also by fluorescence, which, in analogy to the induced-fit binding of preQ$_0$ in the *B. subtilis* enzyme (11), is assumed to preorganize and close up the ecQueF active site. Trp^{198} of ecQueF (like the corresponding Trp^{119} of *B. subtilis* QueF) would thus be placed in a more hydrophobic microenvironment, with consequent effects on their fluorescence properties. The preQ$_0$ complex structure of the C55A variant of *B. subtilis* QueF adopts the "closed" conformation just as the

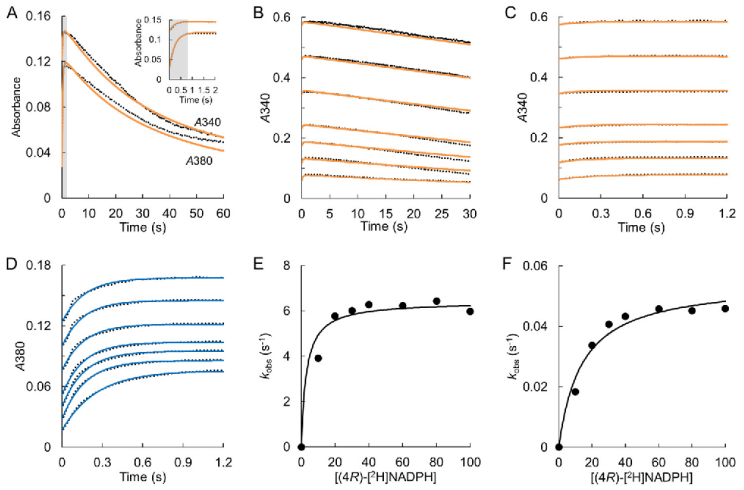

FIGURE 10. **Stopped-flow progress curves of enzymatic reactions under single-turnover and multiple-turnover conditions with 4*R*-[^{2}H]NADPH are shown together with results of kinetic simulation.** *A–D, black dotted lines* are the experimental data averaged from triplicate measurements. *Orange solid lines* in *A–C* present the fit of the data to the two-step binding mechanism described in Scheme 1. The *blue solid lines* in *D* indicate single exponential fits of the data. *A,* single-turnover reaction of preQ$_0$ reduction is shown, recording absorbance. The *gray shaded area* in *A* indicates the phase of covalent thioimide formation, and a close-up view of this phase is shown in the *inset* (*top,* 340 nm; *bottom,* 380 nm). The ecQueF (10 μM) was mixed with preQ$_0$ (10 μM) and (4*R*)-[^{2}H]NADPH (20 μM). *B,* multiple-turnover reaction was recorded at 340 nm. The concentrations of enzyme and preQ$_0$ were constant at 5 and 15 μM, respectively. (4*R*)-[^{2}H]NADPH concentration varied (*bottom to top*: 10, 20, 30, 40, 60, 80, and 100 μM). *C* and *D,* a close-up view (*C,* at 340 nm; *D,* at 380 nm) of covalent thioimide formation in multiple-turnover reaction is shown. *E* and *F,* dependence of k_{obs} on the NADPH concentration is shown. The *circles* are the data, and the *solid line* is a hyperbolic fit. The k_{obs} of thioimide formation (*E*) was obtained from the best fits shown in *D*, and the k_{obs} of NADPH consumption (*F*) was obtained from the linear fits on the data (1–20 s range) shown in *B*.

wild type enzyme does (11), indicating that thioimide formation is not essential for the induced fit. Evidence from the current study adds to the picture, showing that the cyano group of preQ$_0$ is crucial in substrate-binding recognition, for its substitution by a formyl group disrupts entirely the ligand-induced fit in the enzyme. The finding appears relevant biologically in that it suggests a mechanism by which QueF discriminates between its substrate and other metabolites of the queuosine biosynthetic pathway that differ from preQ$_0$ only in the chemical group at position 7 of the deazaguanine core.

The overall ΔG of preQ$_0$ binding to the catalytic Cys variant (C190A) of ecQueF includes a substantial contribution from enthalpy ($\Delta H = -44.7$ kJ/mol; Table 1), which favors binding. Unlike the basal contribution from "desolvation" entropy registered for the binding of 7-formyl-preQ$_0$, the contribution from entropy for preQ$_0$ binding to the C190A variant is nonfavorable ($-T\Delta S > 0$; Table 1) in this case. The favorable ΔH term probably arises from specific non-covalent interactions between the C190A variant and preQ$_0$ (*cf.* Fig. 5), formed as a result of the induced-fit conformational change, which, in turn, according to our interpretation also explains the non-favorable $-T\Delta S$ term in terms of a more compact macromolecular structure. We also note the good agreement between the dissociation constants for non-covalent preQ$_0$ complexes of the wild type enzyme (K_d_kinetic; Table 3) and the C190A variant (Table 1). Most likely in virtue of their effect on substrate positioning, to align precisely the cyano group of the preQ$_0$ with the thiol group of Cys^{190}, these non-covalent interactions are key to promote the covalent thioimide adduct, as shown by the relative inefficacy in that regard of preQ$_0$ analogues lacking the 2-amino or the 6-oxo group. The overall thermodynamic signature of preQ$_0$ binding to ecQueF is strongly shaped by the energetics of covalent bond formation, which almost completely masks the effects of the non-covalent interactions.

On binding of preQ$_0$ at pH 7.5, each ecQueF dimer was shown by ITC to take up 0.78 ± 0.09 protons from the bulk solvent. Preliminary evidence from time-resolved experiments performed in the stopped-flow apparatus and measuring proton uptake with a pH indicator further reveals that the proton uptake occurred concurrently with formation of the thioimide intermediate. A proton is required during conversion of the nitrile to the thioimide group. In the case that the observable proton uptake by ecQueF was an immediate consequence of this reaction, binding of preQ$_0$ by an enzyme variant that is incapable of thioimide adduct formation would accordingly not involve proton uptake. Clear evidence of proton uptake also by the C190A variant therefore eliminated this mechanistic possibility. An alternative mode of protonation, occurring in consequence of the induced-fit protein conformational change in preQ$_0$ binding, is therefore suggested. Identification of the groups involved in the protonation requires further study.

Kinetic Pathway of ecQueF Involves Thioimide Reduction as the Rate-limiting Step—Because preQ$_0$ and NADPH both bind to free ecQueF, the kinetic mechanism appears to be random in principle. However, in the global simulation-fitting analysis with COPASI, binding of NADPH to the free enzyme appeared to be not kinetically significant, at least under the conditions used. In addition, although preQ$_0$ forms a catalytically compe-

tent thioimide adduct with ecQueF even in the absence of NADPH, the preferred reaction path when neither $preQ_0$ nor NADPH is limiting appears to be through the non-covalent ternary complex (Scheme 1). Formation of the thioimide adduct is accelerated about 3.6-fold when NADPH is present, and it is relatively slow compared with the actual substrate binding steps (Table 3). The $preQ_0$ substrate binds in a stoichiometry of 1 per ecQueF dimer. The possibility of half-of-the-sites reactivity was also hinted at by the structure of *V. cholerae* QueF (10), suggesting that only a single NADPH would be bound in two possible orientations to load one of the two active sites. Based on the structural model of ecQueF, Wilding *et al.* (12) arrived at the same conclusion, suggesting however that only one of two catalytic centers in the protein dimer was accessible, whereas the other was buried deeply inside the protein. Evidence from the study of the inactive C190A variant of ecQueF showed that 1 NADPH was bound to each non-covalent complex between enzyme dimer and $preQ_0$.

According to Scheme 1, the observable kinetic parameters from initial rate measurements are related to rate constants as shown in Equations 1 and 2 (19).

$$E/V_{max} = 1/k_9 + 1/k_{11} + 1/k_{14} \quad \text{(Eq. 1)}$$

$$K_M\,(\text{NADPH}) = K_1' + K_2' + K_3' = (k_6 + k_{11})/k_5 + (k_8 + k_9)/k_7 + (k_{13} + k_{14})/k_{12} \quad \text{(Eq. 2)}$$

Because of the slow breakage of the covalent thioimide linkage (Table 3), the $preQ_0$ K_M value tends to be far too low to be experimentally measurable. The results in Table 3 show that V_{max} was limited, to a similar degree, by the rate constants of thioimide and imine reduction. Rate limitation solely by imine reduction, as suggested by Ribeiro *et al.* (14) from their computational study of the reaction of *V. cholerae* QueF, was ruled out for ecQueF based on the kinetic evidence. The stopped-flow progress curves were not consistent with a kinetic mechanism in which the first hydride transfer was faster than the second. The K_M(NADPH) mainly reflects the binding of NADPH to the covalent adduct of ecQueF and $preQ_0$ (K_1). A reaction pathway in which the enzyme "loosens its grip" on NADPH while moving from the non-covalent to the covalent complex with the $preQ_0$ substrate requires comment; however, we believe there might be biological significance to it. Under the premise of ecQueF being present intracellularly in a molar concentration comparable with that of $preQ_0$, thioimide adduct formation from an enzyme-$preQ_0$-NADPH complex, in which the NADPH is bound tightly (K_2), might serve to ensure that the available $preQ_0$ is trapped fast and completely in a covalently enzyme-bound form. Availability of NADPH in relation to K_1 would determine the portion of total enzyme adduct able to undergo conversion into $preQ_1$. The remaining portion, despite being unreactive in the absence of bound NADPH, might still be useful, for it could temporarily "store" part of the $preQ_0$ until reduction occurs. Because flux through the "normal" reaction pathway (k_{cat} = 0.15 s^{-1}, Table 3) exceeds the "off-pathway" thioimide cleavage, loss of adduct to dissociation could thus be prevented effectively. The very small K_3 for the binding of NADPH for imine reduction would help to ensure that any $preQ_0$ that enters the reduction pathway is taken completely to the $preQ_1$ product. Considering that the $preQ_0$-derived imine might immediately hydrolyze to the corresponding aldehyde on being exposed to water, an important task of the enzyme should be to avoid any partial reduction of the nitrile substrate.

Evidence that in each step of the NADPH-dependent reduction by ecQueF the hydride transfer took place by 4-pro-*R* stereoselectivity provided the basis for employing primary deuterium KIEs as selective probes of the enzymatic reaction. There are two isotope-sensitive steps in the enzymatic mechanism (Scheme 1). Results of stopped-flow kinetic analysis suggested a much larger KIE on the thioimide reduction than on imine reduction. The directly measured KIE on V_{max} is explicable as the combined result of the two individual KIEs. According to Scheme 1, the V_{max}/K_M for NADPH includes in principle all steps from the binding of NADPH up to the product release after the imine reduction. However, because K_3 is much smaller than K_1, the actual V_{max}/K_M value for ecQueF reflects the thioimide reduction, and also the KIE is therefore primarily from this step. Note that the V_{max}/K_M value determined at a saturating $preQ_0$ concentration implies reaction via binding of NADPH to the covalent thioimide adduct. The ${}^{D}V_{max}/K_M$ contained a relatively high standard error, but its value of 2.68 (± 0.41) appears largely consistent with the calculated KIE of 3.3 on the thioimide reduction step.

An interesting feature of the $preQ_0$ conversion by ecQueF was that a reverse reaction of $preQ_1$ and $NADP^+$ was not experimentally detectable, despite the use of a broad range of pH conditions to evaluate the reactivity of $preQ_1$ protonated and unprotonated. Note: the pK_a value of the 7-amino group of $preQ_1$ was estimated to be around 8.6. One possibility is that the oxidation of $preQ_1$ was disfavored thermodynamically to an extent that prevented products (*e.g.* NADPH) to accumulate above the detection limit; another possibility is that incorrect protonation of $preQ_1$, enzyme, or both caused the reaction rate to decrease below a level appreciable with the assays used.

The complete lack of activity of ecQueF toward reducing 7-formyl-$preQ_0$ was explicable from the evidence of binding studies that this compound did not elicit a proper substrate-binding recognition in the enzyme. Exclusion already at the level of binding therefore superseded the possible use of 7-formyl-$preQ_0$ as a probe of the imine reduction step in the enzymatic mechanism.

In conclusion, the multistep catalytic reaction pathway of ecQueF was characterized using kinetic analysis and probing with substrate analogues. The key role of the nitrile group for substrate binding recognition was elucidated, and an energetic fingerprint for the different steps of substrate binding was obtained. Hydride reduction of the covalent thioimide intermediate is shown to be the slowest reaction step overall. NADPH binds extremely tightly to the hemithioaminal/imine intermediate compared with its binding to the thioimide intermediate. Therefore, this property of ecQueF may be relevant physiologically, as it ensures that nitrile reduction is always taken completely to the amine when escape of the imine is prevented effectively.

Experimental Procedures

Chemicals—NADPH (purity >98%) and $NADP^+$ (purity >97%) were from Carl Roth (Karlsruhe, Germany). 2-Propanol-d_8 (99.5 atom % D) and alcohol dehydrogenase from *Thermoanaerobium brockii* were from Sigma. Materials were of the highest purity available from Carl Roth and Sigma. The $preQ_0$ and its analogues, 7-cyano-2-deamino-7-deazaguanine (2-deamino-$preQ_0$) and 7-cyano-6-deoxo-7-deazaguanine (6-deoxo-$preQ_0$), were synthesized as described previously (20).

Synthesis of 7-Formyl-7-deazaguanine (7-Formyl-preQ$_0$)—A new synthesis of 7-formyl-$preQ_0$ (systematic name, 2-amino-5-formylpyrrolo[2,3-*d*]pyrimidin-4-one) that, contrary to literature-known procedures (21–23), does not require protecting group chemistry was developed. $PreQ_0$ (808 mg, 4.61 mmol) and sodium hypophosphite dihydrate (1.44 g, 13.6 mmol) were dissolved in the solvent mixture (15 ml of pyridine/acetic acid/deionized water in a ratio of 2:1:1) and stirred under inert atmosphere. Raney nickel catalyst (slurry in water, ~500 mg) was added to the stirred reaction mixture. Safety precaution: dry Raney nickel is pyrophoric and should always be handled under inert atmosphere. The resulting reaction mixture was heated to 50 °C for 5 h. Subsequently, the reaction mixture was cooled to room temperature and filtered over a pad of celite. The filtrate was reduced *in vacuo*. The remaining brown residue was dissolved in 6 M aqueous potassium hydroxide solution. The remaining solids were filtered off. The filtrate was cooled to 0 °C and neutralized by addition of concentrated aqueous HCl. The product precipitated from the solution and was isolated by filtration and washed with copious amounts of ice water and acetone (brown solid, 770 mg, 94%). ^{1}H NMR (DMSO-d_6) δ 6.35 (bs, 2H, NH_2), 7.49 (s, 1H, H-8), 10.04 (s, 1H, CHO), 10.72 (bs, 1H, H-9), 11.96 (bs, 1H, H-1); ^{13}C NMR (DMSO-d_6) δ 98.36 (C-7), 120.34 (C-8), 124.50 (C-5), 153.40 (C-2), 153.83 (C-4), 159.02 (C-6), 185.47 (CHO). NMR data were recorded on a Bruker AVANCE III with autosampler (^{1}H NMR 300.36 MHz, ^{13}C NMR 75.53 MHz).

Enzyme Preparation—Wild type ecQueF and its C190A variant were obtained as N-terminally His-tagged proteins using expression in *E. coli* BL21-DE3 (12). Cells induced with isopropyl β-D-1-thiogalactopyranoside (1 mM; 25 °C, 20 h) were suspended in storage buffer (100 mM Tris, 50 mM KCl, 1 mM tris (2-carboxyethyl)phosphine, and 1% glycerol, pH 7.5) and sonicated. The enzymes were purified from cell extract on a HisTrap™ FF column (GE Healthcare, Buckinghamshire, UK) using a linear gradient of imidazole (10–500 mM) in 50 mM Tris buffer (pH 7.4, 100 mM NaCl, 1 mM DDT, 3 mM EDTA). Fractions containing the enzyme were gel-filtered on a HiPrep™ 26/10 column or PD-10 desalting columns (GE Healthcare) equilibrated with storage buffer. The purified enzyme was concentrated with Amicon Ultra-15 centrifugal filters (Merck Millipore) to about 75–80 mg/ml. The protein concentration was measured with a Pierce BCA protein assay kit (Thermo Fisher Scientific, Germering, Germany). Protein stock solutions were stored at −20 °C and used up within 3 weeks due to enzyme stability.

ITC—A VP-ITC micro-calorimeter from Microcal (Malvern Instruments Ltd., Malvern, UK) was used at 25 °C. The enzyme was gel-filtered twice to sodium phosphate buffer (100 mM NaH_2PO_4·Na_2HPO_4, pH 7.5, 50 mM KCl) using illustra NAP 5 columns (GE Healthcare). Each experiment consisted of an initial 2 μl injection of ligand solution into enzyme solution, followed by 25–29 injections of 6–10 μl of this solution, leaving 300–330 s between each injection. To avoid heat changes due to the DMSO added from the ligand solution, DMSO was also added to the enzyme solution (≤2.5%, v/v). Data were normalized and evaluated using ORIGIN with a single binding site model as described previously (24). The enzyme molar concentration was based on the protein concentration assuming a functional ecQueF homodimer with a molecular mass of 71,772 Da (wild type enzyme) or 71,708 Da (C190A variant). Note that 3-deoxo-$preQ_0$ was not used for ITC measurement because of its prohibitively low water solubility.

ITC measurements were also performed in HEPES and Tris buffer, each 100 mM, at pH 7.5 and 25 °C. The buffers additionally contained 50 mM KCl. Data were acquired and processed as described above. It was shown previously that a comparison of the binding enthalpies (Δ*H*) in HEPES and Tris is applicable to determine the proton uptake or release in conjunction with ligand binding (25, 26). Equation 3 was used, where n_{H+} is the number of protons involved in the binding, and ΔH_{ion} is the ionization enthalpy of the buffer.

$$n_{H+} = (\Delta H_{buffer\ 1} - \Delta H_{buffer\ 2})/(\Delta H_{ion,\ buffer\ 1} - \Delta H_{ion,\ buffer\ 2}) \quad \text{(Eq. 3)}$$

The ΔH_{ion} of phosphate, HEPES, and Tris at pH 7.5 and 25 °C was obtained from the literature as 3.60, 20.40, and 47.45 kJ/mol, respectively (27). The number of protons calculated from three independent sets of experiments was averaged.

The $preQ_0$-C190A complex was prepared by mixing enzyme (105 μM) with $preQ_0$ (548 μM) and incubating for 40 min at 25 °C. The solution of the enzyme complex was then used for titration into the NADPH solution. Using the 5.5 μM K_d from Table 1, the final concentration of $preQ_0$-C190A complex was calculated as 104 μM.

Spectrofluorometric and Spectrophotometric Analysis of Substrate Binding in ecQueF—Quenching of the intrinsic Trp fluorescence was shown for *B. subtilis* QueF to serve as reporter of the formation of the non-covalent complex between enzyme and $preQ_0$ (11). Fluorescence titrations to study with ecQueF in the binding of $preQ_0$ and analogues thereof were performed using a fluorescence spectrophotometer F-4500 (Hitachi, Ltd., Tokyo, Japan). Emission spectra were recorded in the range 300–500 nm at 1200 nm/min with the excitation wavelength at 280 nm. The quenching yield was determined as the ratio $(F_0 - F_s)/F_0$, where F_0 and F_s are the protein fluorescence intensities in the absence and presence of substrate recorded at the same wavelength of emission.

Formation of the thioimide intermediate is traceable in *B. subtilis* QueF by the appearance of a new absorbance band at 370 nm (11, 13). Using ecQueF, we therefore analyzed substrate binding also by absorbance measurements. A Beckman DU 800 spectrophotometer (Beckman Coulter, Inc.) was used. Before and after each addition, a wavelength scan in the range 300–800 nm was performed. The total volume change due to multi-

ple substrate additions was less than 5%, and the final DMSO concentration in the enzyme solution did not exceed 2%. The substrate concentration range used was dependent on the binding affinity (see under "Results"). In both fluorescent and spectrophotometric measurements, Tris buffer (100 mM, pH 7.5) containing 50 mM KCl and 1.15 mM tris(2-carboxyethyl)phosphine) was used. The fluorescence and spectrophotometric data were averaged in triplicate measurements. It was confirmed that the unbound ligands, in the concentrations used, did not interfere with the fluorescence measurements. Also, all ligands had negligible absorbance in the wavelength range of the experiment.

Protein Mass Analysis—The ecQueF solution (130 μM, 0.6 ml) containing preQ$_0$ (130 μM) or 2-deamino-preQ$_0$ (0.13, 0.52, and 2.6 mM) was incubated at room temperature in 1 h and then it was desalted using Amicon Ultra 0.5 ml Centrifugal filters (Merck Millipore). A final protein concentration of 30 pmol/μl was obtained in water containing 5% acetonitrile and 0.1% trifluoroacetic acid. The samples with preQ$_0$ were separated on a capillary HPLC system (1200 Agilent, Santa Clara, CA) equipped with a PepSwift RP monolithic column (500 μm × 50 mm, Thermo Fisher Scientific) at a flow rate of 20 μl/min using a gradient prepared from solvent A (0.05% trifluoroacetic acid in water) and solvent B (0.05% trifluoroacetic acid in acetonitrile), 0–5 min 10% B, 5–55 min 10–100% B, 55–56 min 100–10% B, and 56–71 min 10% B. The injection volume was 5 μl. The column temperature was 60 °C. Mass analysis was performed in a Thermo LTQ-FT mass spectrometer (Thermo Fisher Scientific) operated with an ESI source in positive mode with mass range of 300–2000 *m/z*. The protein mass spectra were deconvoluted (Protein Deconvolution 2.0 software, Thermo Fisher Scientific), using the Xtract algorithm. Enzyme samples incubated with 2-deamino-preQ$_0$ were not detectable on a Thermo LTQ-FT mass spectrometer. These samples were therefore separated on a capillary HPLC system (Dionex Ultimate 3000, Thermo Fisher Scientific) with the protocol described above. The flow rate was 15 μl/min. Solvent A was 0.3% trifluoroacetic acid in water, and solvent B was 0.3% trifluoroacetic acid in acetonitrile. The sample was analyzed in maXis II electron transfer dissociation mass spectrometer (Bruker, Bremen, Germany) operated with the captive spray source in positive mode with a mass range of 250–3000 *m/z*. The obtained protein mass spectra were deconvoluted by data analysis software, using the MaxEnt2 algorithm.

^{1}H NMR Measurement of the Stereochemical Course of Hydrogen Transfer from NADPH—NADPH and (4*R*)-[^{2}H]-NADPH were prepared by using *T. brockii* alcohol dehydrogenase to reduce NADP$^+$ (2.9 mM) from 2-propanol and 2-propanol-d_8 (each 80 mM), respectively (28). Tris buffer (25 mM, pD 9.0; pD = pH meter reading + 0.4) in D_2O (99.8% D) was used. The reaction was stopped after 30 min when about 2 mM NADP$^+$ had been reduced. Enzyme was filtered off (Amicon Ultra-15 centrifugal filter), and 2-propanol and acetone were evaporated at 40 °C and about 20 mbars (Laborota 4000 efficient, Heidolph, Schwabach, Germany). Enzyme and 2-propanol were added fresh to the mixture to reduce all of the remaining NADP$^+$. The NADPH was recovered as described. (4*S*)-[^{2}H]NADPH was obtained via reduction of NADP$^+$ (3 mM) by 1-[^{2}H]-D-glucose (3 mM) and catalyzed by glucose dehydrogenase from *Bacillus megaterium* (0.017 mg/ml) (29) in 25 mM Tris buffer, pH 8.5, containing 125 mM KCl. The pH was controlled at pH 8.5 during the reaction (30 °C, 600 rpm in a Thermomixer Comfort, Eppendorf, Hamburg, Germany). The deuterium content of (4*R*)-[^{2}H]NADPH and (4*S*)-[^{2}H]NADPH thus obtained was determined by ^{1}H NMR and LC-MS to be 98% or greater. The coenzyme preparations were used for reduction of preQ$_0$ with ecQueF. Enzyme was removed by precipitation with methanol (10%, by volume) and the sample analyzed with ^{1}H NMR spectroscopy (Fig. 7).

Spectra were recorded at 499.98 MHz and 30 °C using a Varian INOVA 500 MHz spectrometer (Agilent Technologies). VNMRJ 2.2D software was used to process the spectra. The spectra of coenzymes, preQ$_0$ and preQ$_1$, were compared with the literature-known spectra of these compounds (20, 30, 31). Considering the possibility of deuterium labeling at the C4 of NADP$^+$, reported in the literature to occur in reactions of the *T. brockii* alcohol dehydrogenase under the conditions used here (32, 33), we checked carefully with LC-MS the (4*R*)-[^{2}H]NADPH preparation used. Relevant masses for doubly deuterated forms of NADPH (1H$^+$, 746; 2H$^+$, 373; and K$^+$, 784) were not detected.

Kinetic Studies at Steady State—Experiments were performed in 100 mM Tris-HCl buffer, pH 7.5, containing 50 mM KCl and 1.15 mM tris(2-carboxyethyl)phosphine. BSA (0.2 g/liter) was added to stabilize ecQueF (0.5 μM). DMSO (1–2%, by volume) was used to increase substrate solubility in all reactions. The assay volume was 0.5 ml, and reactions were started by adding enzyme (10 μl) to the substrate (490 μl). Initial rates were determined from the NADPH consumed in the enzymatic reaction at 25 °C, by absorbance at 340 nm (ϵ_{NADPH} = 6.22 mM^{-1} cm^{-1}). It was confirmed by HPLC that the nitrile substrate was converted into the amine product (Fig. 8). Using cuvettes with a 1 cm light path in the Beckman DU 800 spectrophotometer, the lowest substrate or NADPH concentration usable in the assay was about 2 μM. The averaged initial rates from triplicate determinations were used. Kinetic parameters were determined from non-linear fits of the Michaelis-Menten equation to the data. When the preQ$_0$ concentration was constant (5.0, 10.0, 20.0, 50.0, and 100 μM), the NADPH concentration was varied between 2.0 and 330 μM. When the NADPH concentration was constant (30.0, 50.0, 100, 200, or 340 μM), the preQ$_0$ concentration was varied (1.10–200 μM). Using 2-deamino-preQ$_0$, the substrate concentration (10.0–1000 μM) was varied at different constant NADPH concentrations (30.0, 50.0, 100, 200, 300, or 380 μM). Under the conditions used, the decrease in absorbance was linear over 1–10 min.

For the enzymatic conversion of 7-formyl-preQ$_0$, Tris buffer (25 mM, pH 7.5) containing 125 mM KCl was used. The 7-formyl-preQ$_0$ (0.5 mM) was mixed with $(NH_4)_2SO_4$ or NH_4Cl (each at 50 mM) prior to attempted reduction (NADPH, 300 μM or 1 mM) or oxidation (NADP$^+$, 1 mM) in the presence of ecQueF (30 μM) at 30 °C for 16 h.

For the oxidation of preQ$_1$ with ecQueF, preQ$_1$ was prepared by enzymatic reduction of preQ$_0$ and then purified from the reaction mixture by HPLC. After removing acetonitrile and ammonium acetate buffer by vacuum evaporation, the preQ$_1$

was dissolved in DMSO (≧98% purity). Reactions were started with $NADP^+$ and lasted for 90 min. Tris buffer (pH 7.5, 8.0, 8.5, or 9.0) was used.

KIEs on enzymatic $preQ_0$ reduction due to deuteration of the coenzyme were obtained by comparing initial rates measured with NADPH and (4*R*)-[^{2}H]NADPH, both synthesized as described above. The coenzyme concentration was varied (2.0–36 μM) at a constant saturating concentration of $preQ_0$ (10 μM). KIEs were calculated by fitting Equation 4 to the data.

$$V = V_{max}[S]/\{K_M(1 + F{\cdot}E_{V/K}) + [S](1 + F{\cdot}E_V)\} \quad \text{(Eq. 4)}$$

$E_{V/K}$ and E_V are the KIEs −1 on V_{max}/K_M and V_{max}, respectively. F is the deuterium fraction in S. Superscript D is used to indicate a primary deuterium KIE (*e.g.* $^DV_{max}$).

Stopped-flow Kinetic Studies and Time Course Fitting and Simulation—Rapid-mixing kinetic analysis was done at 25 °C using a SX.18 MV stopped-flow spectrophotometer from Applied Photophysics (Leatherhead, UK). Enzyme and substrate solutions were mixed in equal volumes. In a multiple-turnover reaction, the concentrations of enzyme (5 μM) and $preQ_0$ (30, 40, and 60 μM) were constant, whereas NADPH or (4*R*)-[^{2}H]NADPH (10–150 μM) was varied. Reaction progress was monitored by absorbance at 340 and 380 nm recorded simultaneously. A multiple wavelength detector was used. The absorbance data were averaged in triplicate measurements. Time courses were simulated and reaction models fitted to them using the program COPASI (version 4.11_build 65) (34). To translate absorbances and molar concentrations into one another between experiment and simulation, partial overlap in the absorbance spectra of the reaction components had to be taken into account. The $\epsilon_{340\,nm}$ values ($mM^{-1}\,cm^{-1}$) used in analyzing the results were 5.7 (NADPH), 4.5 (thioimide adduct), 0.126 ($preQ_0$), 0.087 ($NADP^+$), 0.63 (ecQueF), and 6.0 or 8.0 (thioimide adduct with NADPH or 4*R*-[^{2}H]NADPH, respectively). The corresponding $\epsilon_{380\,nm}$ values ($mM^{-1}\,cm^{-1}$) were 1.4 (NADPH), 11 (thioimide adduct), 0.07 ($preQ_0$), 0.023 ($NADP^+$), 0.33 (ecQueF), and 7.5 or 10 (thioimide adduct with NADPH or 4*R*-[^{2}H]NADPH, respectively).

The enzymatic reaction model was developed based on the literature (10, 11, 13), and the evidence from this study is as described under "Results." Because the reaction steps of the enzymatic mechanism are all relatively slow, we assumed binding of $preQ_0$ and NADPH in rapid equilibrium. It was furthermore assumed that the dissociation steps are irreversible under the conditions used. Finally, reaction steps were also assumed to be irreversible. A similar approach of reducing the number of model parameters to facilitate convergence of the fitting, also using COPASI, has been applied to enzymatic pathway analysis before (35). Robust parameter estimates with standard deviation ≤5% were obtained.

Reaction rate constants and binding constants were determined by least squares model fitting that employed the evolutionary programming algorithm with a standard setting in COPASI. The units of concentration and time used in the model were micromolars and seconds, respectively. The least sum of squares as objective function was minimized, as described previously (34, 35). Models were evaluated by comparing the objective value of the estimation between the different models. The model described in Scheme 1 was obtained with the lowest objective value, and the best fitting to the experimental data was observed. Unconstrained fitting was used for all parameters. Start values of the parameters were those determined from direct fits of the data. For example, the K_d values for $preQ_0$ (3 μM) and NADPH (10 μM) were used, and the rate constant of thioimide formation in the absence and presence of NADPH was 1.4 and 7.3 s^{-1}, respectively. The hydride transfer rate constants were set to k_{cat}. Using these start conditions, the fitting converged readily to a unique solution with stable and well defined parameter estimates. We also showed that the fitting results were relatively insensitive to change in the initial parameter values by about 5-fold. From covariance analysis it was found that each rate constant was determined largely independently, *i.e.* statistical correlation with other rate constants was low. In addition, we used different algorithms (particle swarm and simulated annealing), but the rate constants shown in Table 3 were hardly changed.

HPLC Analytics—The samples were analyzed using an Agilent 1200 HPLC system equipped with a 5 μm SeQuant ZIC-HILIC column (200 Å, 250 × 4.6 mm; Merck) and a UV detector (λ = 262 and 340 nm). A linear gradient of 90 to 60% buffer B (acetonitrile) in buffer A (100 mM ammonium acetate, pH 6.67) over 15 min was used. The column was washed with 60% B for 5 min and 90% B for 7 min after each analysis. The flow rate was 2.0 ml/min. The column temperature was 30 °C. Optionally, a mass detector (Agilent 6120 Quadrupole) was coupled to the HPLC system equipped with a 2.7 μm Poroshell SB-C18 column (120 Å, 100 × 3 mm; Agilent) and a UV detector (λ = 210, 254, and 340 nm) to analyze the synthesized coenzyme. The mass of the synthesized coenzymes was scanned in a range of 50–1000 with negative mode. A linear gradient of 2–12% buffer B (acetonitrile) in buffer A (5 mM ammonium acetate, pH 6.0 and 7.0) over 12 min was used. The post time was 2 min. The flow rate was 0.7 ml/min. The column temperature was 30 °C.

Author Contributions—J. J. and B. N. designed the research. J. J. and T. C. performed biochemical experiments and analyzed data together with B. N. B. W. and N. K. synthesized the substrates used. J. J. and B. N. wrote the paper. All authors commented and agreed on the final version of the paper.

Acknowledgments—We thank Prof. Hansjoerg Weber (Graz University of Technology) for NMR analysis, Dr. Silvia Wallner (Graz University of Technology) for helpful discussions on ITC measurements, and Prof. Ruth Birner-Grünberger and B. Darnhofer (Medical University of Graz) for protein-mass analysis.

References

1. Adkins, H., and Billica, H. R. (1948) The preparation of raney nickel catalysts and their use under conditions comparable with those for platinum and palladium catalysts. *J. Am. Chem. Soc.* **70,** 695–698
2. Amundsen, L. H., and Nelson, L. S. (1951) Reduction of nitriles to primary amines with lithium aluminum hydride. *J. Am. Chem. Soc.* **73,** 242–244
3. Caddick, S., Judd, D. B., Lewis, A. K. D. K., Reich, M. T., and Williams, M. R. V. (2003) A generic approach for the catalytic reduction of nitriles. *Tetrahedron* **59,** 5417–5423

4. Bagal, D. B., and Bhanage, B. M. (2015) Recent advances in transition metal-catalyzed hydrogenation of nitriles. *Adv. Synth. Catal.* **357,** 883–900
5. Van Lanen, S. G., Reader, J. S., Swairjo, M. A., de Crécy-Lagard, V., Lee, B., and Iwata-Reuyl, D. (2005) From cyclohydrolase to oxidoreductase: discovery of nitrile reductase activity in a common fold. *Proc. Natl. Acad. Sci. U.S.A.* **102,** 4264–4269
6. Harada, F., and Nishimura, S. (1972) Possible anticodon sequences of tRNAHis, tRNAAsn, and tRNAAsp from *Escherichia coli*. Universal presence of nucleoside Q in the first position of the anticodons of these transfer ribonucleic acid. *Biochemistry* **11,** 301–308
7. Durand, J. M., Okada, N., Tobe, T., Watarai, M., Fukuda, I., Suzuki, T., Nakata, N., Komatsu, K., Yoshikawa, M., and Sasakawa, C. (1994) VacC, a virulence-associated chromosomal locus of *Shigella flexneri*, is homologous to tgt, a gene encoding tRNA-guanine transglycosylase (Tgt) of *Escherichia coli* K-12. *J. Bacteriol.* **176,** 4627–4634
8. Iwata-Reuyl, D. (2003) Biosynthesis of the 7-deazaguanosine hypermodified nucleosides of transfer RNA. *Bioorg. Chem.* **31,** 24–43
9. El Yacoubi, B., Bailly, M., and de Crécy-Lagard, V. (2012) Biosynthesis and function of posttranscriptional modifications of transfer RNAs. *Annu. Rev. Genet.* **46,** 69–95
10. Kim, Y., Zhou, M., Moy, S., Morales, J., Cunningham, M. A., and Joachimiak, A. (2010) High-resolution structure of the nitrile reductase QueF combined with molecular simulations provide insight into enzyme mechanism. *J. Mol. Biol.* **404,** 127–137
11. Chikwana, V. M., Stec, B., Lee, B. W., de Crécy-Lagard, V., Iwata-Reuyl, D., and Swairjo, M. A. (2012) Structural basis of biological nitrile reduction. *J. Biol. Chem.* **287,** 30560–30570
12. Wilding, B., Winkler, M., Petschacher, B., Kratzer, R., Egger, S., Steinkellner, G., Lyskowski, A., Nidetzky, B., Gruber, K., and Klempier, N. (2013) Targeting the substrate binding site of *E. coli* nitrile reductase QueF by modeling, substrate and enzyme engineering. *Chem. Eur. J.* **19,** 7007–7012
13. Lee, B. W., Van Lanen, S. G., and Iwata-Reuyl, D. (2007) Mechanistic studies of *Bacillus subtilis* QueF, the nitrile oxidoreductase involved in queuosine biosynthesis. *Biochemistry* **46,** 12844–12854
14. Ribeiro, A. J. M., Yang, L., Ramos, M. J., Fernandes, P. A., Liang, Z.-X., and Hirao, H. (2015) Insight into enzymatic nitrile reduction: QM/MM study of the catalytic mechanism of QueF nitrile reductase. *ACS Catal.* **5,** 3740–3751
15. Liu, Z.-J., Sun, Y.-J., Rose, J., Chung, Y.-J., Hsiao, C.-D., Chang, W.-R., Kuo, I., Perozich, J., Lindahl, R., Hempel, J., and Wang, B.-C. (1997) The first structure of an aldehyde dehydrogenase reveals novel interactions between NAD and the Rossmann fold. *Nat. Struct. Biol.* **4,** 317–326
16. Ge, X., Campbell, R. E., van de Rijn, I., and Tanner, M. E. (1998) Covalent adduct formation with a mutated enzyme: evidence for a thioester intermediate in the reaction catalyzed by UDP-glucose dehydrogenase. *J. Am. Chem. Soc.* **120,** 6613–6614
17. Olson, L. P., Luo, J., Almarsson, O., and Bruice, T. C. (1996) Mechanism of aldehyde oxidation catalyzed by horse liver alcohol dehydrogenase. *Biochemistry* **35,** 9782–9791
18. Ge, X., Penney, L. C., van de Rijn, I., and Tanner, M. E. (2004) Active site residues and mechanism of UDP-glucose dehydrogenase. *Eur. J. Biochem.* **271,** 14–22
19. Ordman, A. B., and Kirkwood, S. (1977) UDPglucose dehydrogenase kinetics and their mechanistic implications. *Biochim. Biophys. Acta* **481,** 25–32
20. Wilding, B., Winkler, M., Petschacher, B., Kratzer, R., Glieder, A., and Klempier, N. (2012) Nitrile reductase from *Geobacillus kaustophilus*: a potential catalyst for a new nitrile biotransformation reaction. *Adv. Synth. Catal.* **354,** 2191–2198
21. Hoops, G. C., Townsend, L. B., and Garcia, G. A. (1995) tRNA-guanine transglycosylase from *Escherichia coli*: structure-activity studies investigating the role of the aminomethyl substituent of the heterocyclic substrate preQ$_1$. *Biochemistry* **34,** 15381–15387
22. Olgen, S., Isgör, Y. G., and Çoban, T. (2008) Synthesis and activity of novel 5-substituted pyrrolo[2,3-d]pyrimidine analogues as pp60c-src tyrosine kinase inhibitors. *Arch. Pharm. Chem.* **341,** 113–120
23. Brooks, A. F., Garcia, G. A., and Showalter, H. D. (2010) A short, concise synthesis of queuine. *Tetrahedron Lett.* **51,** 4163–4165
24. Egger, S., Chaikuad, A., Kavanagh, K. L., Oppermann, U., and Nidetzky, B. (2011) Structure and mechanism of human UDP-glucose 6-dehydrogenase. *J. Biol. Chem.* **286,** 23877–23887
25. Kozlov, A. G., and Lohman, T. M. (1999) Adenine base unstacking dominates the observed enthalpy and heat capacity changes for the *Escherichia coli* SSB tetramer binding to single-stranded oligoadenylates. *Biochemistry* **38,** 7388–7397
26. Leavitt, S., and Freire, E. (2001) Direct measurement of protein binding energetics by isothermal titration calorimetry. *Curr. Opin. Struct. Biol.* **11,** 560–566
27. Goldberg, R. N., Kishore, N., and Lennen, R. M. (2002) Thermodynamic quantities for the ionization reactions of buffers. *J. Phys. Chem. Ref. Data* **31,** 231–370
28. Jeong, S. S., and Gready, J. E. (1994) A method of preparation and purification of (4*R*)-deuterated-reduced nicotinamide adenine dinucleotide phosphate. *Anal. Biochem.* **221,** 273–277
29. Nagao, T., Mitamura, T., Wang, X. H., Negoro, S., Yomo, T., Urabe, I., and Okada, H. (1992) Cloning, nucleotide sequences, and enzymatic properties of glucose dehydrogenase isozymes from *Bacillus megaterium* IAM1030. *J. Bacteriol.* **174,** 5013–5020
30. Ragg, E., Scaglioni, L., Mondelli, R., Carelli, I., Casini, A., and Tortorella, S. (1991) ^{1}H-, ^{13}C-, ^{31}P-NMR studies and conformational analysis of NADP^{+}, NADPH coenzymes and of dimers from electrochemical reduction of NADP^{+}. *Biochim. Biophys. Acta* **1076,** 49–60
31. Klepper, F., Polborn, K., and Carell, T. (2005) Robust synthesis and crystal-structure analysis of 7-cyano-7-deazaguanine (preQ$_0$ base) and 7-(aminomethyl)-7-deazaguanine (preQ$_1$ base). *Helv. Chim. Acta* **88,** 2610–2616
32. Agrawal, N., and Kohen, A. (2003) Microscale synthesis of 2-tritiated isopropanol and 4*R*-tritiated reduced nicotinamide adenine dinucleotide phosphate. *Anal. Biochem.* **322,** 179–184
33. McCracken, J. A., Wang, L., and Kohen, A. (2004) Synthesis of *R* and *S* tritiated reduced β-nicotinamide adenine dinucleotide 2′ phosphate. *Anal. Biochem.* **324,** 131–136
34. Hoops, S., Sahle, S., Gauges, R., Lee, C., Pahle, J., Simus, N., Singhal, M., Xu, L., Mendes, P., and Kummer, U. (2006) COPASI–a COmplex PAthway SImulator. *Bioinformatics* **22,** 3067–3074
35. Leroux, A. E., Haanstra, J. R., Bakker, B. M., and Krauth-Siegel, R. L. (2013) Dissecting the catalytic mechanism of *Trypanosoma brucei* trypanothione synthetase by kinetic analysis and computational modeling. *J. Biol. Chem.* **288,** 23751–23764

Kinetic Analysis and Probing with Substrate Analogues of the Reaction Pathway of the Nitrile Reductase QueF from *Escherichia coli*

Jihye Jung, Tibor Czabany, Birgit Wilding, Norbert Klempier and Bernd Nidetzky

J. Biol. Chem. 2016, 291:25411-25426.
doi: 10.1074/jbc.M116.747014 originally published online October 17, 2016

Evidence of a sequestered imine intermediate during reduction of nitrile to amine by the nitrile reductase QueF from *Escherichia coli*

JBC ARTICLE

Evidence of a sequestered imine intermediate during reduction of nitrile to amine by the nitrile reductase QueF from *Escherichia coli*

Received for publication, June 28, 2017, and in revised form, December 30, 2017 Published, Papers in Press, January 16, 2018, DOI 10.1074/jbc.M117.804583

Jihye Jung[‡§] and **Bernd Nidetzky**[‡§1]

From the [‡]*Austrian Centre of Industrial Biotechnology and the* [§]*Institute of Biotechnology and Biochemical Engineering, NAWI Graz, Graz University of Technology, A-8010 Graz, Austria*

Edited by John M. Denu

In the biosynthesis of the tRNA-inserted nucleoside queuosine, the nitrile reductase QueF catalyzes conversion of 7-cyano-7-deazaguanine ($preQ_0$) to 7-aminomethyl-7-deazaguanine ($preQ_1$), a biologically unique four-electron reduction of a nitrile to an amine. The QueF mechanism involves a covalent thioimide adduct between the enzyme and $preQ_0$ that undergoes reduction to $preQ_1$ in two NADPH-dependent steps, presumably via an imine intermediate. Protecting a labile imine from interception by water is fundamental to QueF catalysis for proper enzyme function. In the QueF from *Escherichia coli*, the conserved Glu^{89} and Phe^{228} residues together with a mobile structural element composing the catalytic Cys^{190} form a substrate-binding pocket that secludes the bound $preQ_0$ completely from solvent. We show here that residue substitutions (E89A, E89L, and F228A) targeted at opening up the binding pocket weakened $preQ_0$ binding at the preadduct stage by up to +10 kJ/mol and profoundly affected catalysis. Unlike wildtype enzyme, the QueF variants, including L191A and I192A, were no longer selective for $preQ_1$ formation. The E89A, E89L, and F228A variants performed primarily (≥90%) a two-electron reduction of $preQ_0$, releasing hydrolyzed imine (7-formyl-7-deazaguanine) as the product. The $preQ_0$ reduction by L191A and I192A gave $preQ_1$ and 7-formyl-7-deazaguanine at a 4:1 and 1:1 ratio, respectively. The proportion of 7-formyl-7-deazaguanine in total product increased with increasing substrate concentration, suggesting a role for $preQ_0$ in a competitor-induced release of the imine intermediate. Collectively, these results provide direct evidence for the intermediacy of an imine in the QueF-catalyzed reaction. They reveal determinants of QueF structure required for imine sequestration and hence for a complete nitrile-to-amine conversion by this class of enzymes.

Sequestration of reactive intermediates, to avoid their release into solvent where they might decompose, is a hallmark of enzyme catalysis (1, 2). Mobile elements of the protein structure are often used to close down over the substrate while it undergoes the catalytic transformation into product. The nitrile reductase QueF deals with a notably difficult problem of intermediate sequestration (3–7). QueF catalyzes a four-electron reduction of a nitrile to an amine in two NADPH-dependent steps, presumably via an imine intermediate. However, imines are extremely unstable molecular groups in water and will hydrolyze to aldehyde immediately. Therefore, to ensure that every substrate "makes it through" to the amine, QueF must both keep a firm grip on the labile imine during the catalytic act and exclude water from the binding site. This study was performed to identify elements of the QueF catalytic apparatus that make nitrile reductases the high-fidelity enzymes they are by nature, converting nitrile to amine without detectable loss of the supposed imine to off-pathway reactions (3–7).

QueF was described from the biosynthetic pathway of the nucleoside queuosine (Q)[2] where the enzyme functions in turning 7-cyano-7-deazaguanine ($preQ_0$) into 7-aminomethyl-7-deazaguanine ($preQ_1$) (8, 9). The $preQ_1$ is inserted into tRNA and subsequently converted to Q. Bound at the wobble position of tRNAs decoding NAC/U codons, Q plays a role in modulating codon-anticodon binding efficiency (8, 10, 11). *De novo* biosynthesis of Q is exclusively found in bacteria (11–13). Although Q is not essential for bacterial life (14), knock out of its biosynthesis can reduce, or eliminate, pathogenicity (15, 16). QueF among all other enzymes of the Q pathway, therefore, presents a potential target for anti-infective strategies directed selectively against bacteria. QueF also has attracted considerable mechanistic interest (3, 5–7, 17), for the reaction catalyzed by it is apparently unique to biology.

2-fold enzymatic reduction of $preQ_0$ is proposed to proceed in three catalytic steps, as shown in Scheme 1 (3–7). A covalent thioimide adduct is formed between the enzyme's catalytic nucleophile (cysteine) and $preQ_0$ (3, 5, 7). Its subsequent reduction by NADPH yields a covalent thiohemiaminal intermediate. After exchange of coenzyme and breakdown of the covalent thiohemiaminal to imine, a second reduction by NADPH gives the amine product. The QueF mechanism necessitates that the

This work has been supported by the Federal Ministry of Economy, Family and Youth (BMWFW), the Federal Ministry for Transport, Innovation and Technology (BMVIT), the Styrian Business Promotion Agency SFG, the Vienna Business Agency, the Standortagentur Tirol, the Government of Lower Austria, and Styrian Provincial Government Economic Affairs and Innovation through the COMET-Funding Program managed by the Austrian Research Promotion Agency FFG. The authors declare that they have no conflicts of interest with the contents of this article.

[1] To whom correspondence should be addressed. Tel.: 43-316-873-8400; Fax: 43-316-873-8434; E-mail: bernd.nidetzky@tugraz.at.

[2] The abbreviations used are: Q, queuosine; $preQ_0$, 7-cyano-7-deazaguanine; $preQ_1$, 7-aminomethyl-7-deazaguanine; T-fold, tunneling-fold; ecQueF, *E.coli* QueF; vcQueF, *V. cholerae* QueF; ITC, isothermal titration calorimetry; KIE, kinetic isotope effect; PDB, Protein Data Bank.

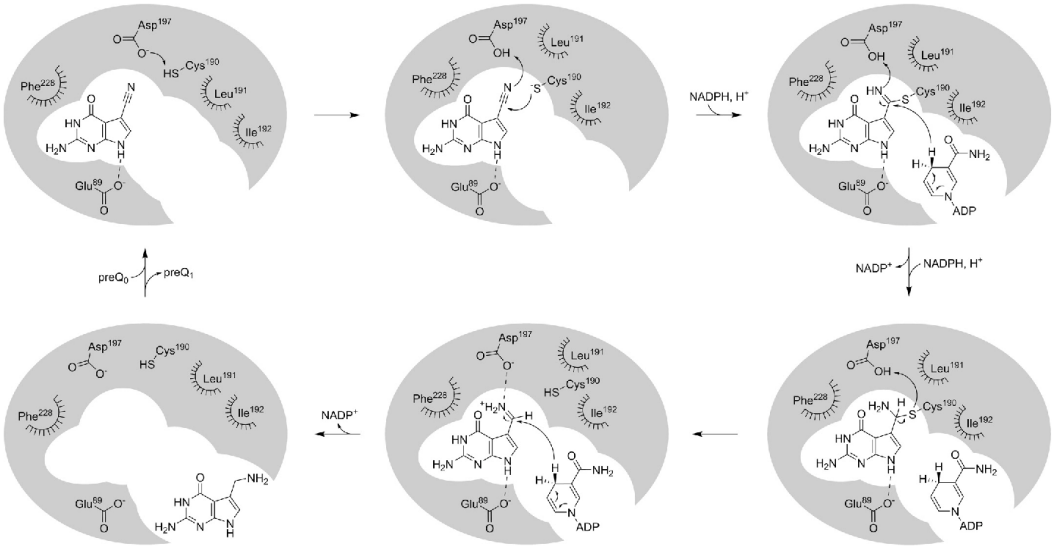

SCHEME 1. **The proposed mechanism of ecQueF reducing $preQ_0$ to $preQ_1$ is shown.** Residues involved in catalysis are indicated. Also shown are residues involved in closing up the binding site of $preQ_0$ and targeted by mutational analysis in this study. The amino acid residues are arranged to indicate their relative positions in the enzyme structure. Amino acid numbering of ecQueF is used. The *dashed line* indicates a hydrogen bond.

different chemical steps of the enzymatic reaction are coordinated exactly with the intermediate physical steps of coenzyme binding and release, and these in turn must be precisely timed with the disengagement of free imine from the covalent thiohemiaminal. The way of how QueF orchestrates these multiple steps (4–6) immediately suggests strategies possibly utilized for intermediate sequestration.

QueF enzymes are oligomeric proteins built from subunits that possess a small, so-called tunneling-fold (T-fold) domain (18). The core T-fold domain consists of a $\beta\beta\alpha\alpha\beta\beta$ arrangement of secondary structure (4, 5, 9). The known QueF enzymes are divided into unimodular (*e.g.* QueF from *Bacillus subtilis*) (3, 5, 19, 20) and bimodular groups (*e.g.* QueF from *Escherichia coli* (ecQueF)) (4, 7, 21–24), depending on whether they comprise subunits containing only a single T-fold domain or two T-fold domains in tandem repeat, respectively. Both types of QueF have their active sites located at the structural interface of two T-fold domains. The active site residues, and their structural arrangement into a functional catalytic center, are highly conserved in both QueF types (4, 5, 21). In addition to the catalytic cysteine (Cys^{190} in ecQueF), there is an invariant pair of acidic residues of which the aspartic acid (Asp^{197} in ecQueF) plays a role in proton transfer, as shown in Scheme 1, and the glutamic acid (Glu^{89} in ecQueF) is involved in binding recognition of $preQ_0$.

Crystallographic studies of QueF from *B. subtilis* (5, 20) and the bimodular QueF from *Vibrio cholerae* (vcQueF; (4)) show that $preQ_0$ binding involves an induced-fit conformational change in protein structure, with the consequence that the substrate binding site, which is quite open in the apoenzyme, is closed up completely in the holoenzyme. The bound $preQ_0$ becomes sequestered completely from the solvent as a result (Fig. 1).

In vcQueF, for which crystal structures of apoenzyme (PDB code 3RJ4), noncovalent complex of a C194A variant with $preQ_0$ (PDB codes 3RZP and 3UXV), and covalent complexes of H233A (PDB code 4GHM) and R262L (PDB codes 3S19 and 3UXJ) variants with $preQ_0$ were determined, the induced-fit binding of $preQ_0$ comprises three main elements in particular. A characteristic device, generally referred to as the "QueF motif," is embedded structurally in a α-helix flanking the active site (5, 9). At its N-terminal end, this helix has a glutamic acid (Glu^{89} in ecQueF), which forms a hydrogen bond with $preQ_0$ (2.8 Å) in the enzyme–substrate complex, as shown in Fig. 1. The glutamic acid is positioned opposite to an adaptable element of the QueF structure (Fig. 1, *B* and *C*) contributing the catalytic cysteine to the active site. This "Cys element," which is completely conserved within bimodular QueF enzymes, additionally comprises Leu^{191} and Ile^{192} (ecQueF numbering). The Cys element rearranges to cover the active site in the $preQ_0$-enzyme complex structure (PDB code 4GHM; Fig. 1*C*). Finally, a conserved phenylalanine (Phe^{228} in ecQueF), which adopts a position to open up the $preQ_0$ binding pocket in the apoenzyme, closes down over the bound substrate, by forming pi-stacking interactions with it (3.7 Å), in the holoenzyme (Fig. 1*C*). Two key residues of $preQ_0$ binding, Glu^{89} and Phe^{228}, and the catalytic Cys^{190} thus get "locked" onto the bound substrate at the end of the structural rearrangement. These features of vcQueF structure important for enzymatic function appear to be completely conserved in ecQueF. Overall, the sequence identity between the two enzymes is 65%.

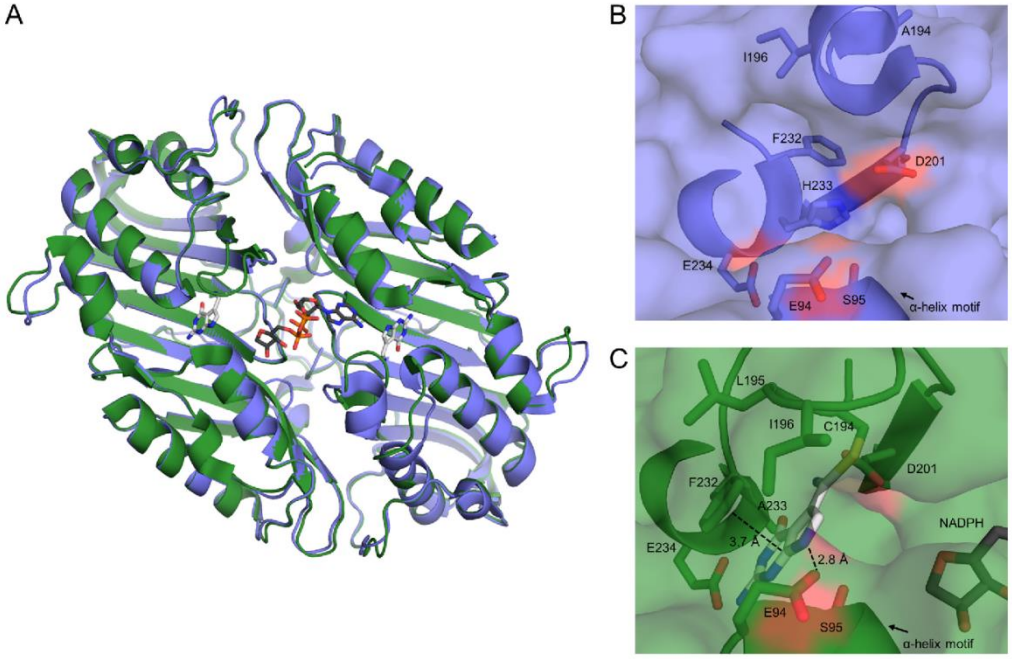

Figure 1. Sequestration of preQ$_0$ is revealed in crystal structures of vcQueF in apoform (C194A variant, *slate*; PDB code 3RJ4) and holoenzyme complex with preQ$_0$ (H233A variant, *green*; PDB code 4GHM). *A*, a superimposition of apoenzyme and holoenzyme structures of the vcQueF homodimer is shown. *B* and *C*, a close-up view of the binding site for preQ$_0$ in apoenzyme (*B*) and holoenzyme (*C*) is shown. The orientation of NADPH binding is from the crystal structure of the ternary complex of enzyme, preQ$_0$, and NADPH (vcQueF R262L variant; PDB code 3UXJ). Despite missing density for the nicotinamide ring in the protein-bound NADPH (*dark gray*), the likely orientation of the nicotinamide moiety can be inferred from the binding positions of preQ$_0$ and the structurally resolved portion of NADPH. Binding of NADPH in ecQueF was also examined with structure modeling (21). The ecQueF residues corresponding to the vcQueF residues shown in *A–C* are Glu^{89}, Ser^{90}, Cys^{190}, Leu^{191}, Ile^{192}, Asp^{197}, Phe^{228}, His^{229}, and Glu^{230}. The preQ$_0$, NADPH, and amino acids in the binding pocket are indicated by element-based colors.

Kinetic studies of ecQueF indicate that NADPH binds to QueF already at the noncovalent complex with preQ$_0$ (7). The presence of NADPH enhances ~4-fold the thioimide formation rate compared with reaction of free enzyme and preQ$_0$. The substrate-binding pocket has a narrow aperture, made up from Glu^{89} and the Cys element, Ile^{192} in particular (Fig. 1), that appears to be used for threading the nicotinamide moiety of NADPH into the active site (21). Structurally, therefore, substrate cannot be released before the coenzyme has dissociated. Accordingly, an important feature of QueF efficiency in intermediate sequestration, suggested from kinetic analysis, is the extremely tight binding of NADPH by the enzyme at the stage of the thiohemiaminal/imine (7).

The evidence just summarized suggests that the residues Glu^{89} and Phe^{228} and also the Cys element are significant for intermediate sequestration in ecQueF. Anchoring the proposed imine through interactions from these QueF structural elements might be crucially important. In this study, therefore, we performed mutagenesis of ecQueF, replacing the "anchoring" Glu^{89} and Phe^{228} by residues (Ala or Leu) unable to fulfill the analogous function. We additionally replaced Leu^{191} and Ile^{192} by Ala with the aim of perturbing the active site-closing movement of the Cys element. Overall, we considered that because of a substrate-binding site not properly closable any more, the ecQueF variants might no longer behave as high-fidelity nitrile reductases. The putative imine intermediate might become intercepted by water able to enter an opened-up active site in the variant enzymes. Detailed characterization of these ecQueF variants reveals two-electron reduction of nitrile to imine for the first time in a nitrile reductase, thus providing direct evidence of the intermediacy of an elusive imine in the native catalytic reaction, and provides a structural and mechanistic explanation for complete nitrile-to-amine conversion by QueF enzymes, emphasizing the critical importance of intermediate sequestration.

Results

Isothermal titration calorimetry study of preQ$_0$ binding to ecQueF variants

Purified ecQueF variants were shown to bind preQ$_0$, and the corresponding thermodynamic characteristics were determined, in ITC experiments. Binding of preQ$_0$ by ecQueF is a two-step process in which an initially formed noncovalent enzyme-preQ$_0$ complex is converted to a covalent thioimide adduct (Scheme 2 and Ref. 7). Note that with ITC, it was not

possible to distinguish between the two steps of $preQ_0$ binding and the data report on the binding process as a whole. The results are shown in Fig. 2, and the parameters calculated from the data are summarized in Table 1.

Strong heat release on titrating enzyme solution with $preQ_0$ solution (Fig. 2), similarly as it occurred with the wildtype enzyme (7), was good evidence that ecQueF variants had retained the ability to bind $preQ_0$. Substitution of Glu^{89} caused substantial weakening of the $preQ_0$ binding as compared with wildtype enzyme, reflected in a smaller negative value of $\Delta G_{binding}$ ($\Delta\Delta G_{binding}$ = +14 kJ/mol) and increased overall apparent dissociation constant K_d (292-fold). The degree of disruptive effect was similar in both enzyme variants. The F228A variant also showed weakened $preQ_0$ binding, reflected in a smaller negative value of $\Delta G_{binding}$ ($\Delta\Delta G_{binding}$ = +10.8 kJ/mol) and 90-fold increased K_d. In terms of $\Delta G_{binding}$ and K_d, $preQ_0$ binding was unaffected by the replacement of Leu^{191} or Ile^{192} with Ala. Interestingly, the $\Delta G_{binding}$ of the E89A, E89L, and F228A variants was comparable to the $\Delta G_{binding}$ of the pre-

$$E + preQ_0 \underset{k_2}{\overset{k_1}{\rightleftharpoons}} E{\bullet}preQ_0 \underset{k_4}{\overset{k_3}{\rightleftharpoons}} E\text{-}preQ_0$$

SCHEME 2. **The two-step kinetic mechanism of $preQ_0$ binding is shown.** *E* is free ecQueF. *E·preQ$_0$* indicates the noncovalent complex. *E-preQ$_0$* indicates the covalent thioimide adduct.

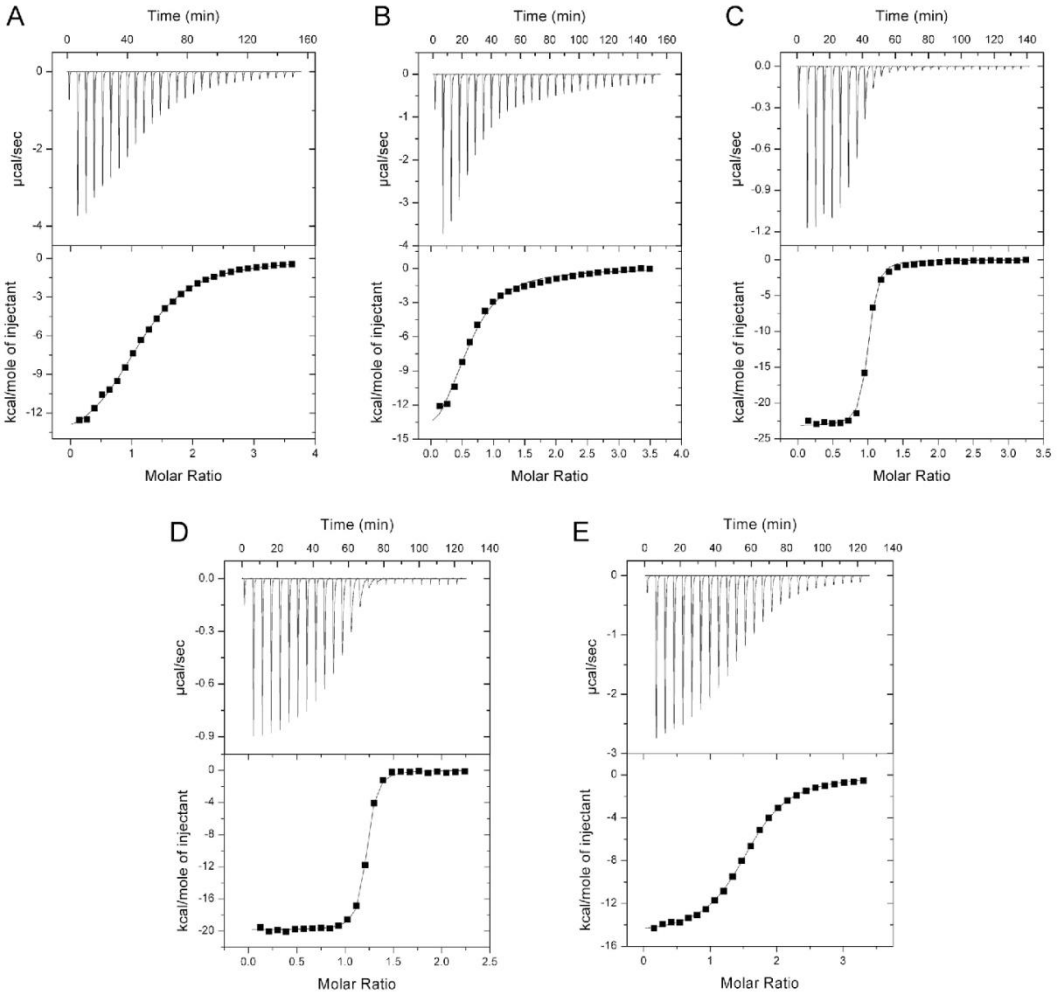

Figure 2. ITC analysis of $preQ_0$ binding to ecQueF variants at 25 °C is shown. E89A (*A*, 58 μM), E89L (*B*, 60 μM), L191A (*C*, 9.4 μM), I192A (*D*, 10 μM), and F228A (*E*, 37 μM) were used. The $preQ_0$ solution (1 mM for E89A and E89L, 0.25 mM for L191A and I192A, and 0.8 mM for F228A) was titrated into the enzyme solution. The obtained thermodynamic parameters are summarized in Table 1. The *c* values (c = [dimeric protein]/K_d) obtained from the experiments were 5 for the E89A, 6 for the E89L, 235 for the L191A, 435 for the I192A, and 11 for the F228A variant.

Table 1
Thermodynamic parameters of $preQ_0$ binding by ecQueF wildtype and variants

	Apparent K_d[a]	$\Delta H_{binding}$	$-T\Delta S_{binding}$	$\Delta G_{binding}$	Reference
	μM	kJ/mol	kJ/mol	kJ/mol	
Wildtype	0.039 ± 0.004	−80.3 ± 0.5	37.9	−42.4 ± 0.5	Ref. 7
C190A	5.5 ± 0.1	−44.7 ± 0.2	14.6	−30.1 ± 0.2	Ref. 7
E89A	11.4 ± 0.4	−63.3 ± 0.7	34.9	−28.4 ± 0.7	This study
E89L	10.3 ± 1.1	−73.3 ± 3.7	44.7	−28.6 ± 3.3	This study
L191A	0.040 ± 0.004	−97.5 ± 0.6	55.1	−42.4 ± 0.6	This study
I192A	0.023 ± 0.011	−82.9 ± 4.0	39.0	−43.8 ± 1.1	This study
F228A	3.3 ± 0.5	−61.7 ± 1.4	30.1	−31.6 ± 0.5	This study

[a] The K_d is denoted apparent because the binding process analyzed involves noncovalent binding of $preQ_0$ and covalent thioimide formation with the enzyme.

viously reported C190A variant, which can bind $preQ_0$ just noncovalently (7). However, contrasting their similarity overall, the $\Delta G_{binding}$ values of these ecQueF variants involved distinct relative contributions from enthalpy ($\Delta H_{binding}$) and entropy ($-T\Delta S_{binding}$). The $\Delta H_{binding}$ became more negative (favorable of binding), and the $-T\Delta S_{binding}$ became more positive (nonfavorable of binding) in going from C190A via the variants. A covalent thioimide formation more pronounced in E89L compared with the E89A and F228A variants and lacking completely in C190A variant could explain these trends in $\Delta H_{binding}$ and $-T\Delta S_{binding}$.

In comparison to the wildtype enzyme, the $\Delta\Delta G_{binding}$ of the E89A variant was primarily due to the effect on $\Delta H_{binding}$. In the E89L and F228A variants, however, the $\Delta\Delta G_{binding}$ involved effects, of a similar degree, on $\Delta H_{binding}$ and $-T\Delta S_{binding}$. The $\Delta G_{binding}$ of L191A variant involved a $\Delta H_{binding}$ lower and a $-T\Delta S_{binding}$ higher than the corresponding $preQ_0$ binding parameters of the wildtype enzyme. However, the $\Delta H_{binding}$ and $-T\Delta S_{binding}$ terms compensated each other in an overall unchanged $\Delta G_{binding}$. A $-T\Delta S_{binding}$ term substantially higher in the ecQueF variants (E89L and L191A) is therefore worth noting. In the I192A variant, the $\Delta H_{binding}$ and $-T\Delta S_{binding}$ terms of $preQ_0$ binding were comparable to what they were in the wildtype enzyme.

Kinetic analysis of covalent thioimide adduct formation in ecQueF variants

Absorbance at 380 nm ($\epsilon = 10.02 \pm 0.14\ mM^{-1}\ cm^{-1}$) indicates the covalent thioimide intermediate of wildtype ecQueF (7). Titration of the enzyme variants with $preQ_0$ also gave rise to a "thioimide" absorbance band, as shown in Fig. 3. Maximum absorption was however shifted to a slightly higher wavelength (≤5 nm) in the Glu^{89} variants. In wildtype ecQueF based on half-of-the-sites reactivity of the enzyme dimer, the molar equivalent of $preQ_0$ was sufficient to convert all enzyme present into the covalent adduct (7). In ecQueF variants, especially the ones having Glu^{89} replaced, excess $preQ_0$ (~10-fold) was required for full conversion of the enzyme (Fig. 3*A*).

In wildtype ecQueF as shown recently (7), the thioimide formation involves a noncovalent enzyme-$preQ_0$ complex in rapid equilibrium, which reacts only relatively slowly to the covalent adduct (Scheme 2). Absorbance time courses from $preQ_0$ binding experiments with the E89A, L191A, I192A, and F228A variant were best fit with single exponentials. The overall fit was not improved when double exponentials were used (data not

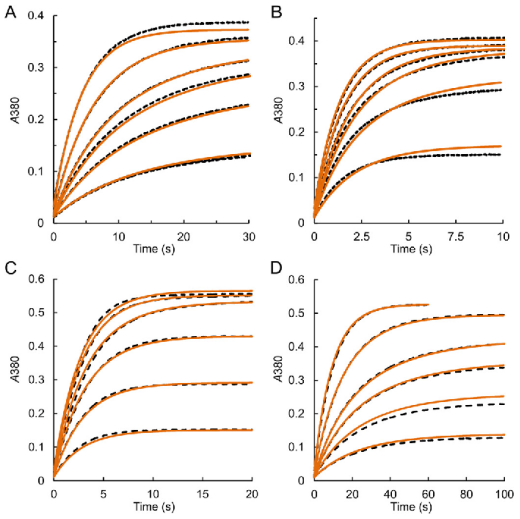

Figure 3. Stopped-flow progress curves of thioimide formation by different ecQueF variants are shown together with fitting results. The thioimide formation by the ecQueF variants was recorded by absorbance at 380 nm. E89A (*A*, 33 μM), L191 A (*B*, 35 μM), I192A (*C*, 57 μM), or F228A (*D*, 53 μM) variant was mixed with varied concentration of $preQ_0$ (*bottom* to *top*: 15, 30, 45, 60, 120, and 300 μM). The DMSO concentration did not exceed 2%. The *black dashed lines* are the averaged data from triplicate measurements. Global fitting was performed using the two-step binding mechanism in Scheme 2. The fits are shown with *orange lines*. The obtained kinetic constants are summarized in Table 2.

shown). The corresponding rate constants and amplitudes (data not shown) were hyperbolically dependent on the $preQ_0$ concentration, as expected if the ecQueF variants reacted in two distinct steps, as shown in Scheme 2, analogous to the wildtype enzyme (7). A global fit of the reaction time courses was therefore performed using the kinetic mechanism in Scheme 2. Experimental data are superimposed in Fig. 3 with the fitting results. Parameters of $preQ_0$ noncovalent binding ($K_{d\,kinetic} = k_2/k_1$) and thioimide formation (k_3, k_4) by the ecQueF variants are summarized in Table 2 along with the corresponding parameters of the wildtype enzyme.

Compared with the wildtype enzyme, the $K_{d\,kinetic}$ was increased in all ecQueF variants (F228A, 59-fold; E89A, 41-fold; and L191A, 7.1-fold), except for the I192A variant that exhibited the same $K_{d\,kinetic}$ as the wildtype enzyme. The k_3 was decreased in all enzyme variants, most strongly so in the F228A variant (10-fold). The ratio k_3/k_4 describes the tightening of $preQ_0$ binding in consequence of covalent thioimide formation. The effect was more pronounced in the L191A variant (k_3/k_4 = 440) than in the E89A (k_3/k_4 = 53), I192A (k_3/k_4 = 26), and F228A variant (k_3/k_4 = 40). Including the wildtype enzyme in this comparison is difficult because only a rough lower limit of 68 could be given for k_3/k_4. Because in kinetic experiments the k_4 was not different from 0 (7), the relationship $K_{d\,overall} = K_{d\,kinetic}/(1+k_3/k_4)$ was used to calculate *the upper bound* of k_4 from the apparent $K_{d\,overall}$ of the wildtype enzyme determined in ITC experiments. The values of $K_{d\,overall}$ determined kinetically and obtained from ITC data agreed for the L191A and

Table 2
Kinetic constants of $preQ_0$ binding by ecQueF wildtype and variants

	$K_{d\ kinetic}$ (k_2/k_1)	k_3	k_4	$K_{d\ overall}$	Reference
	M	s^{-1}	s^{-1}	μM	
Wildtype	$(2.63 \pm 0.01) \times 10^{-6}$	1.63 ± 0.01	$\leq 0.024^a$	$\leq 0.039^b$	Ref. 7
E89A	$(109 \pm 10) \times 10^{-6}$	0.32 ± 0.01	0.006 ± 0.001	2.0	This study
L191A	$(18.7 \pm 7.0) \times 10^{-6}$	0.79 ± 0.02	0.0018 ± 0.0003	0.042	This study
I192A	$(2.8 \pm 1.0) \times 10^{-6}$	0.36 ± 0.03	0.014 ± 0.001	0.10	This study
F228A	$(155 \pm 30) \times 10^{-6}$	0.16 ± 0.02	0.004 ± 0.001	3.8	This study

[a] k_4 was obtained from the relationship $K_{d\ overall} = K_{d\ kinetic}/(1 + k_3/k_4)$ as described in Ref. 7.
[b] As an upper bound of $K_{d\ overall}$ for $preQ_0$ binding to wildtype ecQueF, the apparent K_d from ITC measurement (Table I) was taken.

F228A variant. However, they differed by as much as 5-fold for the E89A and I192A variant. We explain this difference by the fact that in the ITC measurement, both the covalent and the noncovalent complex contribute to the recorded heat signal, whereas absorbance is completely specific for detecting the thioimide adduct. Therefore, only absorbance measurements allow for a clear-cut determination of $K_{d\ overall}$.

Reduction of $preQ_0$ by the ecQueF variants

Direct analysis of the reaction mixtures by ^{1}H NMR (Fig. 4) and HPLC (Fig. 5) was used to examine $preQ_0$ reduction by the ecQueF variants. Initial evidence was that although F228A and both Glu^{89} variants showed conversion of $preQ_0$ at a slow rate, they hardly produced $preQ_1$. We considered that any imine intermediate exposed to water after the first reduction would be detected as 7-formyl-7-deazaguanine. Using authentic reference material from chemical synthesis (7), we identified 7-formyl-7-deazaguanine as the main product of $preQ_0$ reduction by E89A, E89L, and F228A variants, as shown in Figs. 4 and 5. Proton signals characteristic of $preQ_1$ were below detection in these reactions. Conversely, 7-formyl-7-deazaguanine was completely absent from, and $preQ_1$ the only detectable product in, reactions of the wildtype enzyme. Reaction of the L191A variant gave a mixture of products comprising mainly $preQ_1$ (80–90%), but also 7-formyl-7-deazaguanine that accounted for the rest of $preQ_0$ converted. The $preQ_0$ reduction by the I192A variant also proceeded to form both $preQ_1$ and 7-formyl-7-deazaguanine, roughly at a ratio of 1:1.

LC and LC-MS analysis confirmed the ecQueF variants to exhibit the particular change in product formation from $preQ_0$ (Fig. 5). When the $preQ_0$ reduction with the variants were done in Tris buffer, LC traces revealed a putative product peak of unknown identity, appearing always together with the expected product peak for 7-formyl-7-deazaguanine (Fig. 5*B*). The unknown peak exhibited absorbance at 262 and 340 nm, just like 7-formyl-7-deazaguanine but contrary to $preQ_0$ and $preQ_1$, which both show absorbance only at 262 nm. When the same enzymatic reactions were done in phosphate buffer, the second peak was missing, and only the peak for 7-formyl-7-deazaguanine was found (Fig. 5, *C* and *D*). This together with the characteristic mass of the unknown peak ($1H^+$, 282) suggested an imine adduct between 7-formyl-7-deazaguanine and Tris, as shown in Fig. 5, that may have formed in solution already during the enzymatic reaction or during sample preparation.

Ability of the LC and LC-MS analytic method to quantify even small amounts of the secondary reaction product (*e.g.* 5% $preQ_1$ in $preQ_0$ conversion by the E89A variant) made it possible to determine whether the NADPH or the $preQ_0$ concentration had an influence on the product distribution in the enzymatic conversions. Whereas high concentrations of NADPH might prevent the loss of imine intermediate from the enzyme and so pull the enzymatic reaction toward $preQ_1$ formation, the opposite effect, namely preference for formation of aldehyde, could be expected at high $preQ_0$ concentration (Scheme 3). In each enzyme including wildtype ecQueF, there was no effect from variation in [NADPH] between 1 and 10 mM. Note that relatively high NADPH concentrations were used in the experiment to maximize the possible "pull" toward $preQ_1$. The case of the L191A and I192A variants, in which on average one imine was lost in every five (L191A) and two (I192A) $preQ_0$ conversion events, clearly shows that exchange between $NADP^+$ and NADPH for complete 2-fold reduction of $preQ_0$ was still somewhat functional after the replacements of Leu^{191} and Ile^{192}. This result immediately suggests the possibility that imine was intercepted by water in, or escaped into solution from, the L191A and I192A variants before the new NADPH had the chance to bind, implying in turn an early disengagement of the imine from the covalent thiohemiaminal. The alternative possibility is that imine was intercepted by water in, or was released from, the ternary complexes of L191A and I192A variants with NADPH.

Contrary to NADPH, the $preQ_0$ substrate, on variation of its concentration, affected strongly the product distribution from nitrile reduction by the different ecQueF variants. In each enzyme as shown in Fig. 6, the percentage of imine in the total reaction product released increased upon increase in the molar ratio [$preQ_0$]/[enzyme dimer] used in the experiment. The effect was most pronounced in the E89A and F228A variants, which switched from forming primarily $preQ_1$ (80%) when $preQ_0$ was used at the same concentration as the enzyme dimer to being almost completely selective for imine formation (≥95%) at higher [$preQ_0$]/[enzyme dimer] ratios. The E89L variant gave predominantly imine at all conditions used. In the I192A variant, the percentage of imine in total product increased steadily dependent on the [$preQ_0$]/[enzyme] ratio and reached a limiting value of ~50% when $preQ_0$ was added in excess. The L191A variant formed imine as the minor product (≤20%). In all enzyme variants except for F228A, the percentage of imine in total product typically exhibited a roughly hyperbolic dependence on the [$preQ_0$]/[enzyme] ratio used (Fig. 6, *A–D*), from which the maximum imine formation at saturating $preQ_0$ was determined. In the F228A variant, maximum imine formation was established from the data, but the underlying dependence of product selectivity on [$preQ_0$]/[enzyme] ratio appeared complex (Fig. 6*E*).

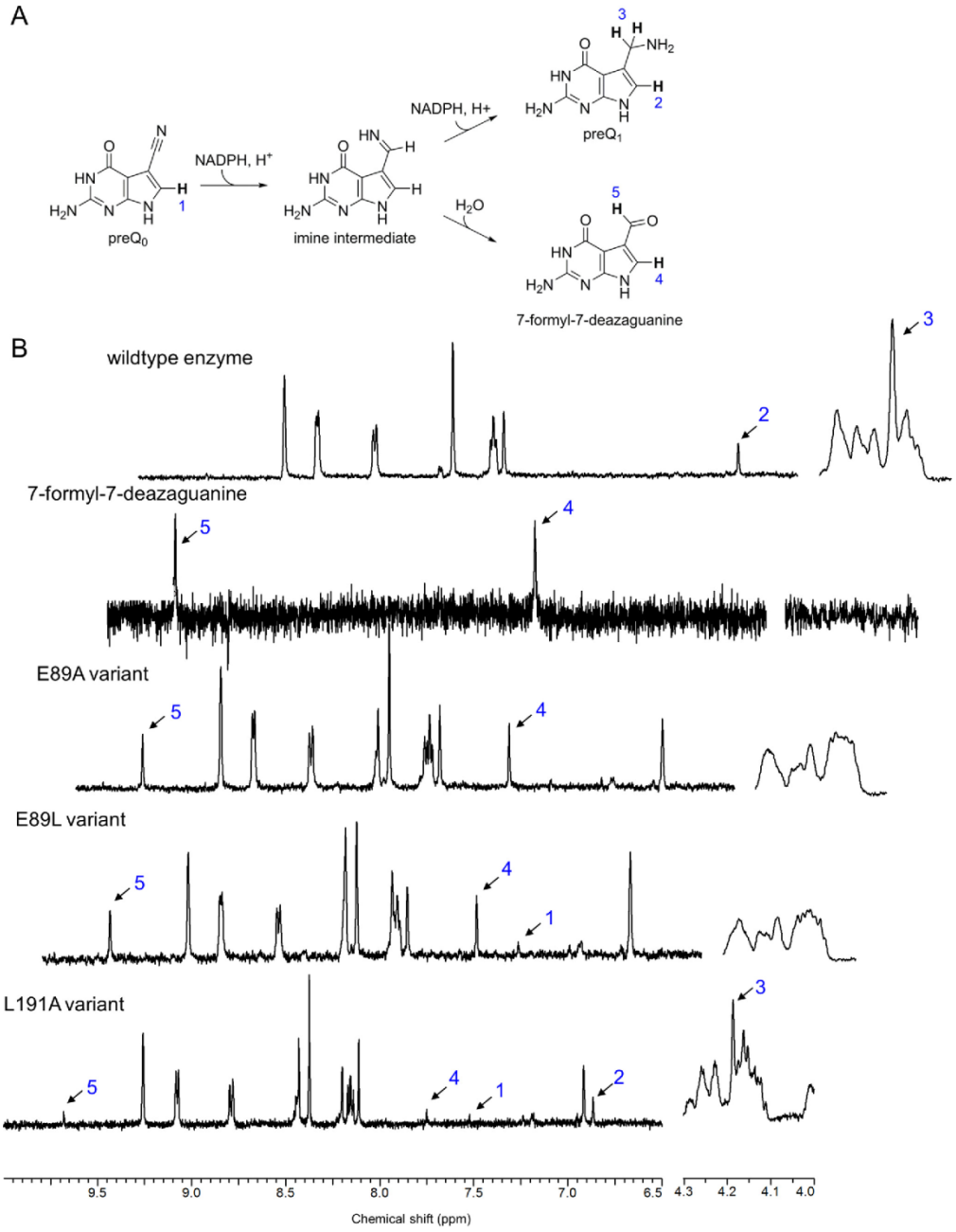

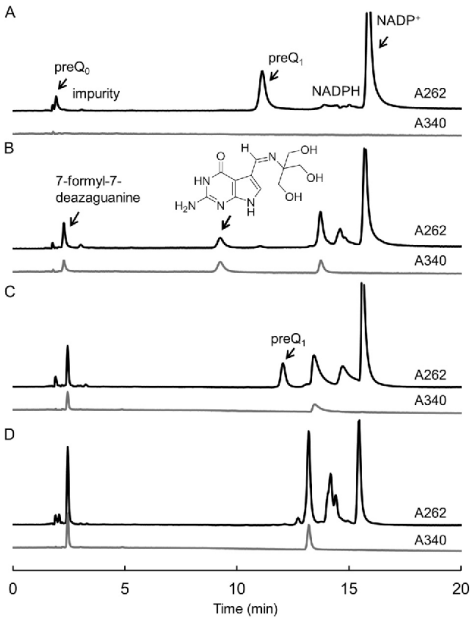

Figure 5. HPLC-MS analysis of the products formed on $preQ_0$ conversion by ecQueF wildtype and variants thereof is shown. The enzyme concentration was varied: 1 μM for wildtype (*A*), 40 μM for E89A (*B*), and 20 μM for each I192A (*C*) and F228A (*D*). The $preQ_0$ concentration was 200 μM, and the NADPH concentration was 500 μM. Incubation at 25 °C proceeded for 3–12 h. The total reaction volume was 1.5 (*A* and *B*) and 0.1 ml (*C* and *D*). *A* and *B*, Tris buffer (100 mM, pH 7.5) containing 50 mM KCl and 1.15 mM tris(2-carboxyethyl)phosphine was used for wildtype enzyme and E89A variant. The Tris-imine complex ($1H^+$, 282) formed in solution between 7-formyl-7-deazaguanine and Tris was separated at 9.2 min. *C* and *D*, phosphate buffer (100 mM Na_2HPO_4-NaH_2PO_4, pH 7.5) containing 50 mM KCl was used for I192A and F228A variant. The $preQ_1$ was separated at 12.8 min (*C*), but it was not detectable in the reaction of the F228A variant (*D*).

Kinetic analysis and KIE studies

To analyze the enzyme kinetics in more detail, and determine primary isotope effects (KIE) from the use of (4*R*)-[^{2}H]NADPH as reductant, we monitored the $preQ_0$ conversion by wildtype and variant enzymes by *in situ* proton NMR and also by LC. Kinetic data obtained from time-course analysis are summarized in Table 3. Material balances were fully consistent with the chemical reaction, $preQ_0 + NADPH + H_3O^+ \rightarrow$ 7-formyl-7-deazaguanine + $NADP^+$ + NH_3, for the variants (E89A, E89L, F228A) carrying out only a single NADPH-dependent reduction of $preQ_0$. At long reaction times (≥24 h), however, decomposition of NADPH became significant as a spontaneous side reaction. The reaction of wildtype ecQueF was confirmed as $preQ_0 + 2\ NADPH + 2H^+ \rightarrow preQ_1 + 2\ NADP^+$. Utilization of NADPH for $preQ_0$ reduction by the L191A and I192A variants was fully consistent with the $preQ_1$ and 7-formyl-7-deazaguanine obtained. Product selectivity of the enzyme variants was confirmed and shown to be constant over the whole time course with prevailing steady-state conditions ([$preQ_0$] > 15 [enzyme dimer]). The specific rate of $preQ_0$ conversion was slowed in the enzyme variants compared with wildtype ecQueF, most strongly in E89L (700-fold), then E89A (160-fold), F228A (140-fold), L191A (24-fold), and I192A (2.7-fold). Using (4*R*)-[^{2}H]NADPH instead of NADPH, we showed that the deuterium was transferred from coenzyme to form 7-formyl-7-deazaguanine (all enzyme variants) and $preQ_1$ (L191A and I192A variants), indicating the same pro-*R* stereoselectivity for NADPH conversion in the variants as in wildtype enzyme (7).

The KIE determined from a direct comparison of reaction rates with NADPH and (4*R*)-[^{2}H]NADPH was 2.9 (±0.7) for the E89A variant, 3.0 (±0.6) for the E89L variant, and 2.8 (±0.4) for the F228A variant. The "reference KIE" for the reaction of the wildtype enzyme was 1.8 (±0.5). The shown KIEs are means (± S.D.) from five independent determinations and represent the averaged isotope effects on the rates of substrate consumption ($preQ_0$, NADPH) and product formation ($preQ_1$ or 7-formyl-7-deazaguanine, $NADP^+$). The L191A and I192A variants differed from the wildtype enzyme and the Glu^{89} and Phe^{228} variants in that their reaction rates based on substrate consumption and product consumption were all affected by a different KIE, as shown in Table 3.

In the reaction of the L191A variant, the KIE on $preQ_0$ consumption was 3.7 (±0.2), higher than the KIE of 2.3 (±0.2) on the release of 7-formyl-7-deazaguanine but lower than the KIE of 5.1 (±0.2) on the main reaction path of the enzyme to $preQ_1$. The KIE on conversion of NADPH to $NADP^+$ was 4.4 (±0.2). Using (4*R*)-[^{2}H]NADPH as coenzyme, the molar ratio between $preQ_1$ and 7-formyl-7-deazaguanine was just 1.8, significantly smaller than the ratio of 4 received from $preQ_0$ reduction by NADPH with the L191A variant.

Using the I192A variant, the ratio of $preQ_1$ to 7-formyl-7-deazaguanine formed in the reaction was 5.4-fold lower when (4*R*)-[^{2}H]NADPH (ratio, 0.48) instead of NADPH was used (ratio, 2.6). The KIE on $preQ_0$ consumption was 4.1 (±0.3), which was higher than the KIE of 1.5 (±0.3) on formation of 7-formyl-7-deazaguanine but lower than the KIE of 8.9 (±0.3) on $preQ_1$ formation. The KIE on conversion of NADPH to $NADP^+$ was 5.0 (±0.6).

There is only one isotope-sensitive step involved in 7-formyl-7-deazaguanine formation: that of reduction of $preQ_0$ to imine. The KIEs for the E89A, E89L, and F228A variants therefore reflect the slowing down of the enzymatic reactions at just this

Figure 4. ^{1}H NMR analysis of the products formed on $preQ_0$ conversion by ecQueF wildtype and variants thereof is shown. *A*, enzymatic routes of conversion of $preQ_0$: 2-fold reduction gives $preQ_1$, whereas single reduction results in an imine that on release to water decomposes to 7-formyl-7-deazaguanine. *B*, ^{1}H NMR spectra of product mixtures obtained with the different enzymes are shown together with spectra of authentic reference material. Phosphate buffer (100 mM, Na_2HPO_4-NaH_2PO_4, pD 7.5, 99.8% D_2O; pD = pH meter reading + 0.4), additionally containing 50 mM KCl and 1.15 mM tris(2-carboxyethyl) phosphine, was used for the reactions of ecQueF wildtype and Glu^{89} variants. NADPH (1.5 mM) and $preQ_0$ (0.5 mM) were added to the enzyme solution. The total reaction volume was 0.6 ml. The spectrum of 7-formyl-7-deazaguanine (3 mM) was obtained in the phosphate buffer. The $preQ_0$ reduction with L191A variant (6 μM) was conducted in Tris buffer (30 mM, pD 7.5) containing 50 mM KCl and 1.15 mM tris(2-carboxyethyl)phosphine). All peaks in the spectra of the ecQueF L191A reaction were slightly shifted by 0.03–0.06 ppm because of the presence of enzyme. The spectra of $preQ_0$, $preQ_1$, and coenzyme were compared with the previously reported spectra of these components (7, 36, 37).

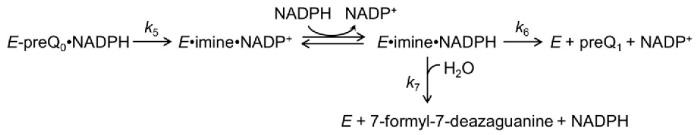

SCHEME 3. **The proposed kinetic mechanism of $preQ_0$ conversion by L191A and I192A variants of ecQueF via partitioning of the imine intermediate between reduction to $preQ_1$ and hydrolysis to 7-formyl-7-deazaguanine is shown.** Covalent (-) and noncovalent (·) binding of substrates/products and coenzymes to the enzyme are indicated. Rate constant numbering starts from Scheme 2 with the assumption that enzyme was saturated with NADPH. Nitrile reduction to imine (k_5) and imine reduction to $preQ_1$ (k_6) are isotope-sensitive steps. Coenzyme exchange in imine intermediate is assumed to be in rapid equilibrium.

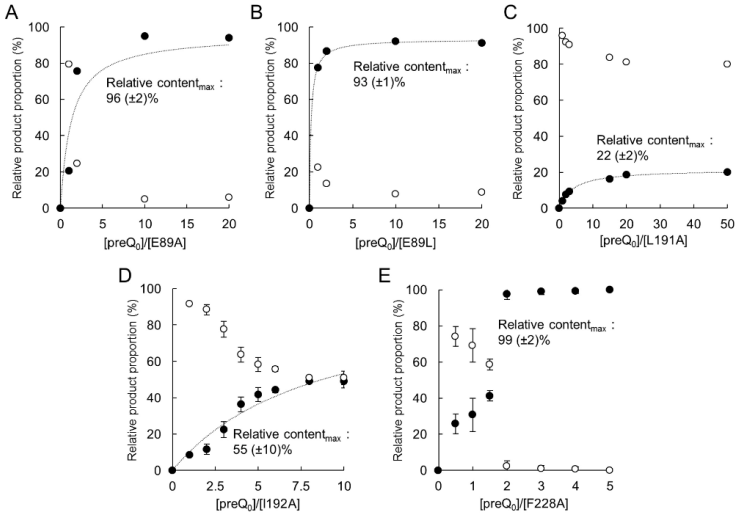

Figure 6. Product distribution analysis for $preQ_0$ reduction by the ecQueF variants is shown. The relative proportion of $preQ_1$ and 7-formyl-7-deazaguanine in total product is shown in dependence of the molar ratio of $preQ_0$ and enzyme ([$preQ_0$]/[E]) used in the reaction. *A*, E89A; *B*, E89L; *C*, L191A; *D*, I192A; *E*, F228A. Phosphate buffer (100 mM Na_2HPO_4-NaH_2PO_4, pH 7.5), additionally containing 50 mM KCl and 1.15 mM tris(2-carboxyethyl)phosphine, was used. The enzyme solution (10, 50, and 100 μM) was mixed with $preQ_0$ (25–500 μM) and NADPH (0.6 or 1.5 mM). After incubation (30 °C, 2–24 h), the samples were analyzed by LC-MS and HPLC. *Open circles* show $preQ_1$, and *closed circles* show 7-formyl-7-deazaguanine. The *dotted line* is a hyperbolic fit to the relative product proportion of 7-formyl-7-deazaguanine, and its maximum relative content is shown.

Table 3

Catalytic reaction rates and their associated KIEs for ecQueF wildtype and variants thereof

The catalytic reaction rates are given as μmol product released (or substrate converted)/(μmol enzyme × min). They were determined individually for each compound participating in the reaction. The reaction rates of substrate ($preQ_0$, NADPH) consumption are negative, and those of product ($preQ_1$, 7-formyl-7-deazaguanine, $NADP^+$) formation are positive. ^DV is the primary KIE, because of deuteration of NADPH, on the catalytic rate. It is the average of the five individual KIEs determined from $preQ_0$, $preQ_1$, 7-formyl-7-deazaguanine, NADH, and $NADP^+$. Each individual KIE is the average of five independent reactions. Note that in reactions of the E89A, E89L, and F228A variants, which perform a single-step reduction of $preQ_0$ to produce 7-formyl-7-deazaguanine, the experimental ^DV equals $^Dk_5$ according to Scheme 3. In the wildtype enzyme, ^DV involves contribution from the KIEs on k_5 and k_6.

	Wildtype enzyme	E89A	E89L	L191A	I192A	F228A
$preQ_0$	−4.1 ± 0.1	−0.025 ± 0.001	−0.006 ± 0.001	−0.17 ± 0.03 (3.7 ± 0.2)[a]	−1.5 ± 0.3 (4.1 ± 0.3)[a]	−0.030 ± 0.006
$preQ_1$	3.9 ± 0.3			0.16 ± 0.02 (5.1 ± 0.2)[a] [2.2][b]	0.8 ± 0.1 (8.9 ± 0.3)[a] [5.4][b]	
7-Formyl-7-deazaguanine		0.022 ± 0.001	0.006 ± 0.001	0.03 ± 0.01 (2.3 ± 0.2)[a]	0.3 ± 0.1 (1.5 ± 0.3)[a]	0.035 ± 0.006
NADPH	−8.4 ± 0.4	−0.018 ± 0.007	−0.005 ± 0.002	−0.27 ± 0.02 (4.4 ± 0.2)[a]	−1.1 ± 0.1 (5.0 ± 0.6)[a]	−0.022 ± 0.005
$NADP^+$	7.6 ± 0.3	0.022 ± 0.001	0.009 ± 0.001	0.29 ± 0.02 (4.4 ± 0.2)[a]	1.8 ± 0.3 (5.3 ± 0.5)[a]	0.024 ± 0.005
^DV	1.8 ± 0.5	2.9 ± 0.7	3.0 ± 0.6	NA[c]	NA[c]	2.8 ± 0.4

[a] In parentheses is shown the primary KIE on the consumption rate or the formation rate of the compound indicated.
[b] The KIE on imine reduction (k_6 in Scheme 3) is shown in square brackets. As explained in text, this KIE is the same as the KIE on the experimental product ratio *R*, $preQ_1$/7-formyl-7-deazaguanine, formed in the reaction.
[c] NA, not applicable. Contrary to the wildtype enzyme and the E89A, E89L, and F228A variants in which ^DV was not dependent on whether substrate consumption or product formation was analyzed and so an average value could be given, the L191A and I192A variants necessitated KIE evaluation separately for each compound involved in the reaction. The concept of an average KIE was therefore not applicable.

step. The individual KIEs associated with reductions of the $preQ_0$ substrate and the imine intermediate by wildtype ecQueF were determined previously as 3.3 and 1.8, respectively (7). Global fitting of reaction time courses of $preQ_0$ conversion were used in our earlier study (7) to obtain these KIEs. The KIEs on conversion of $preQ_0$ to 7-formyl-7-deazaguanine by the

Glu[89] variants and the F228A variant were of a similar magnitude as the first-step KIE, *i.e.* $preQ_0$ reduction to imine, for the reaction of wildtype ecQueF.

In the L191A and the I192A variant, partitioning of the imine intermediate between reaction to $preQ_1$ and reaction to 7-formyl-7-deazaguanine constitutes the point of departure for analyzing the different KIEs in these two enzymes. The molar ratio (R) of $preQ_1$ and 7-formyl-7-deazaguanine reflects the rate constant ratio of imine reduction/imine hydrolysis (k_6/k_7), as shown in the kinetic mechanism depicted in Scheme 3. Because only the imine reduction is sensitive to isotopic substitution in coenzyme, the isotope effect on the product ratio (4/1.8 = 2.22 for L191A; 2.6/0.48 = 5.4 for I192A) is also the KIE on k_6. A KIE on $preQ_0$ conversion smaller than on $preQ_1$ formation arises because partitioning of the imine intermediate is also subject to an isotope effect. The fraction of imine intermediate reacting to 7-formyl-7-deazaguanine is defined from Scheme 3 as $F = 1/(1 + R)$. F has a value of 0.2 and 0.36 in L191A reactions with NADPH (F_H) and NADPD (F_D), respectively. The corresponding F values for the I192A variant are 0.28 (F_H) and 0.67 (F_D). The relative flux from $preQ_0$ to 7-formyl-7-deazaguanine, therefore, increases 1.8-fold (L191A variant) and 2.4-fold (I192A variant) because of deuteration of the coenzyme. Considerations of flux balance reveal the set of KIE data for the L191A and the I192A variant to be internally consistent.

With F_H and F_D known, the KIE on $preQ_0$ consumption obtains, according to Scheme 3, from the KIE on $preQ_1$ formation as $KIE\_preQ_0 = KIE\_preQ_1\ (1 - F_D)/(1 - F_H)$. The calculated value of KIE_preQ_0 is therefore 4.08 for the L191A variant. The same value is obtained for the I192A variant. The KIE on formation of 7-formyl-7-deazaguanine obtains from the relationship, $KIE\_preQ_0\ F_H/F_D$, as 2.27 and 1.70 for the L191A and the I192A variant, respectively. Finally, the KIE on NADPH consumption, which is the same as the KIE on $NADP^+$ formation, is calculated with the relationship, $KIE\_preQ_0\ (2 - F_H)/(2 - F_D)$, as 4.48 and 5.28 for the L191A and the I192A variant, respectively. These calculated KIE data agree well the experimentally obtained values.

Evidence summarized in Table 3 shows that in $preQ_1$ formation the complete reaction of the L191A or the I192A variant was affected by a substantially larger KIE than the partial reaction of imine reduction (k_6) and identifies nitrile reduction to imine as the rate-determining step of the overall $preQ_0$ conversion by these two ecQueF variants. Linear time courses of NADPH consumption by the enzyme, with no sign of a pre-steady state burst, were consistent with this notion (data not shown).

Discussion

Conversion of $preQ_0$ to 7-formyl-7-deazaguanine represents the first reaction of this kind catalyzed by an enzyme. Chemically, it consists in a single hydride transfer reduction of a nitrile group from NADPH followed by the addition of water to the imine thus obtained. Catalysis from the enzyme is required only for nitrile reduction. Imine hydrolysis is a spontaneous reaction, well established from other enzymatic transformations, like those of amino acid dehydrogenases for instance (25–27). Mechanistically, the "interrupted" (two-electron) reduction of

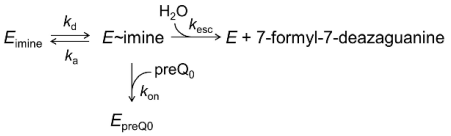

SCHEME 4. **A hypothetical kinetic mechanism of ecQueF-imine complex dissociation induced by $preQ_0$ is shown.** *E* is the free enzyme. The enzyme-bound $preQ_0$ and imine are indicated by *subscript*. *E~imine* indicates a preassociated complex of ecQueF with imine intermediate. The model is adapted from literature (28).

$preQ_0$ is significant, for it provides first-time direct evidence on the occurrence of an imine intermediate in the reaction pathway of QueF nitrile reductases. In addition to reinforcing the current mechanistic proposal for QueF (Scheme 1) (3, 5–7), these results advance comprehension of the mode of action of the enzyme, demonstrating how critically important imine intermediate sequestration is for complete 2-fold reduction of $preQ_0$ to $preQ_1$. The finding that site-directed substitutions interferring most significantly with intermediate sequestration (*e.g.* Glu[89] and Phe[228]) were also strongly disruptive on the hydride transfer revealed that the major physical steps of the enzymatic process proceeded tightly interconnected with the catalytic act(s). It furthermore indicated that ecQueF made parsimonious use of its active-site structural devices to accomplish the different tasks in the overall multistep catalytic reaction. The thermodynamic signatures of $preQ_0$ binding by the different ecQueF variants appear consistent with the enzyme–substrate interactions revealed in the crystallographic evidence on vcQueF (Fig. 1).

The hydride transfers from NADPH are the slowest steps in the overall conversion of $preQ_0$ to $preQ_1$ by ecQueF (7). Evidence that catalytic rates were lowered by up to ~700-fold in the ecQueF variants, whereas their associated KIEs caused by deuteration of the coenzyme were not decreased as compared with the wildtype KIEs, strongly supports the suggestion that catalysis was also rate-limiting in the enzyme variants. The crucial importance of substrate positioning at the stage of imine reduction was most vividly evident from the fact that substitutions of Leu[191] and Ile[192], and even more so those of Glu[89] and Phe[228], caused loss of imine from the enzyme during the reaction. The fraction of $preQ_0$, which on conversion by the ecQueF variants did not make it through to the fully reduced amine $preQ_1$, increased dependent on the substrate amount present. A simple model, having $preQ_0$ compete with imine intermediate for binding to the enzyme in rapid equilibrium, fails to explain the experimental product distributions, for it predicts that at "saturating" [$preQ_0$], no $preQ_1$ will be formed. This is most evidently refuted from the behavior of the L191A and the I192A variants.

Formally, a general model of molecular complex dissociation, induced by a competing ligand as shown in literature (28), would be consistent with the effect of [$preQ_0$] on the product distribution in the ecQueF variants (Scheme 4). The model involves ligand dissociation effectively from a preassociated complex, which enables rapid rebinding of the ligand to give the actual biological form of the complex. The model predicts that competitor molecules will accelerate the breakdown of

enzyme–ligand complexes by occluding the rapid rebinding of enzyme and ligand from the level of their preassociated complex. It is therefore worth noting that the model does not imply the formation of a ternary complex between enzyme, ligand and competitor. The ligand dissociation rate (k_{off}), enhanced in the presence of competitor (C), is thus given by the relationship, derived from Scheme 4, $k_{off}(C) = k_d \times (k_{esc} + k_{on}C) \div (k_a + k_{esc} + k_{on}C)$, where k_a and k_d are first-order association and dissociation rate constants for (rapid) formation of the fully associated complex from the preassociated complex, k_{esc} is the first-order rate constant of ligand release into solution, and k_{on} is the rate constant for competitor binding (28). Note that the k_{esc} step involves hydrolysis of imine. Scheme 4 does not distinguish mechanistically between whether the hydrolysis occurs in solution or, more likely, with imine still bound to the enzyme.

The results in Fig. 6 suggest that the ecQueF variants differed in the relative contribution of k_{esc} and k_{on} to k_{off}. Whereas in the E89L variant the escape of imine appeared to be largely controlled by k_{esc} (because k_{off} was hardly dependent on the $preQ_0$ concentration), the product formation by the L191A and I192A variants reflected a prominent effect from k_{on}. The E89A variant adopted an intermediate position between the two extremes, with both k_{esc} and k_{on} affecting the product distribution dependent on the competitor $preQ_0$. A molecular account of the proposed kinetic scenario for ecQueF is not easy to conceive, and the model is essentially independent of such details. However, a preassociated enzyme–imine complex in a somewhat open conformation might make possible the kinetically implied displacement of the imine by $preQ_0$.

In conclusion, identification of residues in the catalytic apparatus of ecQueF essential (Glu^{89} and Phe^{228}) or auxiliary (Leu^{191} and Ile^{192}) for complete 2-fold reduction of nitrile to amine has led to uncover the imine intermediate, and the necessity of its efficient sequestration in the active site, as central features of the enzymatic mechanism. Structure-based interpretation of the effect of site-directed substitutions on the reaction selectivity of ecQueF is that because of a substrate-binding site (Fig. 1, *B* and *C*) not fully closable any longer, the enzyme variants lose the imine intermediate to hydrolysis, completely in E89A, E89L, and F228A and partly in L191A and I192A. Although not proven by the evidence shown, a likely scenario is that the imine is captured by water now able to enter the partly opened-up active site in the variant enzymes. The hydrolyzed imine, 7-formyl-7-deazaguanine, is not recognized by ecQueF as a substrate of NADPH-dependent reduction, as demonstrated previously (7). It would therefore be released into solvent.

Although in terms of reaction catalyzed, QueF nitrile reductases share commonalities with other four-electron reductases, such as 3-hydroxy-3-methyl-glutaryl-coenzyme A reductase (29–31) and the nonribosomal peptide synthetase module myxalamid reductase (32, 33) that use NAD(P)H to convert thioester-activated forms of carboxylic acids into primary alcohols via an aldehyde intermediate, they are individuated strongly from these other enzymes in having to deal with a highly decomposition-prone intermediate. The central role of intermediate sequestration in the QueF mechanism seems to be reflected in the fact that structural devices used to keep a firm grip on the imine intermediate are likewise involved directly in the catalytic events of the enzymatic reaction.

Experimental procedures

Chemicals and materials used

NADPH (purity, >98%) and $NADP^+$ (purity, >97%) were from Carl Roth (Karlsruhe, Germany). 2-Propanol-d_8 (99.5 atom % D) was from Sigma. All other materials were of the highest purity available from Carl Roth and Sigma. The $preQ_0$ and 7-formyl-7-deazaguanine were synthesized as described previously (7, 19). A pET-28a(+) expression vector encoding *Thermoanaerobium brockii* alcohol dehydrogenase as an N-terminally His-tagged protein was ordered from GenScript (Piscataway, NJ). Standard expression in *E. coli* BL21-DE3 and His-tag purification were used to prepare the enzyme.

Site-directed mutagenesis

Mutagenesis leading to site-directed substitution of Leu^{191} by Ala (L191A) was performed according to a standard two-stage PCR protocol (34, 35). A pEHISTEV expression vector comprising the ecQueF gene was used as the template. The oligonucleotide primers used are shown with the mismatched bases underlined: L191A forward, 5′-GCTGAAATCAAACTGCGCGATCACCCATCAACC-3′; and L191A reverse, 5′-GGTTGATGGGTGATCGCGCAGTTTGATTTCAGC-3′. Mutagenesis to substitute Glu^{89} by Ala or Leu was reported in an earlier study (21). Replacement of Ile^{192} or Phe^{228} by Ala was ordered from Genscript. All mutations were verified by gene sequencing.

Enzyme preparation

The ecQueF wildtype and site-directed variants thereof (E89A, E89L, L191A, I192A, and F228A) were obtained as N-terminally His-tagged proteins using expression in *E. coli* BL21-DE3 as described previously (7, 21). All enzymes were purified by a reported two-step procedure, consisting of immobilized metal ion affinity chromatography and gel filtration (7). Enzyme purity was confirmed by SDS-PAGE. The background of the *E. coli* expression host did not contain QueF activity in amounts detectable with the assays used. Contamination of ecQueF variants with endogenous wildtype activity could thus be ruled out firmly. The protein concentration was measured with a Pierce BCA protein assay kit (Thermo Fisher Scientific). Enzyme stock solutions (0.8–1.2 mM) were stored at −20 °C and used up within 3 weeks because of limited stability.

ITC and spectrophotometric analysis of $preQ_0$ binding in ecQueF variants

A VP-ITC micro calorimeter from Microcal (Malvern Instruments Ltd., Malvern, UK) was used at 25 °C. The enzyme was gel-filtered twice to phosphate buffer (100 mM Na_2HPO_4-NaH_2PO_4, pH 7.5, 50 mM KCl) using illustra NAP 5 columns (GE Healthcare). A DMSO concentration of maximally 2.0% (v/v) was used in both the enzyme and the $preQ_0$ solution. The experiments were conducted, and data evaluation done as described previously (7). The enzyme molar concentration was based on the protein concentration assuming a functional

ecQueF homodimer with a molecular mass of 71,772 Da (wildtype enzyme), 71,656 Da (E89A variant), 71,740 Da (E89L variant), 71,688 Da (L191A or I192A variant), or 71,620 Da (F228A variant).

The covalent thioimide adduct between $preQ_0$ and ecQueF in wildtype or variant form was detected from its characteristic absorbance with maximum absorption at ~380 nm. Absorbance titrations were carried out with a Beckman DU 800 spectrophotometer (Beckman Coulter, Pasadena, CA) as described previously (7). Kinetic study of the thioimide formation was done with a SX.18 MV Stopped flow spectrophotometer (Applied Photophysics; Leatherhead, UK). The experimental progress curves of absorbance (380 nm) increase recorded at different protein, and $preQ_0$ concentrations were analyzed by a global fitting procedure, as previously described (7), that employed the program COPASI (version 4.11_build 65) and used the mechanism in Scheme 2. A least-squares fitting routine implemented in COPASI was used to determine the kinetic rate constants and their standard deviations. In the fitting, k_1 and k_2 were not determined individually, but only their ratio $K_{d\ \mathrm{kinetic}}$ (which equals k_2/k_1) was obtained. We showed that the fitting always converged to a unique and well defined solution that was independent of the parameter start values used. All fitted parameters ($K_{d\ \mathrm{kinetic}}$, k_3, and k_4) were well determined as regards their associated standard deviation. An overall binding constant ($K_{d\ \mathrm{overall}}$) was calculated from the results, using the relationship $K_{d\ \mathrm{overall}} = K_{d\ \mathrm{kinetic}}/(1 + k_3/k_4)$. Note that $K_{d\ \mathrm{overall}}$ thus includes the covalent thioimide formation.

Binding constants were transformed into binding energies using the relationship $\Delta G = -RT\ln K_d$. A 1 M standard state for all reactants was assumed. R is the gas constant (8.314 J/mol·K), and T is the temperature (298.15 K).

Enzymatic reduction of preQ$_0$

Experiments were performed to characterize the $preQ_0$ conversion by the different ecQueF enzymes. In addition to determining the specific rate of substrate consumption, determination of the product(s) formed by $preQ_0$ reduction was of main interest. Reactions were carried out by incubating buffered solutions of enzyme, $preQ_0$, and NADPH on a Thermomixer Comfort (Eppendorf, Hamburg, Germany) at 25 °C with agitation at 700 rpm for ~24 h. The DMSO concentration used was below 2.5%. The concentrations of $preQ_0$ and NADPH were varied as indicated. The enzyme concentration was 50 μM (E89A, E89L, I192A, and F228A variants), 10 μM (L191A variant), and 1.8 μM (wildtype enzyme). The reactions were stopped by precipitating the enzyme with methanol (10%, by volume) at 70 °C for 10 min (1000 rpm in a Thermomixer Comfort) (7). Samples were applied to ^{1}H NMR, HPLC, and LC-MS from comprehensive analysis.

HPLC analytics

The samples were analyzed using an Agilent 1200 HPLC system (Santa Clara, CA) equipped with a 5-μm SeQuant ZIC-HILIC column (200 Å, 250 × 2.1 mm; Merck), the corresponding guard column (20 × 2.1 mm; Merck), and a UV detector (λ = 262 and 340 nm). A 20 mM ammonium acetate buffer (pH 6.67) was used. A decreasing gradient in acetonitrile was applied for compound separation over a 20-min run time. Specifically, the acetonitrile concentration was decreased only slightly from 80 to 78% over 5 min, and a steeper ramp from 78 to 60% was then used from 5 to 20 min. The column was washed with 60 and 80% acetonitrile for 5 min after each analysis. The flow rate was 0.5 ml/min. The column temperature was 30 °C.

Optionally, a mass detector (Agilent 6200 Quadrupole) was coupled to the HPLC system, which in this case was equipped with a 2.7-μm Poroshell 120 EC-C18 column (120 Å, 100 × 3 mm; Agilent) and a UV detector (λ = 210, 262, and 340 nm). The masses of the products from the enzymatic reactions were scanned in a mass range of 100 – 850 using a positive mode. The masses of $preQ_0$ ($1H^+$, 176), $preQ_1$ ($1H^+$, 180), and 7-formyl-7-deazaguanine ($1H^+$, 179) were also analyzed in SIM mode. A linear gradient of acetonitrile was used in water containing 0.01% formic acid. The gradient was from 0% to 25% acetonitrile over 5 min. The column was washed with 90% acetonitrile for 1 min and water for 0.5 min. The post time was 1 min. The flow rate was 0.7 ml/min. The column temperature was 30 °C.

^{1}H NMR measurements

NMR spectra were recorded at 499.98 MHz and 30 °C using a Varian INOVA 500-MHz spectrometer (Agilent Technologies) with VNMRJ 2.2D software. The spectra of coenzymes, $preQ_0$ and $preQ_1$ in D_2O/H_2O solution were reported previously (7, 36, 37). The reduction of $preQ_0$ by the different ecQueF enzymes was monitored by *in situ* ^{1}H NMR measurements that involved presaturation of the residual water signal. Tris buffer (30 mM, pH 7.5) in 120 mM KCl was used that also contained an internal standard solution of 30 μl (trimethylamine hydrochloride, 1.82×10^{-5} mol/liter; trimethylsilylpropanoic acid, 0.05% in 99.5% D_2O) to obtain data for correct integration. The D_2O content was 14% (v/v), and the total reaction volume was 0.6 ml. The reactions were started through addition of the enzyme. Spectra of the reaction with wildtype ecQueF or the L191A variant were collected at every 5–20 min for 5–20 h in the magnet. Because the reactions with the Glu^{89} variants were relatively slow, the spectra were collected for 48 h in the magnet, and the solutions were temporarily kept at room temperature. The data were analyzed in the software program ACD/NMR processor academic edition (version 12.01_build 39104). The total amount of 7-formyl-7-deazaguanine formed in the reaction was determined from the free aldehyde product present and the corresponding imine adduct between 7-formyl-7-deazaguanine and Tris (3.82 ppm in ^{1}H NMR spectra, not shown).

KIE studies

NADPH and (4*R*)-[^{2}H]NADPH were prepared by reducing $NADP^+$ in the oxidation of 2-propanol and 2-propanol-d_8 with *T. brockii* alcohol dehydrogenase. A reported protocol was used for their synthesis (7, 38). Primary KIEs on $preQ_0$ reduction were obtained by comparing initial rates measured with NADPH and (4*R*)-[^{2}H]NADPH, both synthesized as described above. Enzymatic reactions were monitored by HPLC and for certain enzymes (wildtype, E89A, E89L, and L191A) additionally by *in situ* ^{1}H NMR. The initial rates were obtained from linear fits to HPLC or spectral data. Note that because all sub-

strates and products of the reaction were measured in the analysis, a total of four or five reaction rates was obtained: $preQ_0$ and NADPH consumption and $preQ_1$, 7-formyl-7-deazaguanine, and $NADP^+$ formation. The enzyme concentrations used in the reactions were as follows: wildtype, 1.5 μM; E89A and E89L, 25 μM; L191A, 8 μM; I192A, 10 μM; and F228A, 20 μM. The $preQ_0$ concentration was saturating, that is, 500 μM using the wildtype enzyme, the L191A, and the I192A variant and 800 μM using the E89A, the E89L and the F228A variant. The NADPH concentration was 1.5 mM. The temperature was 30 °C. The DMSO concentration was always at or below 2%. Phosphate buffer (100 mM Na_2HPO_4-NaH_2PO_4, pH 7.5) containing 50 mM KCl was used.

Author contributions—J. J. and B. N. designed the research and wrote the paper. J. J. conducted experiments and analyzed data together with B. N. All authors agreed on the final version of the paper.

Acknowledgments—We thank Prof. Norbert Klempier and Dr. Birgit Wilding (Institute of Organic Chemistry, Graz University of Technology) for providing $preQ_0$ and 7-formyl-7-deazaguanine; Dr. Tibor Czabany (Institute of Biotechnology and Biochemical Engineering, Graz University of Technology) for HPLC analysis; Jan Braun (Institute of Biotechnology and Biochemical Engineering, Graz University of Technology) for site-directed mutagenesis; Dr. Hansjörg Weber (Institute of Organic Chemistry, Graz University of Technology) for ^{1}H NMR measurements; and Dr. Gernot Strohmeier (Austrian Centre of Industrial Biotechnology) for HPLC-MS analysis.

References

1. Knowles, J. R. (1991) Enzyme catalysis: not different, just better. *Nature* **350,** 121–124 CrossRef Medline
2. Richard, J. P., Amyes, T. L., Goryanova, B., and Zhai, X. (2014) Enzyme architecture: on the importance of being in a protein cage. *Curr. Opin. Chem. Biol.* **21,** 1–10 CrossRef Medline
3. Lee, B. W., Van Lanen, S. G., and Iwata-Reuyl, D. (2007) Mechanistic studies of *Bacillus subtilis* QueF, the nitrile oxidoreductase involved in queuosine biosynthesis. *Biochemistry* **46,** 12844–12854 CrossRef Medline
4. Kim, Y., Zhou, M., Moy, S., Morales, J., Cunningham, M. A., and Joachimiak, A. (2010) High-resolution structure of the nitrile reductase QueF combined with molecular simulations provide insight into enzyme mechanism. *J. Mol. Biol.* **404,** 127–137 CrossRef Medline
5. Chikwana, V. M., Stec, B., Lee, B. W., de Crécy-Lagard, V., Iwata-Reuyl, D., and Swairjo, M. A. (2012) Structural basis of biological nitrile reduction. *J. Biol. Chem.* **287,** 30560–30570 CrossRef Medline
6. Ribeiro, A. J., Yang, L., Ramos, M. J., Fernandes, P. A., Liang, Z.-X., and Hirao, H. (2015) Insight into enzymatic nitrile reduction: QM/MM study of the catalytic mechanism of QueF nitrile reductase. *ACS Catal.* **5,** 3740–3751 CrossRef
7. Jung, J., Czabany, T., Wilding, B., Klempier, N., and Nidetzky, B. (2016) Kinetic analysis and probing with substrate analogues of the reaction pathway of the nitrile reductase QueF from *Escherichia coli*. *J. Biol. Chem.* **291,** 25411–25426 CrossRef Medline
8. Iwata-Reuyl, D. (2003) Biosynthesis of the 7-deazaguanosine hypermodified nucleosides of transfer RNA. *Bioorg. Chem.* **31,** 24–43 CrossRef Medline
9. Van Lanen, S. G., Reader, J. S., Swairjo, M. A., de Crécy-Lagard, V., Lee, B., and Iwata-Reuyl, D. (2005) From cyclohydrolase to oxidoreductase: discovery of nitrile reductase activity in a common fold. *Proc. Natl. Acad. Sci. U.S.A.* **102,** 4264–4269 CrossRef Medline
10. Harada, F., and Nishimura, S. (1972) Possible anticodon sequences of tRNAHis, tRNAAsn, and tRNAAsp from *Escherichia coli*: universal presence of nucleoside Q in the first position of the anticodons of these transfer ribonucleic acid. *Biochemistry* **11,** 301–308 CrossRef Medline
11. El Yacoubi, B., Bailly, M., and de Crécy-Lagard, V. (2012) Biosynthesis and function of posttranscriptional modifications of transfer RNAs. *Annu. Rev. Genet.* **46,** 69–95 CrossRef Medline
12. Reader, J. S., Metzgar, D., Schimmel, P., and de Crécy-Lagard, V. (2004) Identification of four genes necessary for biosynthesis of the modified nucleoside queuosine. *J. Biol. Chem.* **279,** 6280–6285 CrossRef Medline
13. Vinayak, M., and Pathak, C. (2009) Queuosine modification of tRNA: its divergent role in cellular machinery. *Biosci. Rep.* **30,** 135–148 CrossRef Medline
14. Dineshkumar, T. K., Thanedar, S., Subbulakshmi, C., and Varshney, U. (2002) An unexpected absence of queuosine modification in the tRNAs of an *Escherichia coli* B strain. *Microbiology* **148,** 3779–3787 CrossRef Medline
15. Durand, J. M., Okada, N., Tobe, T., Watarai, M., Fukuda, I., Suzuki, T., Nakata, N., Komatsu, K., Yoshikawa, M., and Sasakawa, C. (1994) VacC, a virulence-associated chromosomal locus of *Shigella flexneri*, is homologous to tgt, a gene encoding tRNA-guanine transglycosylase (tgt) of *Escherichia coli* K-12. *J. Bacteriol.* **176,** 4627–4634 CrossRef Medline
16. Grädler, U., Gerber, H. D., Goodenough-Lashua, D. M., Garcia, G. A., Ficner, R., Reuter, K., Stubbs, M. T., and Klebe, G. (2001) A new target for shigellosis: rational design and crystallographic studies of inhibitors of tRNA-guanine transglycosylase. *J. Mol. Biol.* **306,** 455–467 CrossRef Medline
17. Domínguez de María, P. (2011) Nitrile reductases: a forthcoming wave in biocatalysis? *ChemCatChem.* **3,** 1683–1685 CrossRef
18. Colloc'h, N., Poupon, A., and Mornon, J. P. (2000) Sequence and structural features of the T-fold, an original tunnelling building unit. *Proteins* **39,** 142–154 CrossRef Medline
19. Wilding, B., Winkler, M., Petschacher, B., Kratzer, R., Glieder, A., and Klempier, N. (2012) Nitrile reductase from *Geobacillus kaustophilus*: a potential catalyst for a new nitrile biotransformation reaction. *Adv. Synth. Catal.* **354,** 2191–2198 CrossRef
20. Mohammad, A., Bon Ramos, A., Lee, B. W., Cohen, S. W., Kiani, M. K., Iwata-Reuyl, D., Stec, B., and Swairjo, M. A. (2017) Protection of the queuosine biosynthesis enzyme QueF from irreversible oxidation by a conserved intramolecular disulfide. *Biomolecules* **7,** E30 Medline
21. Wilding, B., Winkler, M., Petschacher, B., Kratzer, R., Egger, S., Steinkellner, G., Lyskowski, A., Nidetzky, B., Gruber, K., and Klempier, N. (2013) Targeting the substrate binding site of *E. coli* nitrile reductase QueF by modeling, substrate and enzyme engineering. *Chem. Eur. J.* **19,** 7007–7012 CrossRef Medline
22. Moeller, K., Nguyen, G. S., Hollmann, F., and Hanefeld, U. (2013) Expression and characterization of the nitrile reductase QueF from *E. coli*. *Enzyme Microb. Technol.* **52,** 129–133 CrossRef Medline
23. Gjonaj, L., Pinkse, M., Fernández-Fueyo, E., Hollmann, F., and Hanefeld, U. (2016) Substrate and cofactor binding to nitrile reductase: a mass spectrometry based study. *Catal. Sci. Technol.* **6,** 7391–7397 CrossRef
24. Li, M., Zhou, Z., Zhang, Z. J., Yu, H. L., and Xu, J. H. (2016) Biochemical properties of a new nitrile reductase cloned from *Pectobacterium carotovorum*. *J. Mol. Catal. B Enzym.* **131,** 47–54 CrossRef
25. Stillman, T. J., Baker, P. J., Britton, K. L., and Rice, D. W. (1993) Conformational flexibility in glutamate dehydrogenase: role of water in substrate recognition and catalysis. *J. Mol. Biol.* **234,** 1131–1139 CrossRef Medline
26. Brunhuber, N. M., and Blanchard, J. S. (1994) The biochemistry and enzymology of amino acid dehydrogenases. *Crit. Rev. Biochem. Mol. Biol.* **29,** 415–467 CrossRef Medline
27. Brunhuber, N. M., Thoden, J. B., Blanchard, J. S., and Vanhooke, J. L. (2000) *Rhodococcus* L-phenylalanine dehydrogenase: kinetics, mechanism, and structural basis for catalytic specifity. *Biochemistry* **39,** 9174–9187 CrossRef Medline
28. Paramanathan, T., Reeves, D., Friedman, L. J., Kondev, J., and Gelles, J. (2014) A general mechanism for competitor-induced dissociation of molecular complexes. *Nat. Commun.* **5,** 5207 CrossRef Medline
29. Friesen, J. A., and Rodwell, V. W. (2004) The 3-hydroxy-3-methylglutaryl coenzyme-A (HMG-CoA) reductases. *Genome Biol.* **5,** 248 CrossRef Medline

30. Haines, B. E., Wiest, O., and Stauffacher, C. V. (2013) The increasingly complex mechanism of HMG-CoA reductase. *Acc. Chem. Res.* **46,** 2416–2426 CrossRef Medline
31. Oliveira, E. F., Cerqueira, N. M. F. S. A., Ramos, M. J., and Fernandes, P. A. (2016) QM/MM study of the mechanism of reduction of 3-hydroxy-3-methylglutaryl coenzyme A catalyzed by human HMG-CoA reductase. *Catal. Sci. Technol.* **6,** 7172–7185 CrossRef
32. Chhabra, A., Haque, A. S., Pal, R. K., Goyal, A., Rai, R., Joshi, S., Panjikar, S., Pasha, S., Sankaranarayanan, R., and Gokhale, R. S. (2012) Nonprocessive $[2 + 2]e^-$ off-loading reductase domains from mycobacterial nonribosomal peptide synthetases. *Proc. Natl. Acad. Sci. U.S.A.* **109,** 5681–5686 CrossRef Medline
33. Barajas, J. F., Phelan, R. M., Schaub, A. J., Kliewer, J. T., Kelly, P. J., Jackson, D. R., Luo, R., Keasling, J. D., and Tsai, S. C. (2015) Comprehensive structural and biochemical analysis of the terminal myxalamid reductase domain for the engineered production of primary alcohols. *Chem. Biol.* **22,** 1018–1029 CrossRef Medline
34. Wang, W., and Malcolm, B. A. (1999) Two-stage PCR protocol allowing introduction of multiple mutations, deletions and insertions using QuikChange site-directed mutagenesis. *BioTechniques* **26,** 680–682 Medline
35. Schmölzer, K., Luley-Goedl, C., Czabany, T., Ribitsch, D., Schwab, H., Weber, H., and Nidetzky, B. (2014) Mechanistic study of CMP-Neu5Ac hydrolysis by α2,3-sialyltransferase from *Pasteurella dagmatis*. *FEBS Lett.* **588,** 2978–2984 CrossRef Medline
36. Ragg, E., Scaglioni, L., Mondelli, R., Carelli, I., Casini, A., and Tortorella, S. (1991) ^{1}H-, ^{13}C-, ^{31}P-NMR studies and conformational analysis of $NADP^+$, NADPH coenzymes and of dimers from electrochemical reduction of $NADP^+$. *Biochim. Biophys. Acta.* **1076,** 49–60 CrossRef Medline
37. Klepper, F., Polborn, K., and Carell, T. (2005) Robust synthesis and crystal-structure analysis of 7-cyano-7-deazaguanine ($preQ_0$ base) and 7-(aminomethyl)-7-deazaguanine ($preQ_1$ base). *Helv. Chim. Acta.* **88,** 2610–2616 CrossRef
38. Jeong, S. S., and Gready, J. E. (1994) A method of preparation and purification of (4*R*)-deuterated-reduced nicotinamide adenine dinucleotide phosphate. *Anal. Biochem.* **221,** 273–277 CrossRef Medline

Evidence of a sequestered imine intermediate during reduction of nitrile to amine by the nitrile reductase QueF from *Escherichia coli*

Jihye Jung and Bernd Nidetzky

J. Biol. Chem. 2018, 293:3720-3733.
doi: 10.1074/jbc.M117.804583 originally published online January 16, 2018

Interplay of nucleophilic catalysis with proton transfer in the nitrile reductase QueF from *Escherichia coli*

Interplay of nucleophilic catalysis with proton transfer in the nitrile reductase QueF from *Escherichia coli*

Jihye Jung[1,2], Jan Braun[1], Tibor Czabany[1,2] and Bernd Nidetzky[1,2*]

From the [1]Institute of Biotechnology and Biochemical Engineering, Graz University of Technology, NAWI Graz, Petersgasse 12/1, and the [2]Austrian Centre of Industrial Biotechnology, Petersgasse 14, A-8010 Graz, Austria

Running title: Catalysis by the nitrile reductase QueF

* To whom correspondence should be addressed: Bernd Nidetzky: Institute of Biotechnology and Biochemical Engineering, Graz University of Technology, NAWI Graz, Petersgasse 12/1, A-8010 Graz, Austria; bernd.nidetzky@tugraz.at; Tel. +43-316-873-8400; Fax. +43-316-873-8434

Keywords: *nitrile reductase, QueF, catalytic mechanism, covalent catalysis, general acid-base, proton transfer, NADPHX, hydration of NADPH*

ABSTRACT

Enzymatic transformations of the nitrile group are important in biology as well as in synthetic chemistry. The enzyme QueF catalyzes conversion of 7-cyano-7-deazaguanine ($preQ_0$) to 7-aminomethyl-7-deazaguanine ($preQ_1$), a unique to biology four-electron reduction of a nitrile to an amine. The catalytic reaction involves a QueF-$preQ_0$ thioimidate adduct that is converted to $preQ_1$ in two NADPH dependent reduction steps via an imine intermediate. The QueF active site comprises a cysteine nucleophile flanked by an aspartic acid and additionally contains a histidine. Here, we used mutagenesis of *E. coli* QueF (C190A, C190S, D197A, D197H, H229A) to study functional interplay between these enzyme residues in covalent catalysis. Substitution of Cys^{190} or Asp^{197} annihilates $preQ_0$ covalent binding and largely disrupts the nitrile-to-amine reductase activity. The H229A variant readily forms the thioimidate adduct and is 24-fold less active for $preQ_0$ reduction than wild-type ecQueF (k_{cat} = 7.2 min^{-1}). Using isothermal titration calorimetry we show that the non-covalent step of $preQ_0$ binding involves proton uptake mediated by Asp^{197} with His^{229} as the likely protonated group. Catalytic proton transfer from the Cys^{190} thiol via Asp^{197} to the nitrile nitrogen promotes the covalent intermediate. We suggest that protonated (charged) His^{229} facilitates polarization of the substrate nitrile for nucleophilic attack on carbon by Cys^{190}; and through proton relay via Asp^{197}, it could provide the proton for re-protonating Cys^{190} during formation of the imine intermediate. Although mostly inactive toward $preQ_0$, the D197A variant promotes the hydration of NADPH at a comparably fast rate (k_{cat} = 0.014 min^{-1}). The enzymatic reaction involves protonation at nicotinamide C5 from Cys^{190}. Addition of water at C6, potentially assisted by Glu^{89}, yields β-6-hydroxy-1,4,5,6-tetrahydronicotinamide adenine dinucleotide phosphate.

Introduction

Enzymatic transformations of the nitrile group are important biologically, in secondary and xenobiotic metabolisms of plants and microorganisms for example (1–3). They also have significant applications in synthetic chemistry wherein nitriles often represent important intermediates (4, 5). The nitrile group is converted by hydrolytic enzymes to an amide or to a carboxylic acid (6–9) and by reductive enzymes to an amine (10–13). Despite the different reactivities, nitrile-converting enzymes share covalent catalysis from an active-site nucleophile as common feature of their mechanisms. Nitrilase (8, 9, 14–16) and nitrile reductase (17–20) both utilize a cysteine to form a thioimidate adduct between enzyme and nitrile substrate (Scheme 1A). The covalent catalysis in each enzyme requires assistance from catalytic proton transfer. The enzyme nucleophile is activated by deprotonation. Conversion of nitrile to the covalent intermediate and further on to product necessitates acid-base catalysis, as shown in Scheme 1A. Nitrile

reductase and nitrilase both have a candidate acid-base residue (Asp or Glu) positioned close to their cysteine nucleophile (8–10, 16, 17, 21), but the precise role of the Asp/Glu remains to be elucidated. Moreover, the critical interplay between general acid-base and nucleophilic catalysis is not well understood in both enzymes. In this study, therefore, we sought to clarify the involvement of catalytic proton transfer in build-up and degradation of the covalent thioimidate intermediate during enzymatic nitrile reduction.

The biological principle of nitrile reduction is embodied in the enzyme QueF (11, 22–26). The natural reaction of QueF is conversion of 7-cyano-7-deazaguanine ($preQ_0$) to 7-aminomethyl-7-deazaguanine ($preQ_1$) by NADPH (Scheme 1B) (17–19, 21, 27, 28). QueF is a bacterial enzyme from the biosynthetic pathway for the modified nucleoside queuosine (Q) (11, 22, 29). Inserted into tRNA as $preQ_1$ and further converted to Q, the queuosine modulates codon-anticodon binding efficiency for decoding NAC/U codons to Asn, Asp, His, and Tyr (22, 29, 30). The proposed catalytic mechanism of QueF is summarized in Scheme 1B. The core characteristics of this mechanism are well supported from enzyme crystal structures and biochemical evidence (17, 18, 21, 27, 28). Therefore, the thioimidate adduct is formed from a non-covalent QueF-$preQ_0$ complex that secludes the nitrile substrate completely from the solvent (Scheme 1B and 2) (17–20). The covalent intermediate is converted to $preQ_1$ in two NADPH dependent reduction steps via an imine. The imine is sequestered effectively in the QueF active site to prevent its decomposition (18, 28). NADPH binds very tightly to the enzyme-imine complex (18). The enzyme thus ensures that every $preQ_0$ converted is reduced fully to $preQ_1$.

QueF structures reveal that the cysteine catalytic nucleophile is flanked by an aspartic acid, which together form the immediate catalytic center (Figure 1A and B) (17, 21, 31). A histidine is additionally present. In the enzyme from *E. coli* studied here (ecQueF), the relevant residues are Cys^{190}, Asp^{197} and His^{229} and this amino acid numbering is used throughout (10, 11, 18, 28). QM/MM computational analysis of the reaction path of QueF (from *Vibrio cholerae*, vcQueF) suggested involvement of Asp^{197} in each catalytic step (Scheme 1B) (27). In thioimidate formation, Asp^{197} would deprotonate Cys^{190} and later protonate the nitrile nitrogen atom of the $preQ_0$ substrate. In the first and second step of reduction by NADPH, respectively, Asp^{197} would stabilize positive charge development on the reactive nitrogen of the protonated thioimidate and imine intermediate. Additionally, upon decomposition of covalent thiohemiaminal to non-covalently bound imine, Asp^{197} would re-protonate the Cys^{190}. In the proposed mechanism (27), the His^{229} had no immediate role and was excluded from involvement in proton transfer. However, the computational study started from the non-covalent complex between enzyme and $preQ_0$, not from the free enzyme; and it did not include macromolecular dynamics in the calculations. It also did not evaluate whether variation in the protonation states of the active-site residues affects the catalytic reaction. Crystal structures of thioimidate enzyme-$preQ_0$ adducts of vcQueF and the QueF from *Bacillus subtilis* (bsQueF) both reveal hydrogen bond network connecting the thioimidate N^{10} via Asp^{197} $O^{\delta 2}$ and an intermediary water to the His^{229} $N^{\delta 1}$, as shown in Figure 1A and B (17, 21). This suggests the possibility of a proton relay involving His^{229}. We have shown in preliminary experiments that $preQ_0$ binding by ecQueF was accompanied by net proton uptake from solution (18). The finding carries immediate implications for the enzymatic mechanism but is unaccounted for in the computational reaction path of QueF.

In this study, therefore, we used mutagenesis of active-site residues in ecQueF (C190A, C190S, D197A, D197H, H229A) to study their functional interplay in covalent catalysis for nitrile reduction. We present evidence from kinetic and ligand binding studies that suggests a refined QueF mechanism. In particular, we show that the non-covalent step of $preQ_0$ binding involves proton uptake from His^{229} via Asp^{197}. Catalytic proton transfer from the Cys^{190} thiol via Asp^{197} to the nitrile nitrogen drives formation of the covalent intermediate. We also show that His^{229} has an auxiliary role in ecQueF catalysis. Positive charge on His^{229} could facilitate polarization of the substrate nitrile for nucleophilic attack on carbon by Cys^{190}. Through proton relay via Asp^{197}, the His^{229} could provide the proton for re-protonation of the cysteine during formation of the imine intermediate. During the mechanistic study we

discovered that most ecQueF enzymes, however the D197A variant in particular, promote hydration of the C5-C6 double bond of the nicotinamide ring of NADPH.

Results

Covalent thioimidate formation – Thioimidate adduct of ecQueF with $preQ_0$ is detectable by absorbance with maximum absorption at 380 nm (ε = 10.02 ± 0.14 $mM^{-1}cm^{-1}$) (18). Assessing ecQueF variants (D197A, D197H, H229A) for thioimidate formation, the incompetent C190A variant served as negative control (10, 18). In absorbance titrations wherein $preQ_0$ was used in up to 5-fold molar excess over enzyme and the wavelength range 300 - 500 nm was scanned for absorbance change, no thioimidate adduct was measured for D197A and D197H variant. Limit of thioimidate detection was ~0.2% of the enzyme concentration used (50 µM). The H229A variant formed the thioimidate adduct similarly as the wildtype enzyme does. The C190S variant could potentially form a covalent imidate involving serine as the enzyme nucleophile. From absorbance titrations, no evidence for such an intermediate was obtained.

Protein mass analysis confirmed the absorbance data. In wildtype ecQueF, covalent adduct (35.906.0 ± 1.7 Da) was detected besides the unliganded enzyme (35,732.1 ± 0.5 Da) (18). Only unliganded enzyme was detected in samples of C190A (35,700 ± 2 Da), C190S (35,716 ± 2 Da) and D197A variant (35,689 ± 2 Da) incubated with $preQ_0$ in 4-fold molar excess over enzyme subunit present. For D197H variant, as shown in Figure 2, mass peaks corresponding to unliganded (35,754 ± 1 Da) and $preQ_0$-bound enzyme (35,929 ± 1 Da) were detected. In the absence of thioimidate adduct as demonstrated in absorbance titrations, the observable enzyme complex likely involved $preQ_0$ tightly but noncovalently bound.

Noncovalent binding of $preQ_0$ – This was analyzed with fluorescence titration. Binding of $preQ_0$ is traceable by quenching of protein tryptophan fluorescence (17, 18). We have shown in an earlier study comparing wildtype and C190A enzyme that the fluorescence quenching arises from the noncovalent step of $preQ_0$ binding (Scheme 2) (18). Results for the different ecQueF variants are shown in Figure 3. The degree of fluorescence quenching at saturating $preQ_0$ was similar in all enzymes (85 - 90%). Dissociation constants (K_d) calculated from the data are summarized in Table 1. Among the enzymes not capable of thioimidate formation, the D197H variant showed the highest affinity for $preQ_0$ binding. Its 0.55 µM K_d was on the same magnitude order as the ~0.1 µM K_d of the H229A variant which binds $preQ_0$ covalently. The D197A variant showed 25-fold loss in binding affinity as compared to the D197H variant. The K_d of the wildtype enzyme is extremely low ($\leq$ 3 nM), reflecting nearly irreversible binding of $preQ_0$ as covalent adduct with enzyme (18).

Binding of $preQ_0$ analyzed with isothermal titration calorimetry – $preQ_0$ binding to ecQueF is a strongly exergonic process that can be monitored well with ITC (18, 28). Of note, a substantial amount (~50%) of the total heat released during $preQ_0$ binding is due to noncovalent complex formation (Scheme 2) (18). ITC data of $preQ_0$ binding to the ecQueF variants in 100 mM phosphate buffer (pH 7.5) are shown in Figure 4. The corresponding thermodynamic parameters are summarized in Table 1. For the ecQueF variants unable to form thioimidate adduct with $preQ_0$, the Gibbs free energy of binding (ΔG) was consistently lower ($\Delta\Delta G$ = + 8 - 12 kJ/mol) than the corresponding ΔG for the wildtype enzyme. The $\Delta\Delta G$ for the enzyme variants involved a large decrease in the enthalpy of binding ($\Delta\Delta H$ = + 36 - 41 kJ/mol), thus rendering $preQ_0$ binding less favorable. However, it also involved significant compensation from the entropy term ($-T\Delta S$), which decreased in the variants as compared to wildtype enzyme. The H229A variant showed a ΔG of binding similar to that for wildtype ecQueF. However, the ΔH was more negative and the $-T\Delta S$ more positive than in the case of the wildtype enzyme.

Kinetic study of wildtype ecQueF showed that NADPH binds to both the covalent and the noncovalent complex of the enzyme with $preQ_0$ (18). Binding of NADPH to the $preQ_0$ complex of C190A variant was previously studied by ITC (Table 1) (18). The 3.6 µM K_d of NADPH binding to this complex was comparable to the corresponding K_d in the wildtype enzyme. Thermodynamic parameters of NADPH binding to the $preQ_0$ complex of D197H variant were determined (Figure 4E and Table 1). They are highly similar to the corresponding parameters of

the C190A variant. Substitution of Asp^{197} with a histidine, therefore, does not interfere with binding of NADPH.

Proton uptake during preQ$_0$ reduction – The enzymatic reaction, $preQ_0 + 2NADPH + 2H^+ \rightarrow preQ_1 + 2\ NADP^+$, implies uptake of two protons for each nitrile substrate converted into amine product. Assuming a protonated amine in $preQ_1$ at pH 7.5, a third proton would additionally be taken up in the reaction. Time-resolved analysis of proton consumption during $preQ_0$ reduction by wildtype QueF is shown in Figure 5. The ratio of steady-state rates of proton uptake and NADPH oxidation was 1.5 (± 0.1), consistent with a proton/$preQ_1$ stoichiometry of 3.

Proton uptake during preQ$_0$ binding – ITC study in buffers (phosphate, Tris, HEPES) differing in ionization enthalpy (ΔH_{ion}) was used to determine proton uptake/release during $preQ_0$ binding (18). Change of binding enthalpy ΔH upon variation in ΔH_{ion} is measured and the number of protons exchanged (n_{H+}) is determined from the slope (positive: proton uptake; negative: proton release) of the linear dependence of ΔH on ΔH_{ion} (32, 33). Results for ecQueF variants are summarized in Table 1 along with previously reported data for the wildtype enzyme and C190A variant. The D197A variant stood out among all other enzymes in that it did not take up protons in conjunction with $preQ_0$ binding ($n_{H+} \approx 0$). Interestingly, the D197H variant recovered proton uptake to a level almost analogous to that seen with the wildtype enzyme. The two variants of Cys^{190} showed reduced proton uptake as compared to the wildtype enzyme. In the H229A variant, the $preQ_0$ binding involved proton uptake larger than in the wildtype enzyme.

Enzymatic reduction of preQ$_0$ – Conversion of $preQ_0$ into $preQ_1$ was measured directly using HPLC (18, 28). NADPH and $NADP^+$ were also determined using the same analytical method (Figure 6A). As shown recently for certain ecQueF variants, 7-formyl-7-deazaguanine is released upon a $preQ_0$ reduction wherein the imine intermediate can hydrolyze due to its incomplete sequestration from solvent in the enzyme (Scheme 1B) (28). Therefore, reactions were also analyzed for 7-formyl-7-deazaguanine.

Under assay conditions routinely used with the wildtype enzyme (18), only the H229A variant showed activity. The k_{cat} of the variant was 0.30 (± 0.06) min^{-1}, that is, 24-fold lower than the k_{cat} of the wildtype enzyme (Table 2). Initial rates of the H229A variant showed saturation at low concentration (≤ 1 μM) of both $preQ_0$ and NADPH. Determination of K_m was therefore not pursued. Using 4*R*-D-NADPH as coenzyme, kinetic isotope effect of 2.2 (± 0.2) on k_{cat} was determined. This is similar to the effect of 2.4 on k_{cat} of the wildtype enzyme.

When incubated for longer times (96 h) at high enzyme concentration (50 μM), a low level of nitrile reductase activity was confirmed for ecQueF Cys^{190} and Asp^{197} variants (Table 2). The loss of activity compared to wildtype enzyme was substantial, about 10^4-fold for the Cys^{190} variants and 10^5-fold for the Asp^{197} variants. Residual activity in these variants is interesting for it implies a nitrile group reduction that proceeds in the absence of a covalent ecQueF-$preQ_0$ intermediate. Careful controls were therefore necessary to ascertain this activity beyond doubt.

First of all, close balance between $preQ_0$ consumption and $preQ_1$ formation was demonstrated in all reactions (Table 2). 7-Formyl-7-deazaguanine was not released. We noted that the $preQ_0$ converted was not matched with the NADPH utilized, which in turn was not balanced to the $NADP^+$ formed (Table 2). Imbalance in reducing equivalents used is clarified in the subsequent section. Non-enzymatic conversion of $preQ_0$ by NADPH was not detected, indicating that catalysis from the ecQueF variants was required for reaction.

Secondly, to ensure that activity could not arise from an endogenous QueF contaminating the recombinant enzyme preparations used, we applied *E. coli* cell extract to $preQ_0$ conversion. One cell extract was from the expression of the D197A variant, which was least active among the enzymes analyzed here (Table 1). The other was from an *E. coli* strain harboring the empty plasmid vector and treated identically as the positive control. Whereas cell-extract containing D197A variant showed $preQ_1$ formation, the negative control was completely inactive. We also considered that proteins were purified by affinity via the His tag; and that the His tag was present in the recombinant but absent in the native enzyme. Therefore, upon applying a purification procedure selective for the His-tagged target protein, it was inconceivable that a contaminating activity not detectable in the cell extract could become

enriched to above detection limit in the course of purification.

Finally, interference from translational error, resulting in amino acid mis-incorporation to yield an active enzyme species, was unlikely due to the particular triplet codon changes used for site-directed mutagenesis. All codon changes involved substitutions of the first or second codon base (C190S, TGC→AGC; C190A, TGC→GCC; D197H, GAT→CAT, D197A, GAT→GCG; H229A, CAC→GCC). Translational misreading is however known to occur chiefly at the third base (34–36). In summary, therefore, these results reinforced the suggestion that Cys^{190} and Asp^{197} variants of ecQueF retained a low level of nitrile reductase activity that was intrinsic to their respective active sites.

Degradation of NADPH via enzyme-catalyzed hydration – Catalytic reactions of the Cys^{190} and Asp^{197} variants with $preQ_0$ were peculiar in that their NADPH consumption exceeded by far the corresponding $preQ_1$ release; and the excess utilization of NADPH was largely uncoupled from the formation of $NADP^+$. The D197A variant represented these features in particular, as shown in Table 2. Being rather unusual among dehydrogenases/reductases, with the exception of glyceraldehyde 3-phosphate dehydrogenase noted and discussed later, the uncoupled utilization of NADPH drew our immediate interest and was therefore analyzed in detail. HPLC absorbance traces revealed two prominent peaks (Figure 6A) whose abundance in reaction samples was correlated with uncoupled NADPH conversion.

We performed experiments in the absence of $preQ_0$ and showed that the uncoupled conversion of NADPH proceeded readily under these conditions (Table 3). Interestingly, in the control reaction lacking the enzyme, some NADPH conversion was observed as well (Figure 6B). It occurred almost exclusively via the uncoupled path (Figure 6B and Table 3) when tris(2-carboxyethyl)phosphine was present. When tris(2-carboxyethyl)phosphine was replaced by dithiothreitol, both the coupled and the uncoupled path contributed to NADPH degradation (Table 3). Note that besides being a reducing agent, tris(2-carboxyethyl)phosphine is a polybasic anion potentially affecting the NADPH degradation (see the Discussion) which dithiothreitol is not. The enzymes used (Table 3) differed in effect on the NADPH conversion. The D197A variant accelerated about 10-fold the uncoupled conversion as compared to the control and nearly all NADPH was degraded enzymatically via this path (Figure 6B). Use of dithiothreitol instead of tris(2-carboxyethyl)phosphine did not affect the degradation path utilized by the D197A variant and only marginally influenced its activity. The other variants and the wildtype enzyme hardly accelerated the overall NADPH conversion in comparison to the control, but caused a marked shift in the conversion path preferentially utilized (Table 3). The wildtype enzyme and the D197H variant utilized both paths (uncoupled: 58-64%) of NADPH degradation. As discussed later, it is mechanistically relevant that NADPH conversion in the presence of the Cys^{190} variants showed the strongest involvement of the coupled path to $NADP^+$ (52-63%; Table 3). The coupled conversion of NADPH was affected by the presence of O_2 and the buffer composition (data not shown). As this is a well-known reaction of NADPH in solution and in enzymes, it was not herein pursued.

From LC-MS analysis we identified the product of uncoupled NADPH conversion to have the mass of NADPH hydrate (763; $1H^-$, 762; $2H^-$, 380.5). Additionally, we observed another species with the same mass as NADPH (745; $1H^+$, 746; $1H^-$, 744). This suggested that two main products arise from the uncoupled degradation. In a UV-Vis spectrum, the products displayed maximum absorption at 266 nm, but unlike NADPH showed no absorption at 340 nm (Figure 7A). These mass data and spectral properties match precisely with the so-called "acid-modified" products of NADH (37) and NADPH (38). At low pH, the coenzymes undergo hydration of the C5-C6 double bond of their dihydro-nicotinamide ring. The hydrated product, which is often referred to as NADHX or NADPHX, reacts further via anomeric epimerization and cyclization at nicotinamide C6 and ribofuranosyl O2. Here, therefore, the product mass of 763 corresponds to *β*-6-hydroxy-1, 4, 5, 6-tetrahydronicotinamide adenine dinucleotide phosphate (NADPX) and the product mass of 745 corresponds to O2'-*β*-6-cyclo-1, 4, 5, 6-tetrahydronicotinamide adenine dinucleotide phosphate ((cTHN)TPN), as shown in Figure 8A. Judging from relative mass intensities in the LC-MS analysis, the ratio of hydrated to cyclized

product was strongly dependent upon the reaction conditions used. When tris(2-carboxyethyl)phosphine was added, spontaneous conversion of NADPH gave a 1:3 ratio for hydrated and cyclized product. When dithiothreitol was used instead, the ratio was changed to 2:1. We also noted that slightly acidic conditions (pH 6.67) in the analysis could cause shift in ratio toward the cyclized product. To prevent this, the analysis was done at pH 7.5.

UV/Vis spectra of hydrated and cyclized product differ in a small "hump" in the region of 280-300 nm that the spectrum of cyclic product characteristically shows (37, 38). As shown in Figure 7A, this hump was absent from the spectrum of the enzymatically formed product. The ^{1}H NMR spectrum of the main product from complete conversion of NADPH in the presence of the D197A variant is depicted in Figure 8B. Comparison of the product spectrum to the ^{1}H NMR spectrum of NADPH reveals complete disappearance of signals from the dihydro-nicotinamide C4 protons of NADPH in the product. Moreover, proton signals diagnostic of the cyclized product, namely those from the tetrahydronicotinamide C5 and the ribosyl C1, were not present in the enzymatically formed product (Figure 8B). Therefore, the actual product from the enzymatic conversion is the NADPH hydrate. Its further rearrangement into the cyclized product most likely occurs spontaneously, particularly during sample preparation for and analysis in LC-MS. We also note that a simple *N*-glycosylase-like degradation of NADPH into adenine (mass = 135) and nicotinamide dinucleotide phosphate (mass = 612), previously considered for *V. cholerae* QueF based on the observation of the 623 mass fragment in the protein crystal (21), is ruled out from these data.

Time courses of enzyme-promoted and spontaneous conversion of NADPH are shown in Figure 7B-D. The kinetics of formation of NADPH degradation products and of $NADP^{+}$ (Figure 7 B-C) indicates that uncoupled and coupled reaction represented two parallel paths of NADPH conversion. In both the enzyme-promoted and the spontaneous conversion, the uncoupled reaction was about 12-fold faster than the coupled reaction. The NADPH conversion detectable in HPLC (Figure 7 B-C) coincided with loss of absorbance at 340 nm, as shown in Figure 7D and Table 3.

Discussion

Catalytic proton transfer coupled to covalent catalysis in ecQueF – QueF crystal structures capture the elementary steps of $preQ_0$ binding (17, 21). Upon noncovalent complex formation, the substrate is anchored tightly between the N-terminal ends of two helices (α2 and α5, in vcQueF; α1' and α2, in bsQueF), as shown in Figure 1D and E. The reactive nitrile group so becomes oriented towards the active-site loop comprising Cys^{190} and Asp^{197}. The side chains of Asp^{197} and His^{229} adopt relatively flexible conformations that enable a dynamic, water-mediated interaction between the two residues (Figure 9A). Upon covalent complex formation, the substrate nitrogen atom develops a hydrogen bond with Asp^{197}, which in turn remains linked via a water molecule to His^{229} (Figure 1A, B, and F). Biochemical evidence from the current study assigns proton relay function to this active-site network of hydrogen bonds.

The mechanism in Scheme 3 is proposed. Asp^{197} is central for proton transfer into and within the ecQueF active site. When $preQ_0$ binds, Asp^{197} picks up a proton from water to protonate His^{229}. The relative proton amount taken up by the enzyme (~0.8 protons/active site) reflects the protonation state of the histidine at the pH of 7.5 used. Replacement of Asp^{197} by an alanine, whose side chain is incompetent in the proton transfer function considered, disrupts completely the proton uptake in conjunction with $preQ_0$ binding. Replacement by a histidine, by contrast, restores proton uptake to a level (~0.6 protons/active site) comparable to that of the wildtype enzyme. The extra positive charge developed on the protonated His^{229} might assist in catalysis to covalent thioimidate formation. It could do so by promoting charge separation in the reactive nitrile group. Nucleophilic attack on carbon and proton transfer to nitrogen would thus be facilitated. Proton uptake by the H229A variant during $preQ_0$ binding was larger (~1.4 proton/active site) than it was in the wildtype enzyme. This probably reflects protonation of a water molecule in the H229A active site. Indeed, the covalent complex structure of the His233A variant of *Vibrio cholerae* QueF reveals a candidate water molecule hydrogen-

bonded to the active-site aspartate (Figure 9B) (21). Interestingly, as demonstrated by proton uptake measurements for the C190A and C190S variants of ecQueF, the catalytic cysteine is not essential for proton uptake during $preQ_0$ binding.

The absolute requirement for Asp^{197} in covalent thioimidate formation is explained by a twofold role of this residue in catalytic proton transfer. First, Asp^{197} activates through deprotonation the Cys^{190} for function as the catalytic nucleophile. Second, Asp^{197} promotes the covalent thioimidate through catalytic proton transfer to the nitrile nitrogen atom. The nucleophilic attack on carbon probably occurs concerted with the Asp^{197}-mediated proton transfer events, as shown in Scheme 3. Evidence in support of this notion is that the D197A and D197H variants were both completely inactive to form the covalent thioimidate even under conditions (pH $\geq$ 9.0) in which a cysteine would be expected to become (partially) deprotonated anyway.

As shown in Scheme 3, conversion of the covalent thioimidate to $preQ_1$ involves partial protonation-deprotonation, hence positive charge development, at the reactive nitrogen atom of substrate. Proton relay via Asp^{197}-water-His^{229} would help delocalizing the charge and could thus facilitate the hydride reduction from NADPH. Upon breakdown of covalent thiohemiaminal to noncovalently bound imine, Cys^{190} would become re-protonated via Asp^{197} in a reversion of the initializing proton transfer event. According to the mechanism proposed (Scheme 3), the $preQ_1$ product would feature an unprotonated amino group and proton uptake by $preQ_1$ probably takes place in solution. The notion is supported from the structure of *V. cholerae* QueF in complex with $preQ_1$ (Figure 9C). The structure shows the amino group of product oriented towards the imidazole ring of His^{229}. The orientation is suggestive of a cation-π interaction between the two groups, assuming the amino group to be protonated. The positioning of $preQ_1$ in the enzyme complex structure thus appears to be unproductive catalytically. Of note, the $preQ_1$ is not detectably oxidized by $NADP^+$ in the presence of ecQueF within a pH range (7.5 - 9.0) accessible to a stable enzyme (18). The amino group pK_a of $preQ_1$ is predicted to be 8.39 (ChemSpider database). It may thus be difficult for the enzyme to bind $preQ_1$ in the presumably active, unprotonated form. From the evidence presented, an auxiliary role of His^{229} in each catalytic step of the QueF reaction is suggested (Scheme 3). This is consistent with the k_{cat} of the H229A variant about 24-fold lower than the k_{cat} of the wildtype enzyme.

QueF and nitrilase appear to utilize a highly similar mechanism to promote the covalent thioimidate intermediate (Scheme 1A) (9, 14, 39). In the nitrilase, a triad of cysteine/glutamic acid/lysine constitutes the active-site apparatus (8, 16, 39). Like Asp^{197} in QueF, the glutamic acid is central for catalytic nucleophile activation and for acid-base catalysis. The role adopted by the positively charged lysine in nitrilase might be similar to that proposed for the protonated His^{229} in QueF (Scheme 3).

Enzymatic nitrile reduction in the absence of covalent catalysis – The conversion of $preQ_0$ to $preQ_1$ by the C190A variant implies a nitrile reduction by NADPH that proceeds in the absence of a covalent enzyme intermediate. The Asp^{197} variants and the C190S variant both could form covalent intermediates with $preQ_0$ in principle, but no evidence in support of such intermediates was found in these enzymes. There is ample precedence for hydride reduction of nitriles to amines in synthetic organic chemistry (40–42). Borane reagents are often used as the hydride source/donor (41). The chemical conversions involve a twofold reduction at the nitrile carbon via imine intermediate (40, 42). The catalytic reactions of the ecQueF variants likely proceed analogously, using NADPH as the hydride donor. From its one-electron redox potential (43–45), NADPH is clearly able to reduce a nitrile group directly. Besides having the ability to position the nitrile substrate for initial reduction, the enzyme variants retain imine intermediate sequestration as a characteristic feature of catalytic function of the ecQueF active site (28). Therefore, each $preQ_0$ reduced by the variants, however slowly, makes it through to the $preQ_1$ product.

Enzymatic hydration of NADPH – Conversion to (cTHN)TPN via hydrated intermediate (Scheme 4) represents a well-characterized route of spontaneous degradation of NADH and NADPH (37, 46, 47). It is facilitated by acidic conditions and by the presence of polybasic anions. It is also promoted by the enzyme glyceraldehyde 3-phosphate dehydrogenase (46). The enzymatic degradation rate was found to depend strongly on

a polybasic anion (e.g., pyrophosphate, phosphate, citrate) present (48). Like QueF, glyceraldehyde 3-phosphate dehydrogenase uses an active-site cysteine as catalytic nucleophile of the reaction (46). NADH was hydrated more rapidly from glyceraldehyde 3-phosphate dehydrogenase with the relevant cysteine acylated than from the corresponding apoenzyme. Hydration of the C5-C6 double bond was suggested to occur from a ternary complex between acylated enzyme, NADH and polybasic anion. The acylated glyceraldehyde 3-phosphate dehydrogenase was shown to bind NADH more tightly than NAD^+ (49, 50).

Although degradation of NADPH by the D197A variant of ecQueF involves the same hydration event on the dihydro-nicotinamide moiety as the conversion of NADH by glyceraldehyde 3-phosphate dehydrogenase does, the underlying mechanisms are clearly different. The activity of the D197A variant does not rely on modification of the active-site cysteine. It is not dependent on the presence of polybasic anions and proceeds readily in their absence at pH 7.5. Mutagenesis results suggest the essential involvement of Cys^{190} in the degradation of NADPH by ecQueF. Considering the relative position of Cys^{190} to the reactive nicotinamide C5 in NADPH, which appears suitable for proton transfer (Figure 10), we would like to suggest a role for the cysteine as catalytic acid of the C5-C6 double bond hydration by the enzyme. Effect of site-directed substitution of Asp^{197} by Ala on enhancing the enzymatic hydration rate is thus explainable in a twofold manner. Firstly, the substitution will enhance the conformational flexibility of Cys^{190}, as indicated in Figure 10, which may be important for the cysteine's proper function as proton donor. Secondly, it will probably stabilize Cys^{190} in a reactive (protonated) state because the Asp responsible for deprotonation of the cysteine in the normal catalytic reaction is replaced by a residue unable to fulfil an analogous function. The enzyme structures (Figure 10) also indicate that a water molecule is positioned suitably for attack on the reactive C6 of NADPH. The addition of water might be facilitated by Glu^{89} providing some base catalytic assistance.

Experimental Procedures

Chemicals – NADPH (purity >98%) and $NADP^+$ (purity >97%) were from Carl Roth (Karlsruhe, Germany). Materials were of the highest purity available from Carl Roth and Sigma-Aldrich (St. Louis, MO, USA). The $preQ_0$ and 7-formyl-7-deazaguanine were synthesized as described previously (12, 18).

Site-directed mutagenesis – Mutagenesis leading to site-directed substitution of Cys^{190} by Ser (C190S), Asp^{197} by Ala (D197A) or His (D197H) was performed according to a standard two-stage PCR protocol (28, 51). A pEHISTEV vector including ecQueF gene (pEHISTEV:EcNRedWT) was used as the template. The oligonucleotide primers are shown with the mismatched bases underlined.

C190S forward 5'-CTGCTGAAATCAAACAGCCTGATCACCCATCAACC-3'

C190S reverse 5'-GGTTGATGGGTGATCAGGCTGTTTGATTTCAGC-3'

D197A forward 5'-CCTGATCACCCATCAACCAGCGTGGGGTTCGCTCC-3'

D197A reverse 5'-GGAGCGAACCCCACGCTGGTTGATGGGTGATCAGG-3'

D197H forward 5'-CCTGATCACCCATCAACCACATTGGGGTTCGCTCC-3'

D197H reverse 5'-GGAGCGAACCCCAATGTGGTTGATGGGTGATCAGG-3'

Mutagenesis to substitute Cys^{190} by Ala (C190A) and His^{229} by Ala (H229A) was reported in an earlier study (10, 18). All mutations were verified by gene sequencing.

Enzyme preparation – The ecQueF variants were obtained as N-terminally His-tagged proteins using expression in *E. coli* BL21-DE3 as described previously (18, 28). All enzymes were purified by a reported two-step procedure consisting of immobilized metal ion affinity chromatography and gel filtration (18, 28). Enzyme purity was confirmed by SDS-PAGE. The HisTrap affinity column (GE Healthcare, Buckinghamshire, UK) was regenerated fully after each use. The PD10-desalting columns (GE Healthcare) were always freshly used. Contamination with protein carried over from previous purification runs was thus ruled out rigorously. Protein concentration was measured with a Pierce BCA protein assay kit

(Thermo Fisher Scientific, Germerin, Germany). Enzyme stock solutions (0.4-0.8 mM) were stored at -20 °C and used up within 3 weeks.

Study of preQ$_0$ binding by ecQueF variants – For isothermal titration calorimetry (ITC), a VP-ITC Micro Calorimeter from Microcal (Malvern Instruments Ltd., Malvern, UK) was used at 25 °C. The enzyme was gel-filtered twice to phosphate buffer (100 mM Na_2HPO_4-NaH_2PO_4, pH 7.5, additionally containing 50 mM KCl) using illustra NAP 5 columns (GE Healthcare). A DMSO concentration of maximally 2% (v/v) was used in both the enzyme and the preQ$_0$ solution. Experiments were conducted and data evaluation done as described previously (18, 28). The enzyme molar concentration was based on the protein concentration assuming a functional ecQueF homodimer with a molecular mass of 71,740 Da (C190S variant), 71,684 Da (D197A variant), or 71,816 Da (D197H variant).

Proton uptake or release in conjunction with ligand binding was determined by ITC experiments done in different buffers. Besides the phosphate buffer described above, HEPES and Tris buffers (each 100 mM, pH 7.5, additionally containing 50 mM KCl) were used, as reported previously (18). The number of protons taken up or released was calculated using the equation, $n_{H+} = (\Delta H_{buffer\ 1} - \Delta H_{buffer\ 2})/(\Delta H_{ion,\ buffer\ 1} - \Delta H_{ion,\ buffer\ 2})$, where n_{H+} is the number of protons involved in the binding, and ΔH_{ion} is the ionization enthalpy of the buffer. The ΔH_{ion} of phosphate, HEPES, and Tris at pH 7.5 and 25 °C was obtained from the literature as 3.60, 20.40, 47.45 kJ/mol, respectively (52). The values of n_{H+} are averages from three independent sets of experiments.

The covalent thioimidate adduct of ecQueF was detected from its characteristic absorbance with maximum absorption at around 380 nm (18). Absorbance titrations were carried out with a Beckman DU 800 spectrophotometer (Beckman Coulter, Pasadena, CA, USA) as described previously (18, 28).

Quenching of the intrinsic Trp fluorescence is a useful reporter of preQ$_0$ binding, as shown previously for bsQueF and ecQueF (17, 18). Fluorescence titrations were performed using a fluorescence spectrophotometer F-4500 (Hitachi, Ltd., Tokyo, Japan). Emission spectra were recorded in the range 300-500 nm at 1200 nm/min with the excitation wavelength at 280 nm. The quenching yield was determined as the ratio $(F_0\text{-}F_S)/F_0$, where F_0 and F_S are the protein fluorescence intensities in the absence and presence of substrate recorded at the same wavelength of emission.

Protein mass analysis—Samples were prepared in Tris-HCl buffer (100 mM, pH 7.5), additionally containing 50 mM KCl and 1.15 mM tris(2-carboxyethyl)phosphine, as described previously (18). The enzyme and preQ$_0$ concentration was 130 µM and 500 µM, respectively. The samples were separated on a capillary HPLC system (Dionex Ultimate 3000, Thermo Fisher Scientific) and analyzed in a maXis II electron transfer dissociation mass spectrometer (Bruker, Bremen, Germany) as described in our earlier study of wildtype ecQueF (18). The obtained protein mass spectra were deconvoluted by data analysis software, using the MaxEnt2 algorithm.

Enzymatic reactions of ecQueF variants – *preQ$_0$ conversion*. Reactions for preQ$_0$ reduction were carried out at 25°C using agitation at 500 rpm in a Thermomixer Comfort (Eppendorf, Hamburg, Germany). The enzyme concentration was 10 µM (wildtype) or 50 µM (Cys^{190} and Asp^{197} variants). The H229A variant was used at 10, 20 and 50 µM. The preQ$_0$ concentration was 250 µM. For the H229A variant, several preQ$_0$ concentrations were used: 50, 100, 150, and 200 µM. The NADPH concentration was 500 µM. Tris-HCl and sodium phosphate buffer (100 mM, pH 7.5), additionally containing 50 mM KCl and 1.15 mM tris(2-carboxyethyl)phosphine, were used. Samples were taken at certain times up to 96 h and analyzed by HPLC with UV/Vis and/or MS detection. All compounds known to be involved in the reaction according to Scheme 1B (preQ$_0$, preQ$_1$, 7-formyl-7-deazaguanine, NADPH, $NADP^+$) were analyzed with the method used. In addition, degradation products of NADPH were revealed.

Absence of nitrile reductase activity in E. coli strain background. The cell-free extract of *E. coli* BL21-DE3 harboring the pEHISTEV vector was used. It was prepared using procedures exactly identical to those used for preparing the enzymes. Cell-free extract from BL21-DE3 harboring the pEHISTEV:EcNRedD197A vector for expression of the D197A variant was used as positive control. The conditions used were as described above, with preQ$_0$ and NADPH concentrations of 250 µM and 500 µM, respectively. The protein concentration in

the reaction was 3.6 mg/mL. For the poistive control this would correspond to an estimated concentration of the D197A variant of 50 µM. Samples were analyzed by HPLC after 24 h. No $preQ_1$ was formed in the negative control above a detection limit of 1 µM $preQ_1$ formed or 5 µM $preQ_0$ consumed. The positive control showed $preQ_1$ formation (3 µM) as expected.

Activity toward NADPH degradation. The enzyme solution (50 µM) was incubated under the above-described conditions in the presence of 500 µM NADPH. Tris-HCl buffer (100 mM, pH 7.5) containing 50 mM KCl was prepared with either 1.15 mM tris(2- carboxyethyl)phosphine or dithiothreitol. Enzyme solution was gel-filtered twice to the used buffer before starting the reaction. After incubation at 25 ºC for up to 26 h (600 rpm; a Thermomixer Comfort), the reaction was stopped by precipitating the enzyme with twice the reaction volume of acetonitrile (15 min on ice). Products of enzymatic and spontaneous reactions were analyzed by HPLC, LC-MS, and ^{1}H NMR.

The "acid-modified" product of NADPH was prepared as described previously (53). NADPH solution in water (20.4 mM) was incubated at pH 3.5 until more than 95% of the NADPH was consumed. The solution was adjusted to pH 8.2 with NaOH to prevent further conversion. The product thus obtained is ((cTHN)TPN), as shown by LC-MS and ^{1}H-, ^{13}C-, HSQC, and HMBC NMR analysis.

Proton consumption during $preQ_0$ reduction. This was measured at 25°C using the pH indicator phenol red using reported protocols (54, 55). Immediately prior to the reaction the wildtype enzyme was gel-filtered twice to a 0.5 mM Tris-HCl buffer (pH 7.51) containing 34 µM phenol red and 150 mM KCl. Reaction mixtures contained 3.6 µM enzyme, 100 µM NADPH and 20 - 40 µM $preQ_0$. The DMSO concentration was 1% (v/v). Proton consumption was determined absorbance increase at 556 nm. The calibration was done with KOH. NADPH conversion was monitored at 340 nm.

^{1}H NMR measurements – NMR spectra were recorded at 499.98 MHz and 30 ºC using a Varian INOVA 500-MHz spectrometer (Agilent Technologies) with VNMRJ 2.2D software. D_2O (99.8% D, 20% v/v) was added into the product solution obtained by enzymatic and spontaneous reaction before the measurements. The (cTHN)TPN obtained from NADPH at acidic conditions was 3-fold diluted by adding D_2O before the measurements. The ^{1}H- and ^{13}C-NMR spectra of coenzymes, the hydration and the cyclisation product of NADPH were reported previously (37, 46, 56, 57). The spectra obtained here were shown to agree well with those earlier spectra.

HPLC analytics – The products of $preQ_0$ reduction were analyzed at 30 °C using an Agilent 1200 HPLC system (Santa Clara, CA, USA) equipped with a 5 µm SeQuant ZIC-HILIC column (200 Å, 250 × 2.1 mm; Merck, Billerica, MA, USA) and the corresponding guard column (20 × 2.1 mm; Merck), and a UV detector (λ = 254, 262 and 340 nm), as described previously (28). The samples of NADPH degradation were analyzed with a 1.15 µm Cromolith High Resolution RP-18 end-capped column (150 Å, 100 × 4.6 mm; Merck). A gradient of 5 to 16% acetonitrile in buffer (50 mM sodium phosphate, pH 6.8, 2 mM tetrabutylammonium bisulfate) over 10 min was used. The flow rate was 2 mL/min. The injection volume was 10 µL. Optionally, a Shimadzu LCMS-2020 system (Kyoto, Japan) equipped with the SeQuant ZIC-HILIC column was utilized to analyze the NADPH rearrangement products, as described above. Note: the method using the Cromolith RP-18 column was incompatible with LC-MS analysis because sodium phosphate and tetrabutylammonium bisulfate used are not volatile. A UV-detector (λ = 254 and 340 nm) was used. Masses were scanned in a range of 100-900 with positive and negative mode. A linear gradient of 80 to 71%, acetonitrile in buffer (5 mM ammonium acetate, pH 6.67 or pH 7.5) over 12 min was used. The column was washed with 80% acetonitrile for 6 min. The flow rate was 0.5 mL/min.

Acknowledgments: We thank Prof. Norbert Klempier and Dr. Birgit Wilding (Institute of Organic Chemistry, Graz University of Technology) for providing $preQ_0$; Prof. Hansjörg Weber (Institute of Organic Chemistry, Graz University of Technology) for ^{1}H NMR measurements; Prof. Ruth Birner-

Grünberger and B. Darnhofer (Diagnostic and Research Institute of Pathology & Omics Center Graz, Medical University of Graz) for protein-mass analysis; and Dr. Gernot Strohmeier (Austrian Centre of Industrial Biotechnology) for HPLC-MS analysis.

Conflict of interest: The authors declare that they have no conflicts of interest with the contents of this article.

Author's Contributions: J.J and B.N. designed the research. J.J. and J.B. performed biochemical experiments and analyzed data together with T.C. All authors commented and agreed on the final version of the paper. J.J. and B.N. wrote the paper.

REFERENCES

1. Howden, A. J. M., Jill Harrison, C., and Preston, G. M. (2009) A conserved mechanism for nitrile metabolism in bacteria and plants. *Plant J.* **57**, 243–253
2. Howden, A. J. M., and Preston, G. M. (2009) Nitrilase enzymes and their role in plant-microbe interactions. *Microb. Biotechnol.* **2**, 441–451
3. Luque-Almagro, V. M., Cabello, P., Sáez, L. P., Olaya-Abril, A., Moreno-Vivián, C., and Roldán, M. D. (2018) Exploring anaerobic environments for cyanide and cyano-derivatives microbial degradation. *Appl. Microbiol. Biotechnol.* **102**, 1067–1074
4. Ramteke, P. W., Maurice, N. G., Joseph, B., and Wadher, B. J. (2013) Nitrile-converting enzymes: An eco-friendly tool for industrial biocatalysis. *Biotechnol. Appl. Biochem.* **60**, 459–481
5. Gong, J.-S., Shi, J.-S., Lu, Z.-M., Li, H., Zhou, Z.-M., and Xu, Z.-H. (2017) Nitrile-converting enzymes as a tool to improve biocatalysis in organic synthesis: recent insights and promises. *Crit. Rev. Biotechnol.* **37**, 69–81
6. Brenner, C. (2002) Catalysis in the nitrilase superfamily. *Curr. Opin. Struct. Biol.* **12**, 775–782
7. Gong, J.-S., Lu, Z.-M., Li, H., Shi, J.-S., Zhou, Z.-M., and Xu, Z.-H. (2012) Nitrilases in nitrile biocatalysis: recent progress and forthcoming research. *Microb. Cell Factories*. **11**, 142
8. Zhang, L., Yin, B., Wang, C., Jiang, S., Wang, H., Yuan, Y. A., and Wei, D. (2014) Structural insights into enzymatic activity and substrate specificity determination by a single amino acid in nitrilase from *Syechocystis* sp. PCC6803. *J. Struct. Biol.* **188**, 93–101
9. Jiang, S., Zhang, L., Yao, Z., Gao, B., Wang, H., Mao, X., and Wei, D. (2017) Switching a nitrilase from *Syechocystis* sp. PCC6803 to a nitrile hydratase by rationally regulating reaction pathways. *Catal. Sci. Technol.* **7**, 1122–1128
10. Wilding, B., Winkler, M., Petschacher, B., Kratzer, R., Egger, S., Steinkellner, G., Lyskowski, A., Nidetzky, B., Gruber, K., and Klempier, N. (2013) Targeting the substrate binding site of *E. coli* nitrile reductase QueF by modeling, substrate and enzyme engineering. *Chem. Eur. J.* **19**, 7007–7012
11. Van Lanen, S. G., Reader, J. S., Swairjo, M. A., de Crécy-Lagard, V., Lee, B., and Iwata-Reuyl, D. (2005) From cyclohydrolase to oxidoreductase: discovery of nitrile reductase activity in a common fold. *Proc. Natl. Acad. Sci. U. S. A.* **102**, 4264–4269
12. Wilding, B., Winkler, M., Petschacher, B., Kratzer, R., Glieder, A., and Klempier, N. (2012) Nitrile reductase from *Geobacillus kaustophilus*: a potential catalyst for a new nitrile biotransformation reaction. *Adv. Synth. Catal.* **354**, 2191–2198
13. Yang, L., Koh, S. L., Sutton, P. W., and Liang, Z.-X. (2014) Nitrile reductase as a biocatalyst: opportunities and challenges. *Catal. Sci. Technol.* **4**, 2871
14. Fernandes, B. C. M., Mateo, C., Kiziak, C., Chmura, A., Wacker, J., van Rantwijk, F., Stolz, A., and Sheldon, R. A. (2006) Nitrile hydratase activity of a recombinant nitrilase. *Adv. Synth. Catal.* **348**, 2597–2603
15. Pace, H. C., Hodawadekar, S. C., Draganescu, A., Huang, J., Bieganowski, P., Pekarsky, Y., Croce, C. M., and Brenner, C. (2000) Crystal structure of the worm NitFhit Rosetta Stone protein reveals a Nit tetramer binding two Fhit dimers. *Curr. Biol.* **10**, 907–917

16. Raczynska, J. E., Vorgias, C. E., Antranikian, G., and Rypniewski, W. (2011) Crystallographic analysis of a thermoactive nitrilase. *J. Struct. Biol.* **173**, 294–302
17. Chikwana, V. M., Stec, B., Lee, B. W. K., de Crécy-Lagard, V., Iwata-Reuyl, D., and Swairjo, M. A. (2012) Structural basis of biological nitrile reduction. *J. Biol. Chem.* **287**, 30560–30570
18. Jung, J., Czabany, T., Wilding, B., Klempier, N., and Nidetzky, B. (2016) Kinetic analysis and probing with substrate analogues of the reaction pathway of the nitrile reductase QueF from *Escherichia coli*. *J. Biol. Chem.* **291**, 25411–25426
19. Lee, B. W. K., Van Lanen, S. G., and Iwata-Reuyl, D. (2007) Mechanistic studies of *Bacillus subtilis* QueF, the nitrile oxidoreductase involved in queuosine biosynthesis. *Biochemistry* **46**, 12844–12854
20. Gjonaj, L., Pinkse, M., Fernández-Fueyo, E., Hollmann, F., and Hanefeld, U. (2016) Substrate and cofactor binding to nitrile reductase: a mass spectrometry based study. *Catal. Sci. Technol.* **6**, 7391–7397
21. Kim, Y., Zhou, M., Moy, S., Morales, J., Cunningham, M. A., and Joachimiak, A. (2010) High-resolution structure of the nitrile reductase QueF combined with molecular simulations provide insight into enzyme mechanism. *J. Mol. Biol.* **404**, 127–137
22. Iwata-Reuyl, D. (2003) Biosynthesis of the 7-deazaguanosine hypermodified nucleosides of transfer RNA. *Bioorg. Chem.* **31**, 24–43
23. Domínguez de María, P. (2011) Nitrile reductases: a forthcoming wave in biocatalysis? *ChemCatChem*. **3**, 1683–1685
24. Moeller, K., Nguyen, G.-S., Hollmann, F., and Hanefeld, U. (2013) Expression and characterization of the nitrile reductase QueF from *E. coli*. *Enzyme Microb. Technol.* **52**, 129–133
25. Li, M., Zhou, Z., Zhang, Z.-J., Yu, H.-L., and Xu, J.-H. (2016) Biochemical properties of a new nitrile reductase cloned from *Pectobacterium carotovorum*. *J. Mol. Catal. B Enzym.* **131**, 47–54
26. Zhou, Z., Li, M., Xu, J.-H., and Zhang, Z.-J. (2018) A single mutation increases the activity and stability of *Pectobacterium carotovorum* nitrile reductase. *ChemBioChem*. **19**, 521–526
27. Ribeiro, A. J. M., Yang, L., Ramos, M. J., Fernandes, P. A., Liang, Z.-X., and Hirao, H. (2015) Insight into enzymatic nitrile reduction: QM/MM study of the catalytic mechanism of QueF nitrile reductase. *ACS Catal.* **5**, 3740–3751
28. Jung, J., and Nidetzky, B. (2018) Evidence of a sequestered imine intermediate during reduction of nitrile to amine by the nitrile reductase QueF from *Escherichia coli*. *J. Biol. Chem.* **293**, 3720–3733
29. El Yacoubi, B., Bailly, M., and de Crécy-Lagard, V. (2012) Biosynthesis and function of posttranscriptional modifications of transfer RNAs. *Annu. Rev. Genet.* **46**, 69–95
30. Harada, F., and Nishimura, S. (1972) Possible anticodon sequences of tRNAHis, tRNAAsn, and tRNAAsp from *Escherichia coli*. Universal presence of nucleoside Q in the first position of the anticodons of these transfer ribonucleic acid. *Biochemistry* **11**, 301–308
31. Mohammad, A., Bon Ramos, A., Lee, B. W. K., Cohen, S. W., Kiani, M., Iwata-Reuyl, D., Stec, B., and Swairjo, M. (2017) Protection of the queuosine biosynthesis enzyme QueF from irreversible oxidation by a conserved intramolecular disulfide. *Biomolecules* **7**, 30
32. Kozlov, A. G., and Lohman, T. M. (1999) Adenine base unstacking dominates the observed enthalpy and heat capacity changes for the *Escherichia coli* SSB tetramer binding to single-stranded oligoadenylates. *Biochemistry* **38**, 7388–7397
33. Leavitt, S., and Freire, E. (2001) Direct measurement of protein binding energetics by isothermal titration calorimetry. *Curr. Opin. Struct. Biol.* **11**, 560–566
34. Ogle, J. M., and Ramakrishnan, V. (2005) Structural insights into translational fidelity. *Annu. Rev. Biochem.* **74**, 129–177
35. Ogle, J. M., Brodersen, D. E., Clemons Jr, W. M., Tarry, M. J., Carter, A. P., and Ramakrishnan, C., V. (2001) Recognition of cognate transfer RNA by the 30S ribosomal subunit. *Science* **292**, 897–902
36. Johansson, M., Zhang, J., and Ehrenberg, M. (2012) Genetic code translation displays a linear trade-off between efficiency and accuracy of tRNA selection. *Proc. Natl. Acad. Sci. U. S. A.* **109**, 131–136
37. Oppenheimer, N. J., and Kaplan, N. O. (1974) Structure of the primary acid rearrangement product of reduced nicotinamide adenine dinucleotide (NADH). *Biochemistry* **13**, 4675–4685

38. Yoshida, A., and Dave, V. (1975) Inhibition of NADP-dependent dehydrogenases by modified products of NADPH. *Arch. Biochem. Biophys.* **169**, 298–303
39. Martínková, L., and Křen, V. (2010) Biotransformations with nitrilases. *Curr. Opin. Chem. Biol.* **14**, 130–137
40. Bagal, D. B., and Bhanage, B. M. (2015) Recent advances in transition metal-catalyzed hydrogenation of nitriles. *Adv. Synth. Catal.* **357**, 883–900
41. Haddenham, D., Pasumansky, L., DeSoto, J., Eagon, S., and Singaram, B. (2009) Reductions of aliphatic and aromatic nitriles to primary amines with diisopropylaminoborane. *J. Org. Chem.* **74**, 1964–1970
42. Bornschein, C., Werkmeister, S., Wendt, B., Jiao, H., Alberico, E., Baumann, W., Junge, H., Junge, K., and Beller, M. (2014) Mild and selective hydrogenation of aromatic and aliphatic (di)nitriles with a well-defined iron pincer complex. *Nat. Commun.* **5**. 4111
43. Burton, K., and Wilson, T. H. (1953) The free-energy changes for the reduction of diphosphopyridine nucleotide and the dehydrogenation of L-malate and L-glycerol 1-phosphate. *Biochem. J.* **54**, 86–94
44. Munro, A. W., Noble, M. A., Robledo, L., Daff, S. N., and Chapman, S. K. (2001) Determination of the redox properties of human NADPH-cytochrome P450 reductase. *Biochemistry* **40**, 1956–1963
45. DeCoursey, T. E., Morgan, D., and Cherny, V. V. (2003) The voltage dependence of NADPH oxidase reveals why phagocytes need proton channels. *Nature* **422**, 531–534
46. Oppenheimer, N. J., and Kaplan, N. O. (1974) Glyceraldehyde-3-phosphate dehydrogenase catalyzed hydration of the 5-6 double bond of reduced β-nicotinamide adenine dinucleotide (βNADH). Formation of β-6-hydroxy-1,4,5,6-tetrahydronicotinamide adenine dinucleotide. *Biochemistry* **13**, 4685–4694
47. Miksic, J. R., and Brown, P. R. (1978) Reactions of reduced nicotinamide adenine dinucleotide in acid: studies by reversed-phase high-pressure liquid chromatography. *Biochemistry* **17**, 2234–2238
48. Rafter, G. W., Chaykin, S., and Krebs, E. G. (1954) The action of glyceraldehyde-3-phosphate dehydrogenase on reduced diphosphopyridine nucleotide. *J. Biol. Chem.* **208**, 799–811
49. Seydoux, F. J., Kelemen, N., Kellershohn, N., and Roucous, C. (1976) Specific interactions of 3-phosphoglyceroyl-glyceraldehyde-3-phosphate dehydrogenase with coenzymes. *Eur. J. Biochem.* **64**, 481–489
50. Kelemen, N., Kellershohn, N., and Seydoux, F. (1975) Sturgeon glyceraldehyde-3-phosphate dehydrogenase. *Eur. J. Biochem.* **57**, 69–78
51. Wang, W., and Malcolm, B. A. (1999) Two-stage PCR protocol allowing introduction of multiple mutations, deletions and insertions using QuikChange Site-Directed Mutagenesis. *Biotechniques* **26**, 680–682
52. Goldberg, R. N., Kishore, N., and Lennen, R. M. (1999) Thermodynamic quantities for the ionization reactions of buffers. *J. Phys. Chem. Ref. Data*. **31**, 231–370
53. Oppenheimer, N. J. (1973) The primary acid product of DPNH. *Biochem. Biophys. Res. Commun.* **50**, 683–690
54. Pival, S. L., Klimacek, M., and Nidetzky, B. (2009) The catalytic mechanism of NADH-dependent reduction of 9,10-phenanthrenequinone by *Candida tenuis* xylose reductase reveals plasticity in an aldo-keto reductase active site. *Biochem. J.* **421**, 43–49
55. Klimacek, M., Brunsteiner, M., and Nidetzky, B. (2012) Dynamic mechanism of proton transfer in mannitol 2-dehydrogenase from *Pseudomonas fluorescens*: mobile Glu ^{292} controls proton relay through a water channel that connects the active site with bulk solvent. *J. Biol. Chem.* **287**, 6655–6667
56. Williams, T. J., Ellis, P. D., Bryson, T. A., Fisher, R. R., and Dunlap, R. B. (1976) Nuclear magnetic resonance studies on pyridine dinucleotides. *Arch. Biochem. Biophys.* **176**, 275–284
57. Ragg, E., Scaglioni, L., Mondelli, R., Carelli, I., Casini, A., and Tortorella, S. (1991) ^{1}H-, ^{13}C-, ^{31}P-NMR studies and conformational analysis of $NADP^+$, NADPH coenzymes and of dimers from electrochemical reduction of $NADP^+$. *Biochim. Biophys. Acta*. **1076**, 49–60

FOOTNOTES

This work has been supported by the Federal Ministry of Economy, Family and Youth (BMWFW), the Federal Ministry for Transport, Innovation and Technology (BMVIT), the Styrian Business Promotion Agency SFG, the Vienna Business Agency, the Standortagentur Tirol, the Government of Lower Austria, and Styrian Provincial Government Economic Affairs and Innovation through the COMET-Funding Program managed by the Austrian Research Promotion Agency FFG.

The abbreviations used are: $preQ_0$, 7-cyano-7-deazaguanine; $preQ_1$, 7-aminomethyl-7-deazaguanine; Q, queuosine; ecQueF, *E.coli* QueF; QM/MM, quantum mechanics/molecular mechanics; vcQueF, *Vibrio cholerae* QueF; bsQueF, *Bacillus subtilis* QueF; ITC, isothermal titration calorimetry; NAD(P)HX, *β*-6-hydroxy-1, 4, 5, 6-tetrahydronicotinamide adenine dinucleotide (phosphate) ;(cTHN)TPN, O2'-*β*-6-cyclo-1, 4, 5, 6-tetrahydro-nicotinamide adenine dinucleotide phosphate; DTT, dithiothreitol

Tables

Table 1. Thermodynamic parameters for $preQ_0$ binding to Cys^{190} and Asp^{197} variants of ecQueF

	K_d (μM)[a]		$K_{d\ app}$ (μM)	ΔH_{app} (kJ/mol)	$-T\Delta S_{app}$ (kJ/mol)	ΔG_{app} (kJ/mol)	n_{H+}	Reference
Wildtype	≤ 0.003	*phosphate*	0.039	-80.3	37.9	-42.4	0.78 ± 0.09	(18)
		HEPES	0.034	-65.7	22.9	-42.8		
		Tris	0.054	-47.7	5.1	-41.6		
C190A	46.5	*phosphate*	5.5 (3.6)[b]	-44.7 (-31.3)[b]	14.6 (0.07)[b]	-30.1 (-31.2)[b]	0.46 ± 0.27	(18)
		HEPES	4.26	-42.3	11.5	-30.8		
		Tris	4.05	-23.2	-7.7	-30.9		
C190S	15.3	*phosphate*	5.3	-38.9	8.7	-30.2	0.31 ± 0.16	This study
		HEPES	4.6	-36.4	5.8	-30.6		
		Tris	3.7	-23.8	-7.3	-31.1		
D197A	13.7	*phosphate*	3.5	-44.3	13.0	-31.3	≈ 0	This study
		HEPES	3.8	-50	18.9	-31.1		
		Tris	3	-42.7	11	-31.7		
D197H	0.55	*phosphate*	1.3 (1.0)[c]	-43.9 (-27.0)[c]	10.1 (-7.5)[c]	-33.8 (-34.4)[c]	0.61 ± 0.05	This study
		HEPES	1.6	-33.1	-0.1	-33.2		
		Tris	1.9	-17.5	-15.3	-32.8		
H229A	≤ 0.1	*phosphate*	0.054	-99.0	57.4	-41.6	1.40 ± 0.37	This study
		HEPES	0.127	-68.9	29.4	-39.5		
		Tris	0.159	-40.2	1.2	-39.0		

[a] Dissociation constants from fluorescence titrations (Figure 3).
[b,c] NADPH binding to the noncovalent complex of C190A[b] and D197H[c] with $preQ_0$

Table 2. Specific rates of substrate consumption and product formation during $preQ_0$ conversion by wildtype ecQueF and variants thereof. The specific rates are expressed as μmol product released (or substrate converted)/(μmol enzyme used × min).

	$preQ_0$	$preQ_1$	NADPH	$NADP^+$	NADPH degradation products [a]
Wildtype	4.1[b]	3.9[b]	8.4[b] (7.2)[c]	7.6[b]	Not detectable
C190A	0.21×10^{-3}	0.15×10^{-3}	1.3×10^{-3}	0.63×10^{-3}	0.65×10^{-3}
C190S	0.25×10^{-3}	0.22×10^{-3}	1.6×10^{-3}	0.67×10^{-3}	0.64×10^{-3}
D197A	0.04×10^{-3}	0.02×10^{-3}	15.3×10^{-3}	0.21×10^{-3}	14.40×10^{-3}
D197H	0.10×10^{-3}	0.09×10^{-3}	2.9×10^{-3}	0.87×10^{-3}	1.93×10^{-3}
H229A	/[e]	/	0.3[d]	/	/

[a] Calculated from the peak areas of peak **1** and **2** (see Figure 6)
[b] From Ref. (28)
[c,d] Obtained by spectrophotometric measurements, and taken from Ref. (18)[c]
[e] Not determined

Table 3. Reaction rates associated with NADPH degradation by wildtype ecQueF and variants thereof. The rates are expressed as µmol product released (or substrate converted)/(L × min). Reactions were carried out in Tris buffer (100 mM, pH 7.5) containing 50 mM KCl and 1.15 mM tris(2-carboxyethyl)phosphine.

	NADPH	$NADP^+$	NADPH degradation products [a]	A340[d]
No enzyme	0.08 (0.08[c])	0.001 (0.036[c])	0.05 (0.037[c])	0.07 (0.09[c], 6.45[e])
Wildtype[b]	0.18	0.062	0.11	
C190A[b]	0.06	0.038	0.03	
C190S[b]	0.08	0.036	0.03	
D197A[b]	0.71 (0.50[c])	0.058 (0.01[c])	0.70 (0.49[c])	0.74 (0.65[c])
D197H[b]	0.19	0.071	0.10	

[a] Calculated from the peak areas of peak **1** and **2** (see Figure 6)
[b] The enzyme concentration used was 50 µM
[c] Reaction in the Tris buffer used, employing dithiothreitol instead of tris(2-carboxyethyl)phosphine
[d] Rates determined from the decrease in absorbance at 340 nm, as shown in Figure 7D, assuming a molar absorption coefficient for NADPH at 340 nm of 6.22 $mM^{-1}cm^{-1}$
[e] Rate of the spontaneous reaction of NADPH at pH 3.5, leading to the "acid-modified" product according to literature (37, 38, 53)

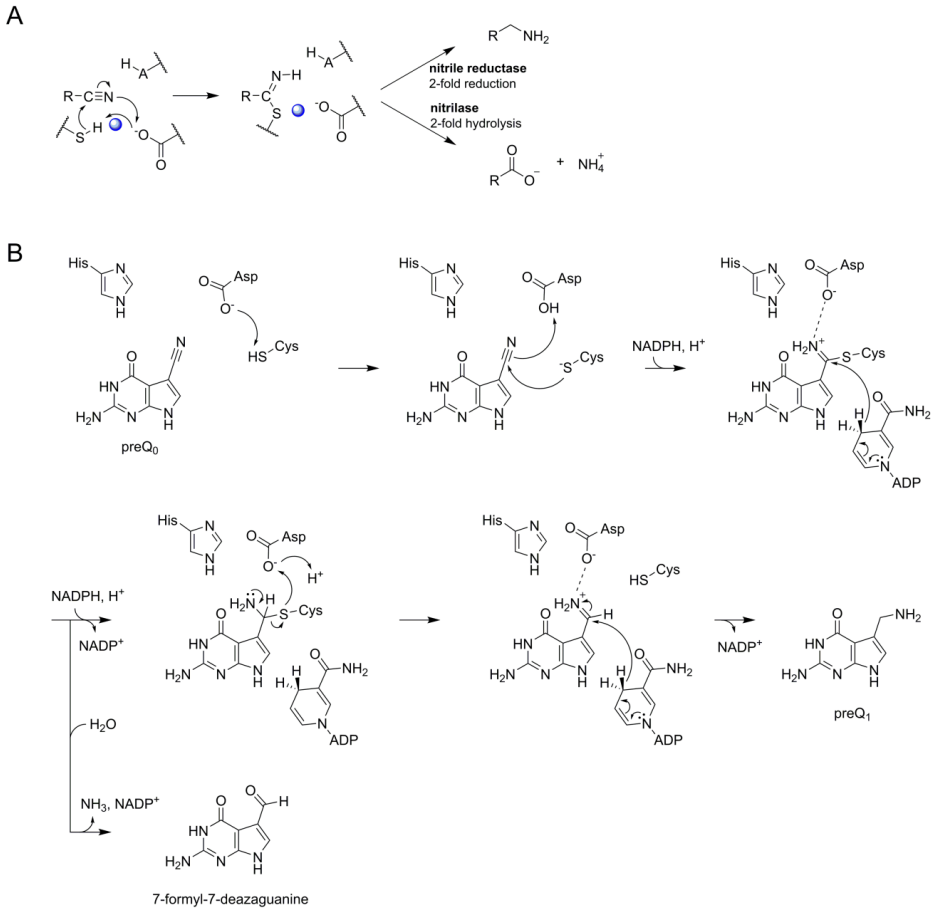

Scheme 1. Mechanistic analogies of nitrile reductase and nitrilase (A) and proposed mechanism of nitrile reduction by ecQueF (B). (A) Catalytic conversion of nitrile substrate via a common covalent thioimidate enzyme intermediate is shown. Base-catalytic activation of the cysteine nucleophile is water-mediated in the nitrilase. The water is shown in blue. Reduction and hydrolysis of the thioimidate both involve general acid-base catalysis. (B) A detailed mechanism of $preQ_0$ reduction is shown. Interception of the imine intermediate by water results in formation of 7-formyl-7-deazaguanine. This off-reaction is not significant in wildtype ecQueF but occurs in certain variants of the enzyme (28).

$$\text{QueF} + \text{preQ}_0 \rightleftarrows \text{QueF}\bullet\text{preQ}_0 \rightleftarrows \text{QueF-preQ}_0$$

Scheme 2. Two-step mechanism of $preQ_0$ binding to QueF. QueF•$preQ_0$, noncovalent complex; QueF-$preQ_0$, covalent thioimidate adduct. In wildtype ecQueF, the conversion of QueF•$preQ_0$ to QueF-$preQ_0$ is irreversible within limits of detection (18).

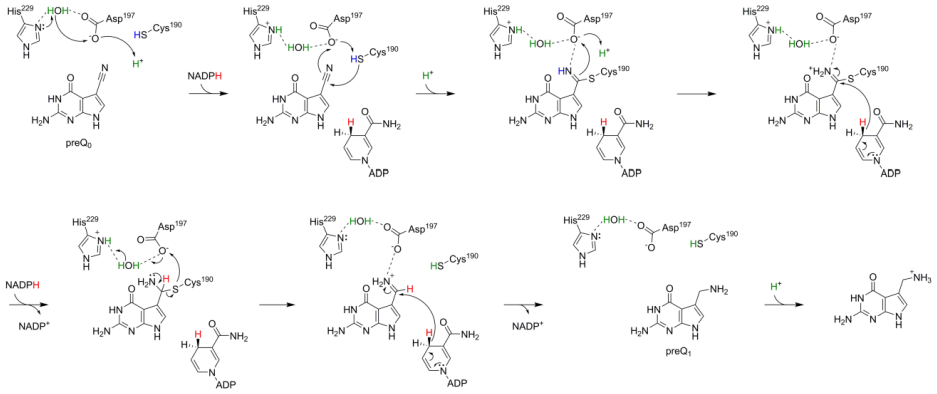

Scheme 3. Proposed enzymatic mechanism of reduction of $preQ_0$ to $preQ_1$ showing the proton transfers involved. Amino acid numbering of ecQueF is used. The dashed line indicates a hydrogen bond. Hydrogen marked in green indicates protons from water. Blue and red indicate protons from the enzyme and hydride from NADPH, respectively.

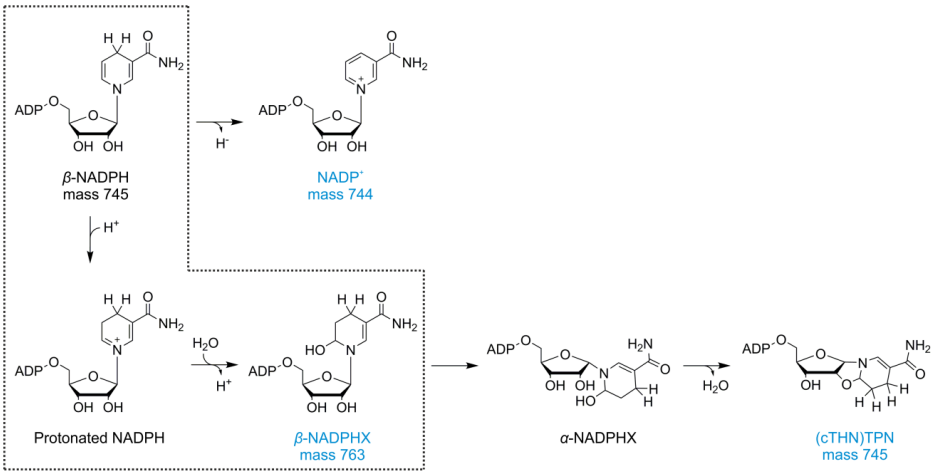

Scheme 4. Proposed paths of NADPH degradation in spontaneous and enzyme-promoted conversions. The uncoupled path involves hydration of NADPH to NADPHX followed by epimerization-cyclization to (cTHN)TPN. The reaction promoted by the D197A variant is marked by the dotted box. Conversion of NADPHX to the cyclic product is a spontaneous reaction. The coupled path entails formation of $NADP^+$ by known oxidation reactions of NADPH, for example by O_2.

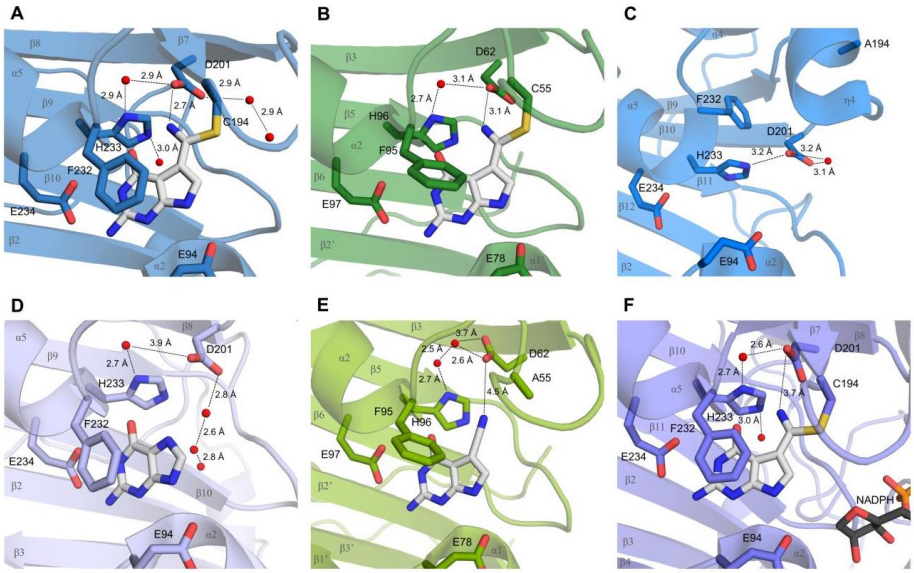

Figure 1. Crystallographic evidence for a possible proton relay involving the conserved Asp and His residues in QueF active sites. (A-B) The covalent thioimidate adducts between $preQ_0$ and the enzymes are shown for vcQueF (A, R262L variant, PDB code: 3S19) and bsQueF (B, wildtype, PDB code: 4F8B). Water molecules are shown as red balls. The full proton relay involving the substrate, Asp, water and His is established. (C) The apo-enzyme of vcQueF (C194A variant, PDB code: 3RJ4) is shown. (D-E) Noncovalent complexes of vcQueF with guanine (D, C194A variant, PDB code: 3BP1) and bsQueF with $preQ_0$ (E, C55A variant, PDB code: 4FGC) are shown. In panel E, a proton relay involving Asp, water and His is suggested. (F) The covalent $preQ_0$-vcQueF complex with NADPH (R262L variant, PDB code: 3UXJ) is shown. The full proton relay may be functional. In panels A-F, active-site residues are indicated and numbered. Note: the ecQueF residues corresponding to the vcQueF residues are Glu^{89}, Cys^{190}, Asp^{197}, Phe^{228}, His^{229}, and Glu^{230}. Elements of secondary structure are indicated. In bsQueF (panels B and E) the prime is used to indicate secondary structure elements from another protein subunit. Crystal structures of vcQueF and bsQueF are from Refs. (17, 21) and from unpublished data in the database.

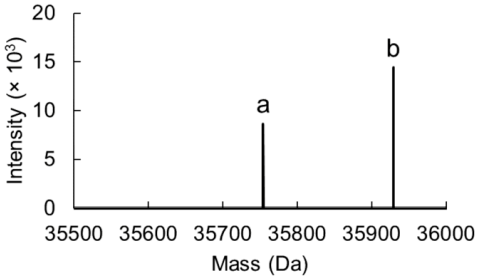

Figure 2. Protein mass analysis for the D197H variant of ecQueF after incubation with preQ$_0$ is shown. The sample is shown to contain both preQ$_0$-free monomeric protein (a, 35,754 ± 1 Da) and preQ$_0$-bound monomeric protein (b, 35,929 ± 1 Da).

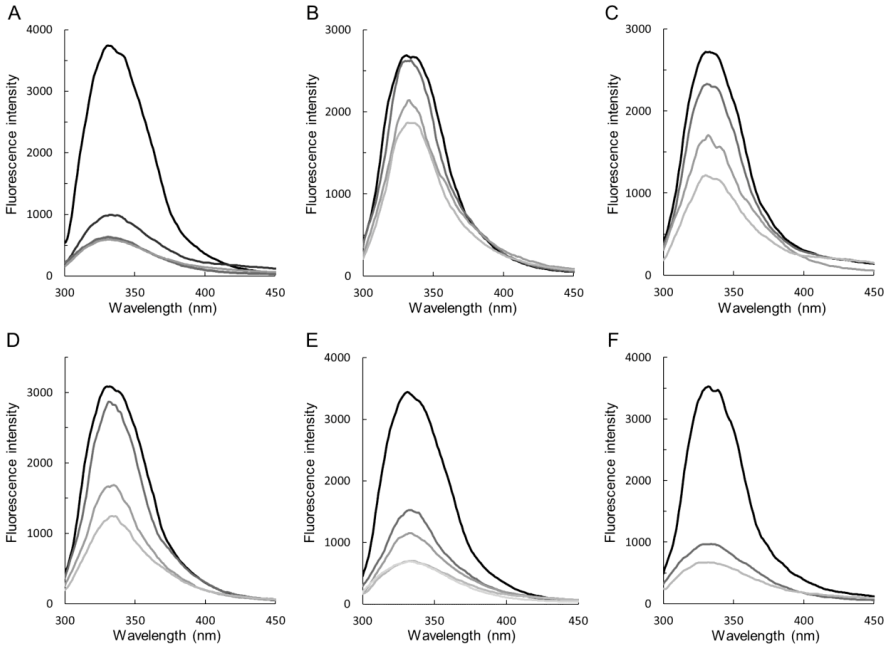

Figure 3. Fluorescence titration analysis of preQ$_0$ binding to ecQueF variants. The enzymes used are wildtype ecQueF (A), C190A (B), C190S (C), D197A (D), D197H (E), and H229A variant (F). The enzyme concentration was 3 µM. Protein fluorescence was quenched upon addition of preQ$_0$ (top to bottom: no preQ$_0$; 1.5, 3, 7.5, 15, 30 µM preQ$_0$). The K_d values obtained from the data are summarized in Table 1.

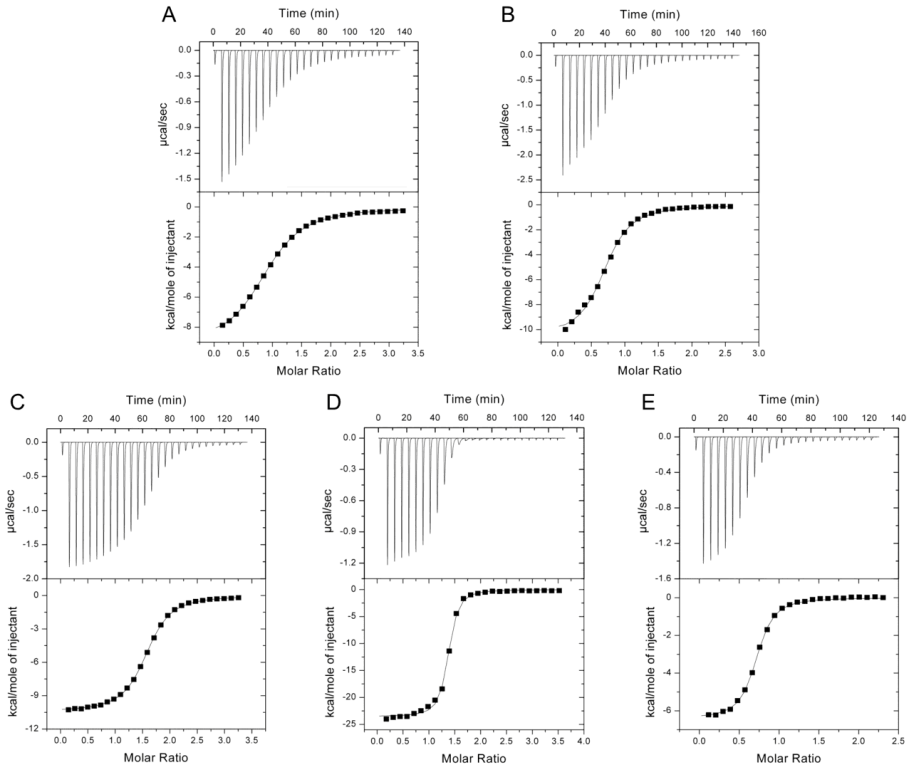

Figure 4. ITC analysis of $preQ_0$ and NADPH binding to ecQueF variants at 25 °C is shown. Phosphate buffer (100 mM Na_2HPO_4-NaH_2PO_4, pH 7.5) containing 50 mM KCl was used. (A-D) C190S (A, 39 µM), D197A (B, 60 µM), D197H (C, 39 µM), and H229A (D, 8 µM) were used. The $preQ_0$ solution (800 µM for C190S, D197A, and D197H; 250 µM for H229A) was titrated into the enzyme solution. The DMSO concentration did not exceed 2% in both the enzyme and the substrate solution. The *c* values (c = [dimeric protein]/K_d) obtained from the experiments were 7 for C190S, 17 for D197A, 30 for D197H, and 148 for H229A. (E) NADPH (1 mM) was titrated to the noncovalent $preQ_0$-D197H complex (59 µM). The *c* value obtained from the experiment was 59. Results of fits of the data are summarized in Table 1.

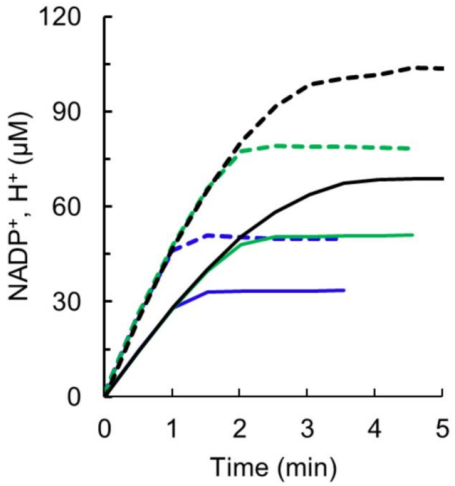

Figure 5. Proton uptake (dashed lines) and $NADP^+$ formation (solid lines) during $preQ_0$ reduction by wildtype ecQueF are shown. Reaction conditions: 3.6 µM enzyme; 100 µM NADPH; 20, 30 and 40 µM $preQ_0$ (bottom to top, purple, green, and black). A Tris buffer (0.5 mM, pH 7.51) additionally containing 150 mM KCl and 34 µM phenol red was used.

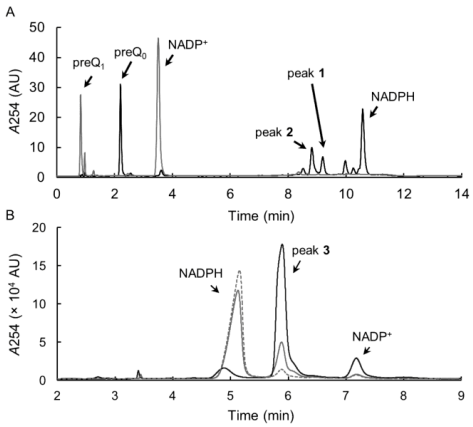

Figure 6. HPLC analysis of $preQ_0$ reduction by wildtype ecQueF and D197A variant (A) and degradation of NADPH by the D197A variant (B) are shown. Reaction conditions: wildtype enzyme (5 µM), D197A variant (50 µM); 250 µM $preQ_0$, 500 µM NADPH. Tris buffer (100 mM, pH 7.5) containing 50 mM KCl and 1.15 mM tris(2-carboxyethyl)phosphine was used. (A) Absorbance traces of the wildtype reaction (gray) and the reaction of D197A variant (black). The D197A variant shows NADPH degradation but almost no $preQ_0$ reduction. The peaks labeled **1** and **2** are from NADPH degradation. (B) Rearrangement of NADPH (500 µM) by D197A variant (50 µM, black) and spontaneous reaction (gray) after an incubation at 25 ºC for 26 h. The NADPH solution at reaction start is shown by a gray dashed line. Note: the degradation product peaks were not separated in the LC-MS analysis shown. Peak **3** therefore involves both peak **1** and peak **2** from the analysis shown in panel A. Mass analysis shows that peak **3** comprises a 745 mass as well as a 763 mass species. The mass intensity ratio for the two species was changed depending on the conditions used in the reaction and in the analysis procedure.

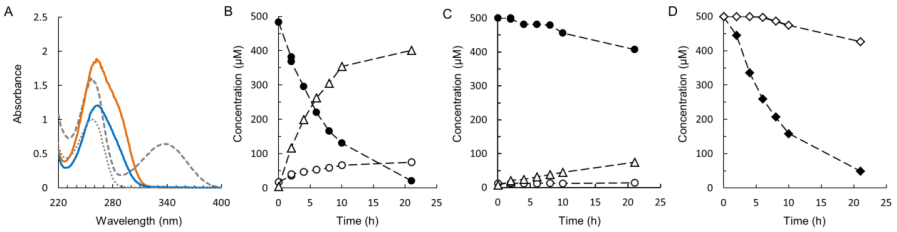

Figure 7. Conversion of NADPH promoted by the D197A variant and occurring spontaneously in solution. (A) The UV-Vis spectra of the main rearrangement product obtained through enzymatic conversion (blue, 80 µM) is compared to the spectra of the cyclisation product (orange, 87 µM), NADPH (gray dashed line, 103 µM), and $NADP^+$ (gray dotted line, 40 µM). (B-D) Time course analysis of NADPH degradation is shown. Experiments were done in Tris-HCl buffer (100 mM, pH 7.5), additionally containing 50 mM KCl and 1.15 mM tris(2-carboxyethyl)phosphine. The enzyme concentration was 50 µM. (B-C) Enzymatic (B) and spontaneous (C) degradation of NADPH is shown. Reactions were monitored by LC-MS analysis. Closed and open circles indicate NADPH and $NADP^+$, respectively. Open triangles indicate the NADPH degradation products obtained from the sum of peak **1** and **2** in Figure 6. (D) Degradation of NADPH (enzymatic: closed diamonds; spontaneous: open diamonds) monitored by loss of absorbance at 340 nm is shown. Reaction rates obtained from the time courses are summarized in Table 3.

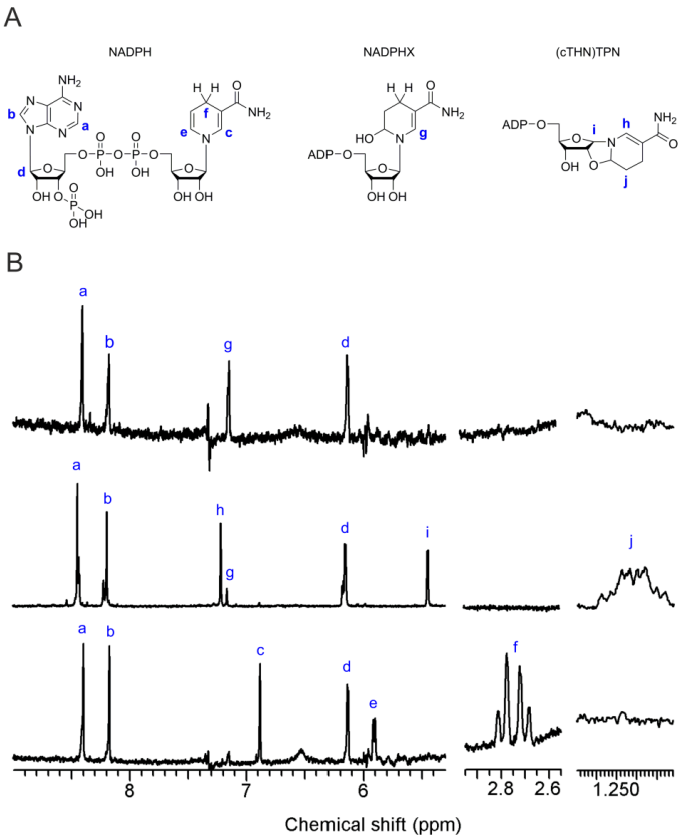

Figure 8. ^{1}H NMR analysis of the main hydration product released during conversion of NADPH by D197A variant. (A) Chemical structures of NADPH, NADPH hydrate (NADPHX), and the cyclic rearrangement product ((cTHN)TPN) are shown. (B) The ^{1}H NMR spectrum (top) of the product obtained from full conversion of NADPH (0.5 mM) with enzyme (50 µM) is shown. The reference spectrum of cyclic product (middle, 5.8 mM) and NADPH (bottom, 0.5 mM) are also shown. Tris-HCl buffer (100 mM, pH 7.5) containing 50 mM KCl and 1.15 mM tris(2-carboxyethyl)phosphine was used for reaction. Proton peaks of adenine C2 (b, 8.18 ppm), C8 (a, 8.41 ppm), and ribose C1 (d, 6.14 ppm) were not shifted in the products. The proton peak of dihydronicotinamide C2 of NADPH (c, 6.88 ppm) was shifted in the enzymatically formed product (g, 7.15 ppm) and in the cyclic product (h, 7.22 ppm). Proton peaks of nicotinamide C4 (f, 2.72-2.81 ppm, 2-times magnified) and C6 (e, 5.90-5.92 ppm) of NADPH were not present in the degradation products. The cyclic product showed proton signals from the tetrahydronicotinamide C5 (j, 1.22-1.24 ppm, 2-times magnified) and ribosyl C1 (i, 5.45 ppm), which were not present in the product obtained from the enzymatic reaction. Ribosyl protons were overlapped with water signal. The spectra of NADPH and the degradation products were validated with the previously reported spectra of these components (37, 46, 57).

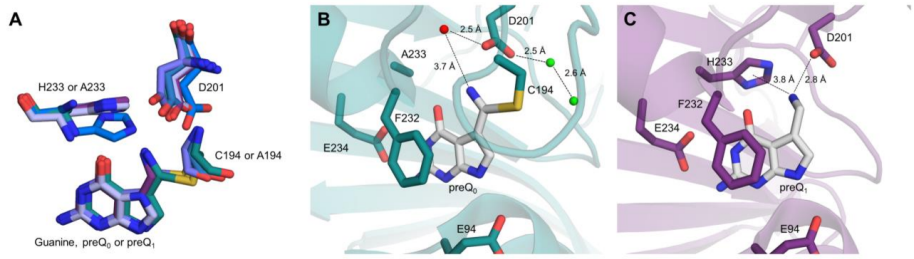

Figure 9. Conformational flexibility of His and Asp residues in the vcQueF active site and binding of the preQ$_1$ product to the enzyme. (A) A structural overlay of vcQueF structures, used in Figures 1 and 9, is shown: apo-enzyme (blue, C194A variant), holo-enzyme (deep blue, preQ$_0$-R262L variant; light blue, guanine-C194A variant; teal blue, preQ$_0$-H233A; violet, preQ$_1$-C194A variant) and ternary complex structures (purple blue, preQ$_0$-R262L variant-NADPH). (B) The covalent thioimidate complex of the vcQueF H233A variant with preQ$_0$ (PDB code: 4GHM, teal blue) is shown. The structure reveals that Asp^{201} interacts with water molecules both inside (red sphere) and outside (green sphere) of the active site. This could establish a proton relay despite the absence of His. (C) The complex of vcQueF with preQ$_1$ (C194A variant, PDB code: 3RZP, violet) is shown. Crystal structures of vcQueF are from Ref. (21) and from unpublished data in the database.

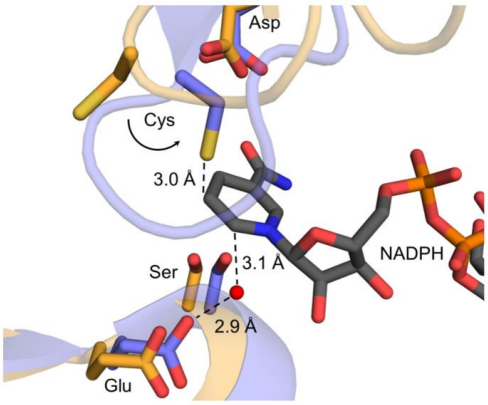

Figure 10. Structural interpretation and proposed mechanism of catalytic hydration of NADPH by the D197A variant of ecQueF. An overlay of the structural model of ecQueF (orange, wildtype; Ref. (10)) and the experimental crystal structure of vcQueF (light blue, R262L variant, PDB cod: 3UXJ) is shown. The bound NADPH is from the structural model of ecQueF. The catalytic cysteine is on a flexible loop in the QueF structures. Substitution of Asp^{197} by Ala is expected to enhance the inherent conformational flexibility of the cysteine, allowing it to be brought into proton transfer distance to the dihydro-nicotinamide C5 of NADPH. Cys^{190} variants of ecQueF are no longer able to promote the hydration of NADPH. A water molecule (red sphere) is present in the structure at a position suitable for attack on C6. The addition of the water may be assisted by Glu^{89}. Amino acids and NADPH are indicated by element-based colors.

Scientific records

Publications

Kinetic analysis and probing with substrate analogues of the reaction pathway of the nitrile reductase QueF from *Escherichia coli*

J. Jung, T. Czabany, B. Wilding, N. Klempier, and B. Nidetzky, *J. Biol. Chem.* 291 (**2016**), 25411–25426

Evidence of a sequestered imine intermediate during reduction of nitrile to amine by the nitrile reductase QueF from *Escherichia coli*

J. Jung, B. Nidetzky, *J. Biol. Chem.* 293 (**2018**), 3720–3733

Oral presentations

Kinetic analysis and substrate binding studies of the *Escherichia coli* nitrile reductase QueF

J. Jung, T. Czabany, and B. Nidetzky, *44th ACS Middle Atlantic Regional Meeting*, **2016**, Riverdale, New York, United State